A novel nanosized layered double hydroxide ceramic based extended release drug delivery system for cancer therapy

Thesis Submitted by,

Suman Saha

For the degree

of

Doctor of Philosophy (Pharmacy)

Department of Pharmaceutical Technology
Jadavpur University
Kolkata, India
2022

Name, Designation & Institution of the Supervisor/s:

Prof. (Dr.) Tapan Kumar Chatterjee
Dean, Dept. of Pharmaceutical Science and Technology
JIS University, Kolkata
Former Professor, Division of Pharmacology
Former Director, Clinical Research Centre (CRC)
Jadavpur University
Kolkata-70032, India

Dr. Jui Chakraborty
Principal Scientist
Bioceramics and Coating Division
CSIR-Central Glass & Ceramic
Research Institute
Kolkata-700032

List of publication in peer reviewed journals

1. Saha S, Ray S, Acharya R, Chatterjee T K, Chakraborty J. Magnesium, zinc and calcium aluminium layered double hydroxide-drug nanohybrids: a comprehensive study. **Applied Clay Science. (Elsevier)**. 2017, 135, 493-509. (SCI Impact Factor **3.64**).

2. **Saha S**, Ray S, Ghosh SK, Chakraborty J, pH-dependent facile synthesis of CaAl-layered double hydroxides and its effect on the growth inhibition of cancer cells, **Journal of the American Ceramic Society**, **Wiley publication,** 2018, 101(9), 3924-3935. (SCI Impact Factor **2.96**).

3. **Saha S**, Bhattacharjee A, Rahaman Sk H, Basu A, Chakraborty J, Synergistic anti metastatic activity of etoposide loaded calcium aluminium layered double hydroxide nanoconjugate in the management of non small cell lung carcinoma, **Applied Clay Science (Elsevier), 2020, 188, 105496** (SCI Impact Factor **3.64**).

4. **Saha S,** Bhattacharjee A, Rahaman H Sk, Ray S, Marei M K., Jain H , Chakraborty J, Prospects of antibacterial bioactive glass nanofibres for wound healing: an in vitro study. International Journal of Applied Glass Science. **Wiley publication**, (**Accepted**, **doi: 11.1111/ijag.15029**) (SCI Impact Factor **1.85**).

5. Ray S, **Saha S**, Sa B, Chakraborty J. *In vivo* pharmacological evaluation and efficacy study of methotrexate-encapsulated polymer coated layered double hydroxide nanoparticles for possible treatment of osteosarcoma. **Journal of Drug Delivery and Translational Research (Springer)**. 2017, 7(2), 259-275. (SCI Impact Factor **3.39**).

6. Acharya R, **Saha S**, Ray S, Hazra S, Mitra M K, Chakraborty J. siRNA-nanoparticle conjugate in gene silencing: A future cure to deadly diseases? **Materials Science and Engineering C (Elsevier)** 2017, 76 1378–1400 (SCI Impact Factor **5.08)**

7. Rahaman Sk. H, Bhattacharjee A, **Saha S**, Chakraborty M, Chakraborty J, shRNA intercalation in CaAl-LDH nanoparticle synthesized at two different pH conditions and its comparative evaluation, **Applied Clay Science. (Elsevier).** 2017, 135, 493-509. (SCI Impact Factor **3.64**)

8. Bhattacharjee A, Rahaman Sk. H, **Saha S**, Chakraborty M, Chakraborty J, Determination of half maximal inhibitory concentration of CaAl layered double hydroxide on cancer cells and its role in the apoptotic pathway, **Applied Clay Science. (Elsevier).** 2019, 171, 57-64. (SCI Impact Factor **3.64**)

Book chapter

1. **Suman Saha,** Payal Roy and Jui Chakraborty, Mesoporous silica-biopolymer based systems in drug delivery applications, Tailor-Made and Functionalized Biopolymer Systems, Elsevier, ISBN 978-0-12-821437-4, DOI: https://doi.org/10.1016/B978-0-12-821437-4.00002-5.
2. Acharya R, **Saha S**, Ray S, Chakraborty J, Nanoparticulate Immunotherapy: an intelligent way to tailor makes our defense system. Jana S and Jana S (Eds) Particulate Technology for Delivery of Therapeutics. Springer Nature Publication, New York, USA, ISBN 978-981-10-3646-0, 393642_1_En, (13) 2017, 419-451.

List of Patent

1. An inorganic base antacid compound with improved and novel properties, authored by Jui Chakraborty, Sayantan Ray, **Suman Saha**, Biswanath Sa, The Indian patent application number 0097NF2017, Docket no. 37407. CBR. No. 20680, Patent office application no. 201711020405, dated 12/06/2017. **(Indian) (Granted)**
2. Bioactive glass particles and micro nano fibre based wound care compositions dressing, suture and matrices thereof, Jui Chakraborty, Suman Saha, Payal Roy, Rupam Saha, Application No: 202111046618, dated 12.10.2021. Council for Scientific and Industrial Research (Filed)
3. New compositions of bioactive glass based hemostatic matrices and preparation thereof, Puja Srivastava, Jui Chakraborty, Payal Roy, Suman Saha, Rupam Saha, Defence Research and Development Organization (Filed)

List of Presentations in National/International/Conferences/Workshops :

1. Saha S, Participated in "First International Conference on Emerging Materials: Characterization & Application" held on December 4-6, 2014 at CSIR- Central Glass and Ceramic Research Institute, Kolkata, India.

2. Saha S, Ray S, Joy M, Chakraborty J, "A layered nanocarrier in anticancer drug delivery path to a new horizon" in 6th East zonal & 24th state conference of Indian Pharmacological Society, WB branch, February 5- 6, 2015,West Bengal University of Animal and Fishery Sciences, Kolkata, India.

3. Saha S, Ray S, Chakraborty J, "CSIR-CGCRI developed novel inorganic based antacid: efficacy and toxicity study" in International Conference on Biomaterials, Biodiagnostics, Tissue Engineering, Drug Delivery and Regenerative Medicine 2016, held on April 15-17, 2016 at Indian Institute of Technology Delhi.

4. Saha S, Ray S, Chakraborty J, "A unique mouth melting inorganic antacid developed at CSIR-CGCRI for the treatment of hyperchlorhydria", at the International Conference on Biotechnology and Biological Sciences (Biospectrum 2017), during August 25-26, 2017, held at University of Engineering and Management, Kolkata, India.

5. Saha S, Bhattacharjee A, Rahaman Sk H, Basu A, Chakraborty J, Synergistic anti metastatic activity of etoposide-CaAl layered double hydroxide nanoconjugate: A novel treatment approach for non small cell lung carcinoma, on Current Trends in Materials Science and Engineering 2019 on 18th-20th July 2019, held at S. N. Bose National Centre For Basic Sciences, Kolkata

6. Ray S, **Saha S**, Acharya R, Chakraborty J, "Value added multifunctional injectable bone augmentation material for treatment of osteoporotic vertebral compression

fracture in elderly patients" in International Conference on Energy, Functional Materials and Nanotechnology 2016 held on March 27-29, 2016 at Nanotechnology Center, Kumaun University, Kumaun University, Nainital, India.

7. Ray S, **Saha S**, Acharya R, Sa B, Chakraborty J, "Unique bioactive glass based bone augmentation material for treatment of geriatric population suffering from osteoporotic vertebral compression fracture", at the International conference on advances in glass science and technology held on January 23-25, 2017 at CSIR-Central Glass & Ceramic Research Institute.

Awards

1. Young Scientist Award from Material Research Society of India (MRSI), held at Indian Association for the cultivation of Sciences, Kolkata-700032 on 21.08.2018.

2. Best Oral Award at International Conference on Current Trends in Materials Science and Engineering 2019 on 18th-20th July 2019, held at S. N. Bose National Centre For Basic Sciences, Kolkata

3. Excellence in Research work Award at 2nd National Biomedical Research Competition, NBRCom 2019 organized by Postgraduate Medical Education & Research, Chandigarh and Society of Young Biomedical Scientists (SYBS), India. Dated 17th November 2019.

4. Best Oral Presentation Award at International Conference on Synthesis, Characterization and Application of Nanomaterials (SCAN) organized by The Institution of Engineers (India), Dated 1-2 November 2019, Kolkata.

Statement of originality

I, Suman Saha a PhD registered candidate of Jadavpur university having **enrolment No D-7/ISLM/69-16 dated 08.09.2016** do hereby declare that this thesis entitled **"A novel nanosized layered double hydroxide ceramic based extended release drug delivery system for cancer therapy**" contains literature survey and original research work done by the undersigned candidate as part of doctoral studies.

All information in this thesis have been obtained and presented in accordance with existing academic rules and ethical conduct. I declare that, as required by these rules and conduct, I have fully cited and referred all materials and results that are not original to this work.

I also declare that I have checked this thesis as per the "Policy on Anti Plagiarism, Jadavpur University, 2019", and the level of similarity as checked by iThenticate software is __%.

Signature of the candidate

Signature and seal of Supervisors

Prof.(Dr.) Tapan Kumar Chatterjee, (Supervisor)
Dean, Dept. of Pharmaceutical Science and Technology
JIS University, Kolkata
Former Professor, Division of Pharmacology
Former Director, Clinical Research Centre (CRC)
Jadavpur University
Kolkata-70032, India

Dr. Jui Chakraborty(Supervisor)
Principal Scientist
Bioceramics and Coating Div
CSIR-Central Glass and
Ceramic Research Institute
Kolkata-700032

CERTIFICATE FROM THE SUPERVISOR

This is to certify that the thesis entitled "**A novel nanosized layered double hydroxide ceramic based extended release drug delivery system for cancer therapy**" submitted by Suman Saha, who got his name registered having enrolment No D-7/ISLM/69-16 dated 08.09.2016 for the award of Ph.D. (Pharmacy) degree of Jadavpur University is absolutely based upon his own work under the supervision of the undersigned and that neither his thesis nor any part of the thesis has been submitted for any degree/diploma or any other academic award anywhere before.

Signature & Seal

Prof (Dr.) T. K. Chatterjee
Dean,
Dept. of Pharm. Science and Tech.
JIS University, Kolkata
Former Professor, Division of Pharmacology
Former Director, Clinical Research Centre (CRC)
Jadavpur University
Kolkata-70032, India

Dr. Jui Chakraborty
Principal Scientist
CSIR-Central Glass &
Ceramic Research Institute
Jadavpur, Kolkata-70032
India

Acknowledgement

First of all, I pay tribute to Lord Shiva, the almighty for giving me the chance to pursue the doctoral degree and provide me the capability to proceed successfully. The tenure of PhD has been a truly life-changing experience for me and it would not have been possible to do without the support that I received from many people. I would therefore like to offer my sincere thanks to all of them.

Foremost, I would like to express my sincere gratitude to Dr. K. Murleedharan, Ex-Director, and Dr. Suman Kumari Mishra, Director, CSIR-Central Glass and Ceramic Research Institute, Kolkata for their kind co-operation throughout my research work.

I would like to thank to Dr. V. K. Balla (HOD), Dr. S. Bandyopadhyay (Ex-HOD) and Dr. S. Dasgupta (HOD) of Bioceramics and Coating Division, CSIR-Central Glass and Ceramic Research Institute, Kolkata, for their encouragement, insightful comments, and allowing me to use departmental facilities and ample amount of freedom during my work here.

I would like to express my sincere gratitude to my supervisor Prof. (Dr.) T. K. Chatterjee, Professor, Department of Pharmaceutical Technology, Jadavpur University, Kolkata, for the insightful discussion and valuable advice during the period of my study. I am very much grateful to him for his support, immense knowledge in drug delivery makes him a great mentor.

I would like to say a very big thank you to my supervisor Dr. Jui Chakraborty, Principal Scientist, Bioceramics and Coating Division, CSIR-Central Glass and Ceramic Research Institute, Kolkata, for all the support and encouragement she gave me, during my entire tenure at CSIR-CGCRI Kolkata. She was always available for discussion

despite of her busy schedule. I am very much grateful for her constant support, motivation, enthusiasm.

I want to convey my sincere thanks to Dr. Samar Chakraborty, Consultant Anaesthesiologist, AMRI Hospital, Kolkata for arranging the drug Etoposide for the entire thesis work.

I also appreciate the financial support of the INSPIRE programme (IF 140912) under Department of Science & Technology, GOI, New Delhi, India, during my PhD work.

I thank my seniors including Dr. Sayantan Roy, Dr. Mathew Joy and Dr. Mayur Shukla, and fellow juniors Ms. Payel, Ms. Rupam, in Bioceramics and Coating Division, CSIR-CGCRI for valuable discussions. I want to convey my sincere thanks to my best friend Anuradha who helped me throughout my PhD tenure. I can remember the pleasant days we worked together in our respective work and for all the fun we have had in the last few years.

I would also like to express my appreciation to all the staff members at the Central Characterization facility, CSIR- Central Glass and Ceramic Research Institute, Kolkata for assistance in characterization of different samples.

Last but not the least my family. I warmly thank my father Late Ajit Kumar Saha for his blessings and my mother Mrs. Rita Saha for her constant support and blessings in all aspects of life. I also would like to thank my wife Mrs. Moumita Kundu for constant support and tolerating me throughout my PhD tenure.

Suman Saha

List of Figures

Figure 5.11. (B) Hydrodynamic diameter of (a) sample A (b) sample B.

Figure 5.12. FESEM image of (a) sample A (b) sample B.

Figure 5.13. Thermogravimetric analysis (TG-DTA) and DSC of (a, a') ETO (b,b') sample A and (c,c') sample B.

Figure. 5.14 (a) Calibration curve of etoposide gained from UV-VIS spectroscopy; (b) In vitro release of ETO from (a) Physical mixture of sample A and ETO (1:1, w/w) (b) sample B in phosphate buffer saline at pH 7.4; (c)-(f) Release kinetics models (a) First-order model; (b) Hixon Crowel model; (c) Higuchi model (d) Korsmeyer-Peppas model.

Figure 5.15. The half maximal inhibitory (IC50) concentration of (a) ETO treated on A549 cell line (b) sample B treated on A549 cell line

Figure 5.16. (A) In vitro cell viability study of the ETO, sample A and sample B on A549 cell line in varying time including 24, 48 and 72 h respectively; (B) In vitro cell migration assay shows (a) Confluent cells in 6 well plate (b) scratch by micropipette on the confluent plate (c) A549 cells without treatment (d) Cells treated with sample A (e) Cells treated with ETO (f) A549 cell treated with physical mixture (1:1, w/w) (g) Cells treated with Sample B

Figure 5.17 Exhibits uptake of FITC tagged sample B into A549 cell line, showing internalization of the nanoconjugate into the cell (sample B)

Figure 5.18. Confocal image of (a) DAPI image (b) FITC image (c) superimposed image**.**

Figure 5.19. exhibits (a) CAMKIIα expression assay; (b) SOD expression assay.

List of Tables

Dedicated to

my beloved parents…

Preface

This thesis is being submitted in accordance with the rules and regulations for the degree of Doctor of Philosophy in Pharmacy in the Department of Pharmaceutical Technology, Jadavpur University and the entire work in this thesis was undertaken by me in CSIR-Central Glass and Ceramic Research Institute, Kolkata.

Malignancy is one of the most dangerous health concerns, and it is the second leading cause of mortality worldwide. Although numerous epidemiologic criteria play a pivotal role in cancer prediction, they can be further expanded to include family history, genetic predisposition, and environmental or cultural habits. Chemotherapy has a substantial advantage over other forms of treatment since it has fewer side effects. However, there are various challenges connected with eradicating all cancer cells, and it is difficult to control when the cells have spread to other vital organs. Chemotherapy's failure in cancer treatment might be attributed to several factors. Selectivity of inappropriate drugs/cycles, multi-drug resistance, and heterogeneous biological causes for cancer are some of the significant aspects. Furthermore, there are numerous other characteristics linked with the drug itself, such as low solubility at physiological pH, drug targeting, and so on. Because of these reasons, current anticancer medication treatment strategies necessitate high dosages, which can induce a variety of side effects such as nausea and vomiting, muscle pain, hair loss, headaches, diarrhoea, appetite loss, throat discomfort, and so on, resulting in poorer patient compliance. Further most of the anticancer drugs are insoluble or have lower solubility in aqueous medium therefore for solubilization of the drug, various toxic chemical substances are in use which often exhibits several adverse events hence increase the morbidity and mortality rate. Anticancer drugs that delivered directly do not have the best therapeutic efficacy owing to several problems, including low absorption, enzymatic degradation, adverse drug reactions due to high

dosage, and systemic toxicity due to local accumulation. Further higher dosage of a drug is required in case of short plasma half-life which further leads to nonspecific toxicities to the proliferating cells. Therefore, it is of prior importance to choose an efficient delivery system that can effectively deliver the drug for a prolonged time thus resulting in reduce the dosage which ultimately results in better patient compliance.

Herein, lung carcinoma is a malignant lung tumour marked by uncontrollable cell proliferation in the lungs. By metastasizing into neighbouring tissue or other sections of the body, this abnormal tissue growth might expand beyond the lung. Herein the first line of drug incudes Etoposide although high dose of this drug can lead to various systemic toxicities. Herein to overcome the problem an effort has been made to synthesize a novel (CaAl based) nanoceramic layered double hydroxide (LDH) based nanocarrier that can effectively address the issues related to the bare drug.

In this study, a novel ceramic-based calcium aluminium layered double hydroxide (CaAl-LDH) nanoparticles were synthesized at three different pH conditions and all the physicochemical characterization of the same were undertaken to optimize the phase pure CaAl-LDH. Herein it has to be mentioned that At pH 8.5, a well crystallised hydrotalcite-like phase with typical (00l) reflections for layered clays was observed, which was indexed to hexagonal lattice with rhombohedral space group. The basal spacing (d002) of 8.66 A, which matches to CaAl-(002) LDH's peak, confirms the phase pure CaAl-LDH (JCPDF 01-089-6723). Further increase in pH upto 12.5 leads to formation of $CaCO_3$ (aragonite and calcite polymorphs) which was further evaluated by many other analytical techniques. The concentration of the leached Ca^{2+} was found to be 13.91 ppm after 72 hours for the sample synthesized at pH 8.5 which was decreased to 6.42 ppm in case of sample synthesized at a pH of 12.5. There after all the samples were taken to carry out the *invitro* cytotoxicity study on colon and breast cancer

cell lines (HCT116 and MCF7 as a sample cell line) and healthy bone cells (MC3T3) (osteoblast precursor) to check the viability. A strong suppression of cell growth on HCT116 was 70.77% at 72 hours was observed in phase pure CaAl-LDH synthesized at a pH of 8.5 whereas no such observation with other two synthesized CaAl-LDH nanoparticles. Moreover, all the samples show good viability in healthy MC3T3 cells. This observation was first time reported in any peer reviewed journal that phase pure CaAl-LDH exhibits a cytotoxic potential in cancer cell.

Further to evaluate the potential of the phase pure CaAl-LDH as a delivery vehicle and owing to its cytotoxic property, synergistic activity was assessed in lung cancer. Herein anticancer drug Etoposide (ETO) was selected and successfully intercalated by simple ex-situ anion exchange techniques to develop ETO intercalated CaAL-LDH nanohybrid. The basal spacing (d002) of 8.5764 corresponds to the (002) diffraction peak of phase pure CaAl-LDH (JCPDF 01-089-6723), which rose to 17.18 owing to the enlargement of the interlayer space caused by the drug ETO being inserted into the LDH nanoparticle along the z-axis. Thermogravimetric analysis exhibits increased thermal stability of the encapsulated ETO in the LDH nanoparticles. Further *invitro* release kinetics shows the cumulative release of ETO from the vehicle exhibits an initial burst release of nearly 40% within the first 2 h owing to the loosely bound drug on the surface of the nanoparticle and the leftover drug, intercalated within the nanoparticle follows ETO's prolonged release for up to 72 hours, which could be due to ETO's slow diffusion from the interlayer space. Notably *In vitro* cell viability and cell migration assay was carried out on A549 cell line (lung carcinoma) using the bare drug and nanoconjugate to assess the synergistic anti-cancer potential of the nanoconjugate. The cell viability was reduced to 21.56 % after 72 hours when compared to bare ETO and nanoparticle which showed a viability of 37.45 % and 61.85 %, respectively ($P<0.05$).

The results were corroborated by cellular uptake study and cellular internalization study respectively. Cellular internalization of the nanoconjugate was found to be 19.30 % after 72 hours of incubation. This finding backs with evidence from an *in vitro* cytotoxicity study, which implies that ETO intercalated phase pure CaAl-LDH nanoconjugate has a synergistic anti-cancer effect towards lung carcinoma. This research findings have a great potential to revolutionize the lung cancer treatment.

Contents

Experimental: Part 2

Chapter: 5

5. Results & Discussion

Results & Discussion: Part 1

Results & Discussion: Part 2

Chapter 1

Introduction

1. Introduction

Malignancy is one of the most important hazardous health issues and is the second common factor associated with death worldwide. Though there are many epidemiologic parameters involved in the prognosis of cancer it can be further expanded to many other parameters including family history, genetical predisposition, environmental or cultural habits. These parameters often contribute to the development of cancer (Reichert, and Wenger, 2008; Vasir, and Labhasetwar, 2005). However, pathogenesis of cancer is diverse and most of the time is associated with physico-chemical and biological occurrence (Doll, and Petro, 1981). In cancer there is a series of abnormal mutations in the genetic code which leads to uncontrolled cell growth. Therefore, the function of the cells are hampered, and abnormalities are noted (Siegel RL et al., 2016). This gene mutation is primarily due to many environmental pollutants and/or other chemical substances which has carcinogenic potential that influences directly or indirectly to the cytoplasm of the cell resulting in genetic disorders as well (Poon SL et al., 2014, Trafialek J et al., 2014, Cumberbatch MG et al., 2015). In case of cancer prognosis, the proto-oncogenes are held responsible for cell division and growth under normal condition though in some special occasions during the mutation phase these oncogenes mutate abnormally and becomes dangerous. In male, prostate, lung and colon cancer is predominant whereas in case of female breast, uterine corpus, thyroid, lung cancer contributes to significant health burden.

Although there are hundreds of cancer type and all are different in each other in all aspect including pathogenesis involved, prognosis, treatment strategies, life expectancy and many more, however regular screening, high risk patient with significant family history, early diagnosis have improved the patient prognosis and health outcome (Parkin et al., 1997). It is evident that almost 80% of the cancers are solid tumours

which can be surgically removed, prior to which chemotherapy and radiotherapy is the main choice of treatment for the reduction in tumour size and association of other organs at the tumour site (Jang et al., 2003). Moreover other treatment strategy includes immunotherapy/immunosuppression, gene and hormonal therapy, transplantation etc. (Leach, 1999). Chemotherapy predominates significantly owing to its lower adverse effect compared to other means of treatment however, there are several obstacles associated to killing of all the cancer cells and difficult to manage when the cells are metastasized to other organs of importance. There are several reasons that contribute to the failure of the chemotherapy in cancer treatment. The notable parameters including selectivity of inappropriate drugs/cycles, multi drug resistance, heterogenous biological factors for cancer etc. Moreover, there are many other parameters associated with the drug itself including poor solubility at physiological pH, targeting of the drug to the site etc. Because of these factors, the present treatment strategy with anticancer drugs require high dosage which can exhibit multitude of adverse events including nausea and vomiting, pain in muscle, hair loss, headaches, diarrhoea, appetite loss, throat scores, etc. resulting in lower patient compliance (Minchinton, and Tannock, 2006). Further most of the anticancer drugs are insoluble or have lower solubility in aqueous medium therefore for solubilization of the drug, various toxic chemical substances are in use which often exhibits several adverse events hence increase the morbidity and mortality rate (Feng, and Chien, 2003; Torchilin, 2004).

Though there are improvements in the conventional chemotherapy, still there is dearth in satisfactory performances and requires further improvisation of the same. The major concern persists with the conventional chemotherapy related to the pharmacological and physicochemical properties of the drug molecule. Anticancer medications delivered directly do not have the best therapeutic efficacy owing to several problems,

including low absorption, enzymatic degradation, adverse drug reactions due to high dosage, and systemic toxicity due to local accumulation [Saha et al., 2016]. Further higher dosage of a drug is required in case of short plasma half-life which further leads to nonspecific toxicities to the proliferating cells. Therefore, it is of prior importance to choose an efficient and safe delivery system of anticancer drug. Therefore, nanoparticle mediated drug delivery is an important choice as it allows a controlled release of the moiety to the target site thereby reduced accumulation of drugs in the body that results in reduced toxic side effects and dosage frequency. When compared to typical bare pharmaceuticals, the employment of suitable nanoparticles (e.g., biocompatible and biodegradable) in drug delivery applications is a significant topic because of their small size, enhanced solubility which is expected to display maximal performance. Nano drug delivery is one of the most challenging approaches towards the treatment of many diseases including cancer that helps to overcome several conventional drug delivery related drawbacks. As a result, in recent years, several nanoparticles, including as polymeric, liposomes, metal oxide, composites, and ceramics, have been extensively explored for the above-mentioned use (Hassan et al., 2020).

Pharmacokinetic properties of the nanoparticles are largely dependent on the matrix system. Furthermore, the size of the matrix carrier should be more than 100 nm as to prevent the opsonisation of the surface that leads to phagocytic uptake by liver (Maeda et al., 2003). Further several studies have demonstrated that owing to the increased permeability and the retention effect of the nanoparticular drug delivery system, it becomes the most significant choice of treatment in cancer chemotherapy (Moghimi et al., 2001).

As the nanoparticle-based drug delivery is gaining popularity among the formulation scientists, both small and large drug molecules are under investigation for the treatment

of cancer which has a significant potential to revolutionize the landscape of biopharmaceutical field.

1.1 Nanoparticle-based drug delivery system and its advantages

Nanoparticles can be defined as colloidal particle in submicron size range (10-1000 nm) that are widely used in drug delivery system (Wagner et al., 2006). There are different types of nanoparticles are in use including biodegradable polymeric nanoparticle, nanoliposome, micelle, gold nanoparticles, dendrimers, carbon nanotubes, magnetic nanoparticles, quantum dots etc (Moses et al., 2003). The drugs are incorporated, surface adsorbed or intercalated into the nanoparticle that exhibits a sustained release action thereby modifying the pharmacokinetics of the entrapped molecule resulting in optimum therapeutic efficacy with null or less toxicity compared to the conventional dosage form (Ferrari, 2005). There are many advantages of the nanoparticle-based drug delivery formulations over the conventional one (De- Jaeghere et al., 1999). This includes:

a.) During the transportation of the drug molecule to its site of action in a controlled/ sustained manner alters the pharmacokinetic property of the drug in term of biological half life of the drug, biodistribution, renal clearance so as to achieve the maximum therapeutic efficacy with low toxicity owing to less chances of accumulation of the drug in the body (Brigger et al., 2002; Couvreur et al., 1995).

b.) It can improve the bioavailability of the drug molecule by enhancing aqueous solubility of the hydrophobic drug for administration through intravenous route (Linhardt, 1989).

c.) Nanocarrier can also act as the safeguard of various sophisticated biomolecules including proteins or DNA, RNA from the environmental damage (e.g., pH, temperature, enzymatic degradation etc) thereby enhancing the physico-chemical stability of the biomolecule (Haixiong, and Ge, 2002).

d.) Nanoparticles helps in cellular entry of the biomolecule by phagocytic or endocytosis pathway (Haixiong, and Ge, 2002).

e.) Efficient delivery of the optimum drug concentration leads to reduce the dosage frequency of the same thus improves patient compliance (Guzman et al., 1996).

f.) Due to the high surface area to volume ratio its conjugation with targeting ligands allows the nanoparticle for active targeting for the encapsulated biomolecule thereby enhancing the bioavailability in a great extent without destroying the healthy cells (Lockman et al., 2002).

g.) Drug leakage is also reduced owing to the reduction in mobility of the encapsulated biomolecule.

h.) This delivery system is perfectly suitable for different route of administration including oral, nasal, intraocular and parenteral etc.

All of the aforementioned factors may contribute to the nanoparticulate drug delivery system becoming the pharmaceutical industry's fastest-growing field. Furthermore, clinical trials have shown that nanoparticles are effective in identifying and treating a wide range of disorders, including cancer.

1.2 Different nanoparticle-based delivery systems

A myriad of nanoparticles is currently in use for the diagnostic/ medicine purpose significantly in case of various diseases including cancer. Among them various polymer-based nanoparticle (micelles or dendrimers), different liposomal formulation, viral nanoparticles, inorganic nanoparticle (carbon nanotubes), gold nanoshells, magnetic nanoparticles, quantum dots, dendrimers, micelles etc. (Cho et al., 2008). Of these, polymeric nanoparticles have attracted much attention in pharmaceutical application owing to their biocompatibility and biodegradability. In this regard, many polymers are in use including e.g., poly (lactic-co-glycolic acid) (PLGA), poly (epsilon caprolactone) (PCL), polyglycolic acid, polylactic acid, poly(methylmethacrylate), poly(alkylcyanoacrylate), poly(butyl)cyanoacrylate and various natural polymers including poly (amino acids), albumin, hyaluronic acid, gelatin polysaccharides, dextran, proteins, polypeptides, and chitosan etc. Biodegradable polymer PLA and PLGA have been approved by US FDA for use (Cho et al.., 2008). This polymer matrix helps preventing drug degradation by various physicochemical factors and further modifying the drug release kinetics based on the preparation of the nanoparticle thereby effectively controlling the pharmacokinetic parameters of the same (Salla et al., 2021)

Even though drug delivery systems are mostly polymer based, in recent past there was a constant search for an alternate low cost with similar potential material having good biocompatibility which has led to use of ceramic nanoparticle as a drug delivery vehicle (Yang et al., 2010). The ceramic nanoparticles have many advantages including the ease of administration, low/null nontoxicity and highly penetrable to the mucus barrier as has been detected by different in vitro/in vivo experiments. With its extraordinary physicochemical properties including tailor

made structure, size, surface structure and modification, low cost and good biocompatibility makes this ceramic material an emerging platform in the field of drug delivery by means of transportation of the biomolecule to the target site and maintaining the release properties in a controlled manner at par with the available polymer-based nanoparticles with a lesser cost (Hnatyszyn et al., 1994). In the year 1980 the first ceramic nanocarrier was introduced and that was based on aluminium calcium phosphorous oxide (ALCAP) ceramic capsules (Bajpai and Graves, 1980). In continuation to the same later various research studies have been done based on the delivery of the different drugs including anticancer, antibiotic, steroids etc.

Other ceramic nanoparticles include calcium phosphate hollow apatite nanospheres (Cai et al., 2007, 2008), iron oxide nanoparticles (Nawroth et al., 2004), nanocomposites (Shen et al., 2004), titania nanotubes (Yao and Webster), silica nanoparticles (Roy et al., 2003; Bechet et al., 2008, 2009), apatite nanocrystals (Dai and Shivkumar, 2008), calcium carbonate hollow spheres (Cai et al., 2008), alumina hollow nanoshells (Wang and Tseng, 2009), etc. have also been explored.

In this regard, layered double hydroxide (LDHs), a type of ceramic material (anion exchanger clay substance), has long been utilised as a catalyst, ceramic precursor, and additive for polymers, among other things. Although the nanoscale production of materials has opened up a new arena in the field of drug/gene delivery with applications in nanomedicine (Choy et al., 2007). Moreover, their intrinsic extraordinary features including pH dependant degradability, high swelling propery, ease of surface functionization, tailor made anion exchange capacity and chemical inertness, it can be used as an excellent carrier of drug/biomolecule, genes, small interfering RNA (siRNA)/ other small molecules (Figure. 1.1) and thereby the controlled release property of the material makes it a suitable alternative to

polymeric nanoparticle in the field of drug delivery (Kriven et al., 2004; Choi et al., 2009).

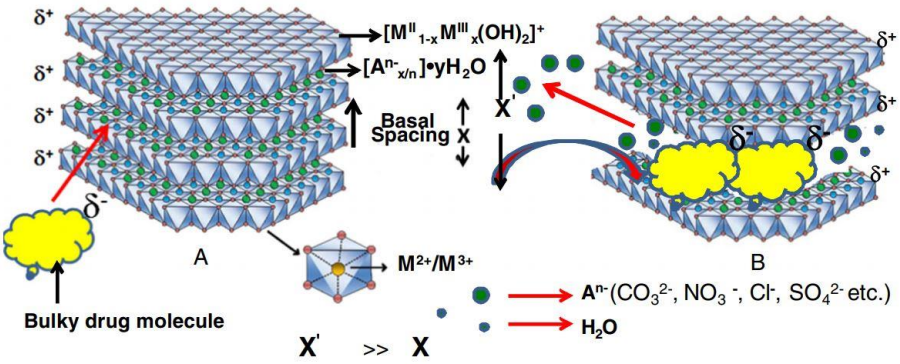

Figure. 1.1 Ion exchange allows the molecule to be inserted into the interlayer/interlamellar space of the bilayer via cationic layers of LDH (Saha et al., Appl. Clay Sci. 2016)

An anionic layered mineral (LDH) is composed of charge-balancing hydrated gallery anions and charged metal hydroxide layers. $[M^{II}_{1-x}M^{III}_{x}(OH)_2]^{+}[A^{n-}_{x/n}]\bullet yH_2O$, in which M^{II} denotes bivalent metal ions such as Mg, Ca, Zn, Ni, Cu, Co, and M^{III} denotes trivalent metal ions such as Al, Cr, Fe, Ga, and so on. The ions are able to occupy octahedral core of brucite layers, e.g., M^{II}-O- M^{III}-OH, that forms positive layers which exhibits strong interaction between the layers and the electro neutrality of the structure is maintained by the presence of hydrated exchangeable anions. CO_3^{2-}, NO_3^{-}, Cl^{-}, SO_4^{2-} etc (Figure 1.1), and x= molar ratio of M^{II}/ (M^{II}+M^{III}) comes within the range of 0.25 - 0.33, yields LDH structure (either 2:1 or a 3:1) respectively. Moreover, function of the anion is denoted by y and the x/n term achieves charge neutrality throughout the LDH structure (Chakraborty et al., 2013).

Table 1: Different drugs that are intercalated in various LDH nanoparticles (MgAl/ZnAl and CaAl-LDHs) (Saha et al., 2016)

MgAl-LDH in drug delivery

Category	Method of preparation	Important findings	Reference
NSAIDs	Co-precipitation	Loading was 30.8% (w/w), stability increased upto 6 times,	Alcantara et al. 2010
Anti inflammatory	Ion exchange	Particle size is around 60 nm, Optimum release of drug takes 2h	Li et al. 2004
Antiarthritic	Co-precipitation	Loading was 45% of Ibuprofen and 25% of glucoronate, thermal stability increased.	Ay et al. (2009)
NSAIDs	Co-precipitation	Loading was 50% (w/w) and stability was good.	Ambrogi et al. 2001
Anticancer agent	Co-precipitation	lower paricle size of 10-100 nm at pH 9 and loading was 33.2% at pH 11, l	Chakraborty et al. 2012
Anticancer agent	Co-precipitation	Particle size in the range of 50–800 nm which showed moderate stability and sustained release upto 190 h	Chakraborty et al. 2013b
Anticancer agent	Anion exchange and soft hydrothermal	Anion exchange is better than soft hydro-thermal in drug delivery	Chakraborty et al. 2010a,b

Anticancer agent	Direct co-precipitation and hydrothermal	Good stability and particle size is about 100 nm, excellent targeting in cervical cancer	Choi et al. 2016
Anticancer agent	Ion exchange	Loading is lower about 9.6% and Particle size is about 50-150 nm	Chen et al. 2014
Bactericides	Ion exchange, coprecipitation and reconstruction methods	Particle size is similar for Hexaconazole-LDHs by three method but in Triadimenol-LDHs particle size is higher in co-precipitation method which is about 260 nm compared to others	Zhenlan et al. (2009)
Anticancer agent	Co-precipitation	Drug accumulation in tissues and favourable blood clearance noticed	Choi et al. 2010
Antibiotic	Co-precipitation	high solubility and loading was 19%,	Khan et al. 2015
Anticancer agent	Co-precipitation	Particle size is about 127 nm, LDH nanoparticles are internalized via clathrin-mediated endocytosis.	Oh et al. 2006a

NSIDs	Co-precipitation	Hydrothermally prepared drug LDH nanoconjugate having larger particle size (194–332 nm) than without hydrothermal treatment	Gu et al. 2014
Anticancer agent	Co-precipitation	Size range should be 100-200 nm, did not exhibit any toxicity.	Choi et al. 2009
NSIDs	Co-precipitation	Slower release, half life and biodistribution are significantly increased.	Dong et al. 2013
Antibiotic	Coating	Effective drug against Ps. Aeruginosa	Hesse et al. 2013
Anticoagulant	Co-precipitation	Lower crystallinity and reduced particle size, drug release upto 108 h.,	Gu et al. 2008
NSAIDs	coprecipitation	lower density and less aggregation	Gunawan et al. 2009
NSAIDs	Hydrothermal and co-precipitation	150–530 nm particle size and release rate is sequentially reduced with	Huang et al. 2010

		increasing particle sizes		
ZnAl-LDH in drug delivery				
Citric acid, Salicylic acid,	Anti-acne, anti-aging and anti-wrinkle	Co-precipitation	Particle size is about 100 nm,	Hwang et al. (2001)
Naproxen	NSAIDs	Ion exchange	Uptake of is appropriate in the pH range of 6-11.5 and uptake is small at above pH 11.	Hou et al. (2007)
5-fluorouracil	Anticancer	Ion exchange	drug was released faster at alkaline pH compared to acidic pH	Jin et al. 2010
Levodopa	Dopamine precursor	Ion exchange	Acute toxicity of levodopa loaded LDH is 2000 mg/kg	Kura al. 2015
Hippuric acid	Antibiotic	Direct reaction	Loading was about 38.7% (w/w) and synergistic action with tamoxifen.	Ali et al. 2011
Perindopril erbumine	Antihypertensive	Co-precipitation and ion exchange	Release is slower in co-precipitation method compared to ion exchange.	Hussein et al. 2012
Cetirizine HCl	Antihistaminics	Direct reaction	Loading was 49.4% (w/w).	Ali et al. 2012

Sodium Dodecyl Sulfate	Emulsifying agent	Co-precipitation	Crystallinity increases with amount of drug increased	Babakhani et al. 2014
Chlorogenic acid	Anticancer agent	Ion-exchange and co-precipitation	Loading was 43.2% by ion exchange method, release rate at pH 7.4 is markedly lower than pH 4.8	Barahuie et al. 2014
Diclofenac	NSAIDs	Co-precipitation	C_{max} and AUC increased by 5.3 and 6.0 fold.	Cao et al. 2011
ascorbic acid and topopherol acid succinate	Vitamin	Ion exchange or Co-precipitation	Safe maintenance of bioactivities without having deterioration of chemical and structural properties	Choi et al. 2004
Methotrexate	Anticancer agent	anion exchange	Loading: 34.50 %.Particle size ranging from 100-300 nm,	Chakraborty et al. 2011b
CaAl-LDH in drug delivery				
Vitamin C	Vitamin	Co-precipitation	Loading: 36.4 %, thermal stability enhanced,	Gao et al. 2014
-	Calcium supplement	Co-precipitation	Eudragit coating preserves the molecule from hostile acidic environment	Kim et al. 2014
Methotrexate	Anticancer	Anion Exchange	Loading of 53.3 wt% was observed	Chakraborty et al., 2016

1.3 Lung Cancer and treatment options

Lung carcinoma is a malignant lung tumour marked by uncontrollable cell proliferation in the lungs. By metastasizing into neighbouring tissue or other sections of the body, this abnormal tissue growth might expand beyond the lung (Cooper GM et al., 2000). Most malignancies begin in the lungs, which are referred to as primary lung cancers. The two types of lung cancer that have been identified are small-cell lung carcinoma (SCLC) and non-small-cell lung carcinoma (NSCLC). Coughing (including coughing up blood), shortness of breath, normal weight loss, and chest pains are the most prevalent symptoms of lung cancer (Cooper GM et al., 2000). People who have never smoked account for roughly 10–15 percent of instances. Chest radiography and computed tomography (CT) scans can both be used to diagnose lung cancer. A biopsy, which is commonly conducted under bronchoscopy or CT guidance, is also used as a confirmatory test for lung carcinoma (Manhire et al., 2003). Although various therapeutic options for lung cancer exist, such as surgery, radiation therapy, chemotherapy, targeted therapy, and immunotherapy, the majority of them lack specificity and hence fail (Maeda et al., 2018).

1.4 Drug encapsulated nanoparticular delivery system-drawbacks

Although various methods are adapted to formulate different anticancer drug encapsulated nanoparticles, these have few drawbacks too. There are many class III toxic organic substances are in use for the synthesis of the nanoparticle which has some adverse effect in the body. Further there is variability in the encapsulation efficiency of the nanoparticle-based drug delivery system which further modify the initial burst release that significantly affect the pharmacological action of the drug. Moreover, particle size, high surface energy often leads to particle aggregation that

ultimately results in accumulation/ retention of the particle *in vivo*. (O'Donnell et al., 1997; Ruan et al., 2002).

1.5 Brief description of the drug under discussion

Etoposide

Trade names: Toposar®, Etopophos® VePesid®,

Other name: VP-16, Etoposide phosphate

Mechanism of action:

Etoposide is an anticancer drug under the categories of "topoisomerase II inhibitor." The topoisomerase II enzyme (which participates in DNA unwinding) prevents the strands of DNA from re-ligating, resulting in strand breaking.

Use:

The drug etoposide is used in many cancers apart from non small cell lung carcinoma including testicular, bladder, prostate, Hodgkin's and non-Hodgkin's lymphoma etc.

Side effects:

Side effects of ETO includes low lymphocyte count that enhances the chance of infection and low platelet count that yields to high clotting time. Many other side effects of etoposide include alopecia, chemotherapy-induced menopause, infertility, nausea and vomiting, hypotension and so on.

Physicochemical Properties

Molecular formula: $C_{29}H_{32}O_{13}$

Molecular mass: 588.55658 g/mol

Description: White to yellow-brown, crystalline powder.

Solubility: Etoposide is poorly water soluble but soluble in organic solvents such as ethanol, methanol and DMSO to different extents.

Dose: 35 mg/m^2 i.v. once a day for 4 days to 50 mg/m^2 i.v. once a day for 5 days in combination with platinium derivatives.

Chapter 2

Literature Survey

2. Literature survey

2.1 FDA approved nanoparticles in cancer therapy.

In recent times nanoparticle-based drug delivery systems are of utmost important in the field of drug delivery. Recently numerous numbers of nanoparticle-based drug delivery have been under different phases of Clinical trials and some of them are approved by Food and Drug Administration (FDA). Out of which, apart from other diseases there are few formulations currently approved by FDA owing to the high advantageous properties with respect to the conventional formulations. In the year 1995 the first anticancer formulation of doxorubicin was approved, which was based on pegylated liposome that has been indicated for different types of cancer including ovarian carcinoma or Kaposi's sarcoma (Park, 2002; Gordon et al., 2000; Gordon et al., 2001; Pillai, 2014). In this formulation doxorubicin was incorporated into unilamellar liposome having in the size range of 80-90 nm coated with PEG which helps the nanoparticles to stay for a long time in the blood stream that results in increase in therapeutic efficacy of the dosage form by reaching more amount of drug to the target cancer cells (Working et al., 1994; Park, 2002). Further another PEGylated liposomal doxorubicin citrate formulation was approved by different regulatory bodies by the brand name of 'Myocet' which is indicated in the treatment of metastatic carcinoma of breast (Swenson et al., 2003; Leonard et al., 2009). Moreover, daunorubicin which is an anthracycline derivative of antibiotic and antineoplastic drug has been approved by FDA in the year 1996 for the treatment of Kaposi's sarcoma associated with HIV (Lowis et al., 2006; Gill et al., 1995). In 2005, Abraxane was introduced in the market after obtaining approval from FDA in the treatment of NSCLC. Further many research studies were conducted in pancreatic cancer and US FDA has granted the approval of Abraxane in 2013 for the treatment of advanced pancreatic carcinoma (Glill et al., 1995;

Guarneri et al., 2012; Desai et al., 2004). EndoTag® was approved by FDA in the year 2012 for the indication of breast cancer (Strathopoulos et al., 2012). Another very known anticancer alkaloid drug vincristine was approved by FDA in the form of a liposome injection in 2012 for the use in Philadelphia chromosome-negative acute lymphoblastic leukemia. In liposomal formulation the clearance of vincristine was low thus exhibit higher AUC and results in higher efficacy compared to bare drug (Sankaram, 2002; Shih-Hung et al., 2012). Further another liposomal formulation of the said drug was developed for the treatment of Non-Hodgkin‘s lymphoma (Shih-Hung et al., 2012). A sustained formulation containing liposome based cytarabine which was approved by FDA in 2007 for the use in lymphomatous meningitis. Depocyt is a sustained release liposomal formulation (Angst et al., 2006; Benesch et al., 2008). Owing to the unique properties including encapsulation efficiency of both hydrophilic and hydrophobic drugs, easy functionalization properties most of the marketed nano formulation are based on liposome (Strathopoulos, 2012; Lei et al., 2003, Angst et al., 2006; Dullaart, 2006).

2.2 Inorganic nanoparticle-based drug delivery

2.2.1 An overview

As mentioned earlier that most of the FDA approved formulations are liposome based whereas polymeric micelle formulations are either in clinical trial or in other phases of their research and development. Some polymeric nanoparticles have been suffered from leakage of drugs under the severe environmental stressed condition resulting in altered pharmacokinetic properties of the drug owing to the uncontrollable amount of drug release in vivo (kamaly et al., 2016). In recent times owing to development in the

nanotechnology field, various inorganic nanoparticles including ceramic nanoparticle have gotten a lot of attention.

Inorganic nanoparticles have many advantages including ease of synthesis technique, and the size, shape and morphology could be controlled during the fabrication process of the nanoparticles (Yang et al., 2003; Goldberg et al., 2007). Moreover, owing to the optical or magnetic properties, various nanoparticles are currently in use in the field of bioimaging as well (Lei et al., 2003). Further in comparison with the organic nanoparticles, inorganic ones are resistant to growth of microorganisms, devoid of pH dependent swelling properties and relative stability in physiological pH (Yang et al., 2003; Bechet et al., 2008). A plethora of metals/oxides based inorganic nanoparticles have been explored in last few years. These materials are of varying size, shape, difference in porosity and surface composition thereby protecting the drug molecule from hazardous physiological conditions in vivo. Though inorganic nanoparticles are comparatively in stable form w.r.t different temperature and pH of the medium, the biogedradation property often arises some concern related to safety issue especially using the nanoparticle for a prolonged period of time.

In recent times a wide range of ceramic nanoparticles including apatite nanocrystals (Dai and Shivkumar, 2008), calcium phosphate hollow apatite nanospheres and nanocomposites (Shen et al., 2004, Cai et al., 2007, 2008,), iron oxide nanoparticles (Nawroth et al., 2004), silica (Bechet et al., 2008, Roy et al., 2003), alumina nanoshells (Wang and Tseng, 2009), titania nanotubes (Yao and Webster, 2009) and calcium carbonate hollow spheres (Cai et al., 2008) etc. have been explored widely for their advantageous properties in the field of drug delivery.

2..2.2. Layered double hydroxides (LDHs)

In this regard, for the last few years a special class of metal hydroxides, clay material layered double hydroxide (LDHs), were known for the application in the field of catalyst, additives for polymers, ceramic precursor, etc. Further the nanoscale LDHs have gained attraction as a novel material for the potential use in drug delivery and gene delivery which has opened a new area in the field of nanodelivery system (Choy et al., 2007). Moreover, the extraordinary intrinsic feature of the nanomaterial along with pH dependant biodegradability, high resorption ability, improved swelling properties, tailor made synthesis characteristics, unique surface properties and inertness makes it an excellent vehicle for transportation of the biomolecules including drugs, siRNA, genes etc into the systemic circulation along with controlled release of the same (Kriven et al., 2004; Choi et al., 2009). Clay products containing calcium carbonate have been employed in the treatment of gastrointestinal problems for many years (Mahaney et al., 1996;; Carretero, 2002, Viseras and Lopez-Galindo, 1999). LDHs are an anionic ceramic/clay material made up of charged metal hydroxide layers and charge-balancing gallery anions that keep the charge balance between the layers balanced.

2.2.3. Structure of the LDH

LDH typically represents by general formula $[MII_{1-x}MIII_x(OH)_2]^{+}[An_{-x/n}]\cdot yH_2O$, where MII stands for the bivalent metal ions including Ca, Zn, Mg, Ni, Co, Cu, and MIII represents trivalent metal ions including Fe, Al, Cr, Ga, etc. These metal ions can inhabit the octahedral core of a brucite structure, such as MII-O-MIII-OH, which is made up of positively charged layers, resulting in strong electrostatic interactions and a high planar charge density. (Figure 2.1). Therefore, the presence of exchangeable anions (A^{n-}) make this structure electroneutral. The typical anions present in the

structure would be carbonate (CO_3^{2-}), Nitrate (NO_3^-), chloride (Cl^-), sulphate (SO_4^{2-}) etc. Further x = molar ratio of MII/(MII + MIII) that typically comes in between 0.25 $\leq x \leq 0.33$ which ultimately results in LDH (2:1 or 3:1), respectively. Furthermore, y is a function of the anion present in the structure, and the values for the anion (A) are determined by its charge in relation to the amount of trivalent anion present, resulting in x/n reaching charge neutrality throughout the LDH structure (Palmer et al., 2009). Herein the mobility of interchangeability of the anion determines the anion exchange behaviour of the LDH nanoparticle. (Choy et al., 1999; Xu et al., 2006a, 2006b).

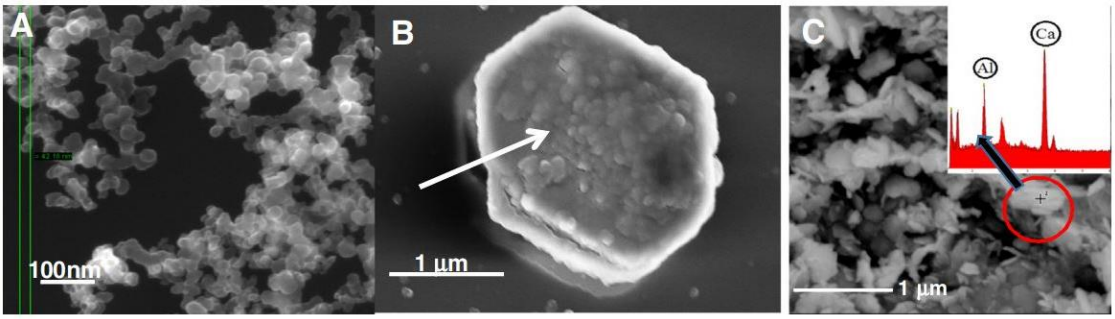

Figure 2.1. Images of (A) Magnesium Aluminium LDH (MgAl-LDH) (B) Calcium Aluminium LDH (CaAl-LDH), demonstrating nanoparticles deposited on a massive calcium carbonate ($CaCO_3$) crystal generated during the precipitation process, and (C) Energy Dispersive X-ray Spectrometry (EDX) reveals elemental composition (indicated by circle).

LDH can be synthesized via aqueous coprecipitation route at ambient temperature under the influence of constant flow of nitrogen and argon (Choi and Choy, 2011a, Oh et al., 2006a, 2006b). During last few years various structure of LDH including powder, sphere, belt, fibrous structure has been studied (Xu et al., 2006a, Gunawan and Xu, 2008, 2009; Du et al., 2009; He, 2008, Hu and O'Hare, 2005, Martínez-Ortiz et al., 2008, Gao et al., 2006; Choi et al., 2008). Surprisingly, flakes and rod-like crystals were

discovered in the ZnAl-LDH structure (Babakhani et al., 2014). Furthermore, utilising a soft template, sodium dodecyl sulphate (SDS), an anionic surfactant found in nature, a flower-like hierarchical structure of LDH comprising Mg and Al has been produced (Sun et al., 2016). Further, particle size and morphology of bare CaAl-LDH and polymer coated CaAl-LDH (Eudragit®L 100) were determined to be around 200-500 nm, with only minor morphological alterations in coated nanoparticle (LDH) (Kim et al., 2014b). Moreover 'cauliflower like' structure of LDH have been obtained by another group of researchers as well (Liu et al., 2006; Lü et al., 2008). The hexagonal structure of ZnAl-LDH was synthesised using the sol-gel technique, then heat treated for 30 minutes at 400 °C (Yamaguchi et al., 2006). Moreover, Colloidal MgAl-LDH drug delivery system has been developed by simple coprecipitation technique followed by controlled hydrothermal treatment. In this method, LDH having a size range of 50-300 nm have been synthesized in which there is agglomeration in the nanoparticle which further yields particle having a size range of 1-10 µm. In this method, LDH is generated as platelets with diameters ranging from 50 to 300 nm, as opposed to the traditional co-precipitation method, which produces aggregates with sizes ranging from 1 to 10 µm (Xu et al., 2006a). This technique of synthesis has also been used to other forms of LDH, such as bivalent transition metals like Fe^{2+}, Fe^{3+}, Ni^{2+}, and Gd^{3+}. Firecracker-like heterostructures of ZnAl-LDH has been synthesized that comprising ZnO nanorods standing in a order at the edges of 2D surface of ZnAl-LDH nanoparticle as well (Liu et al. 2006b). This phenomenon also leads to development of complex structures that is effectively achieved by changing the volume of $NH_3 \cdot H_2O$ (Liu et al., 2006b). By using decarbonated methanol, an engineered MgAl-LDH nanoparticles in the size range of 35–50 nm has been synthesized by simple coprecipitation technique

which ultimately leads to better stability of the nanoparticle (at least for a month) in aqueous suspension (Dong et al., 2014).

2.2.4. LDH preparation

Despite the availability of several approaches such as co-precipitation, ion exchange, urea hydrolysis, hydrothermal, sol-gel, or electrochemical procedures, the majority of LDHs such as MgAl, ZnAl, and CaAl-LDHs are successfully produced using coprecipitation techniques alone (Braterman et al., 2004; He et al., 2006; Barahuie et al., 2014b). In the synthesis technique, the experimental condition including temperature, concentration of the salts, pH of the medium, reactant's flow rate, aging time are the most vital parameters in the synthesis of LDH. The experimental procedures entail the formation of a metal hydroxide layer by combining bivalent and trivalent metal ions in aqueous medium in the presence of an alkaline medium containing a strong or weak base such as sodium hydroxide or ammonium hydroxide (Chakraborty et al., 2013a). It has been observed that the ideal pH of the LDH synthesis comes in between a pH condition of 7-11 and the solution temperature will be in the range of 25-75º C. Further it has been observed that the morphology of the nanoparticle could be obtained with high specific surface area at constant pH of the medium in comparison with the variable pH condition (Newman and Jones, 1998).

The synthesis reaction of a simple MgAl-LDH by coprecipitation technique is as follows:

$2Mg^{2+}+Al^{3+}+3OH^{-}\rightarrow Al(OH)_3\downarrow + 2Mg^{2+}$

$2Mg^{2+}+Al(OH)_3(s)+3OH^{-} \rightarrow [Al(OH)_4]^{-}$ (anionic complex) $+ 2OH^{-}+ 2Mg^{2+} \rightarrow [Mg_2Al(OH)_6]^{+}$

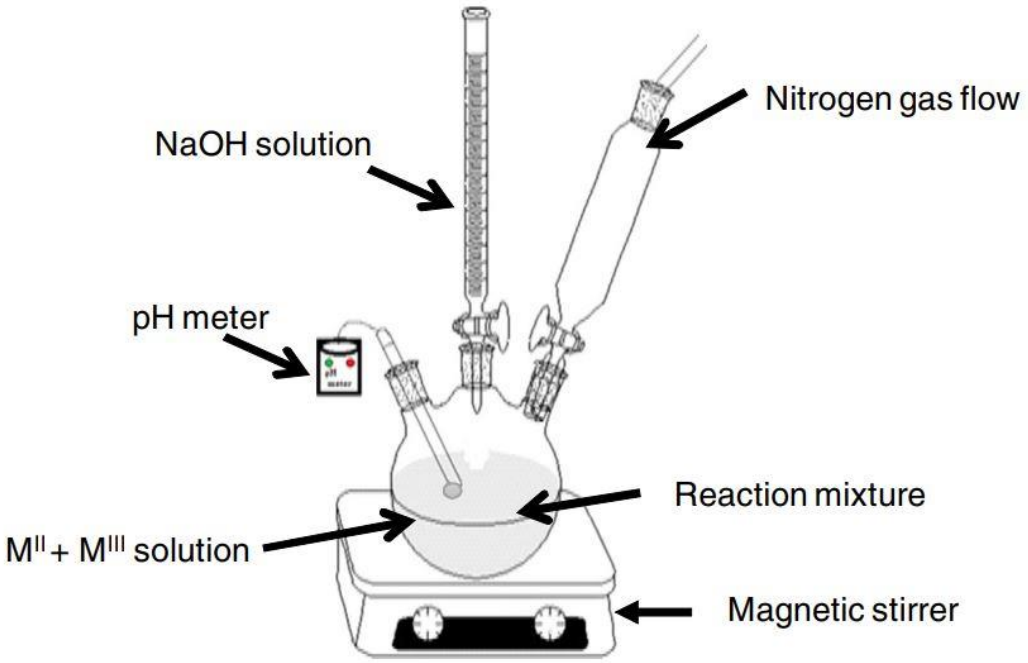

Figure. 2.2. Simple synthesis technique of LDHs by co precipitation method

During the synthesis of MgAl-LDH, aluminium hydroxide will precipitate from the less soluble aluminum salt while the magnesium ion remains in the solution (Eq. (1). Further addition of excess alkaline solution into the synthesis medium leads to formation of the anionic complex (Jeffery et al., 1980) (Eq. (2) that readily reacted to the magnesium which is in the solution. After aging of the solution leads to precipitation of MgAl-LDH nanoparticles and the water is separated out in the solution. Moreover, it is worth mentioning that a similar trend of formation of the nanoparticles have been observed in case of both Zn-Al and Ca-Al LDH, contemplating the solubility product (Ksp) in aqueous medium of hydroxide form of Ca or Zn respectively (Olfs et al., 2009). Further many research exhibits comparison between constant pH and variable pH condition during the synthesis procedure of LDH nanoparticles. It was observed that in case of both low and high super saturation, at constant pH condition co-precipitation reaction exhibits good crystallinity, smaller particle size and hydrodynamic diameters, in

comparison to those produced with variable pH. Further this method accurately controls the charge density of the bivalent and trivalent metal ions in the brucite layered structure. The value of x (molar ratio) of the two stands in between 0.25-0.33 in case of synthesis of phase pure LDH nanoparticle (M^{2+}/ (M^{2+} + M^{3+}) is in between 2-4 (Chakraborty et al., 2013b).

However, at a ratio of less than 2, there is a high chance of the density in the octahedral structure of the brucite layer which further leads to growth of the $M(OH)_3$ and at a density of more than 4 leads to form $M(OH)_2$ (Chakraborty et al., 2013b, Olfs et al., 2009;). Moreover, pH dependent stability of ZnAl containing LDH nanoparticles have been studied extensively with respect to MgAl-LDH nanoparticles as well.

2.2.5. Effects of synthesis techniques in drug incorporation

The impact of the LDH nanoparticle manufacturing method alters not just the material's crystallinity, but also the content of biomolecules (Braterman et al., 2004) that has been encapsulated in the interlayer space of the nanoparticle. Further it has been noted that hydrothermal technique of synthesis was found to have great influences on the physicochemical characteristics of the drug incorporated LDH nanoparticles (Gu et al., 2014). In this study, NSAIDs like ibuprofen (IBU) and diclofenac (DIC) have been incorporated into Mg-Al-LDH synthesized via coprecipitation technique followed by hydrothermal treatment at 150 °C, for 4 h or without the same. It was observed that the hydrothermal treated nanoparticles show better particle size and crystallinity, basal spacing of different planes which in turn maintains the interlayer structure of the nanoconjugate. (Gu et al., 2014). Moreover, it is further established that the synthesis condition including metal ion ratios, aging time and temperature of the medium significantly influence the crystallinity of the drug incorporated nanoconjugate

(Chakraborty et al., 2011b). Nanosized MgAl-LDH nanoparticles have been also obtained by dissolving the metal containing salts in the methanol in the presence of sodium hydroxide (NaOH) which further expanded to synthesis of LDH's having Al^{3+} in the structure (Gursky et al., 2006). Further varying the reaction conditions with aqueous ammonia/potassium hydroxide and varying the ratio of $Mg^{2+:}Al^{3+}$ at 2:1 and 5:1, MgAl-LDH nanoparticle has been synthesized and the structural and anion exchange properties have been verified with respect to the synthesis parameters. It was observed that 2:1 Mg:Al exhibited highest basal spacing of the crystalline structure whereas highest specific surface area (SSA) was obtained in case of the LDH synthesized at a ratio of 5:1. (Olfs et al., 2009). In another study comparison has been made between the synthesis techniques including MgAl oxides by co-precipitation and sol gel methods. In the case of the sol gel process, increased crystallinity was seen at a molar ratio of magnesium to aluminium in the range of 2 to 4, but a lower molar ratio of 0.15 denotes maximal modification in the physicochemical properties of the nanoparticles (Bolognini et al., 2003). Template directed synthesis of MgAl-LDH by urea hydrolysis method have been reported further under hydrothermal treatment condition (Li and He, 2008).

NO^{3-} and CO_3^{2-} comprising MgAl-LDH has been successfully synthesized by low supersaturation mnethod (Yun and Pinnavaia, 1995, Meyn et al., 1993). It was also observed that the hydration processes can result in the creation of bigger crystals, which is proportional to the media's temperature. (Klemkaite et al., 2011). Using a low supersaturation synthesis approach, a well-arranged crystalline material with irregular circular or hexagonal form in the region of 50-200 nm has been generated (Balcomb et al., 2015) Although the high supersaturation technology can also be employed to synthesise LDH nanoparticles utilising the co-precipitation method (Fornasari et al.,

1995). Further research revealed that the size, shape, and orientation of the biomolecule are the primary parameters that influence the LDH separation process, according to the intercalation chemistry of the nanoconjugate (Wang and Khan and O'Hare, 2002, O'Hare, 2012). It was further observed that the particle of the size range 100-200 nm exhibits highest efficiency in terms of delivery of the active therapeutics inside the structure following clarithrin- mediated endocytosis and after that release the biomolecule in a controlled manner which ultimately leads to better therapeutic efficacy of the nanoconjugate in vivo (Choi et al., 2008; Oh et al., 2006b; Chakraborty et al., 2011b). In another study CaAl-LDH has been successfully synthesized by varying the drying parameters and concluded that though the drying parameters in the synthesis process does not have any role in the influence of the basal spacing in the crystalline structure, they have a substantial impact on the particle size of the nanoparticle (Kim et al., 2014b).

It was further noticed that during the synthesis of CaAl-LDH, adding the NaOH can leads to precipitation of a small amount of $Ca(OH)_2$ (Tóth et al., 2014). Further research explored the impact of pre-milling rate, temperature, sonication to optimize the ideal synthesis procedure (Szabados et al., 2016). Like that the effect of various synthesis steps on different physicochemical properties have been studied by different groups. Herein, NO_3^{2-} comprising CaAl-LDH has been synthesized via simple coprecipitation route followed by hydrothermal treatment which resulted in particles in the size range of 2–8 μm, however stable homogeneous suspension was obtained. Furthermore, hydrothermal treatment improves particle size and crystallinity in this case. Furthermore, the sample is harmless in nature. (Shafiei et al., 2013).

2.2.6. Versatility of different bivalent metal containing (Ca, Zn and Mg,) LDHs as pools for biomolecule

Owing to the anion and the water molecules that are present in the interlayer structure of LDH nanosheet are labile in nature, many drugs/biomolecules can be incorporated into that space by simple anion exchange technique. Further it has been observed that the replacement of the drug molecule with the anions depends on several factors including the selectivity of the anion into the structure of the LDH nanoparticles. It must be mentioned that the ion selectivity is as follows as $I^- < NO_3^- < Br^- < Cl^- < OH^-$ whereas in case of the divalent anions, the sequence will be $SO_4^{2-} < CrO_4^{2-} < HAsO_4^{2-} < HPO_4^{2-} < CO_3^{2-}$. Moreover, due to the higher charge density, the selectivity is much higher in case of divalent anions in comparison with monovalent anions (Bish, 1980).

Asper the following reactions the anion exchange of the drug molecule into the LDH structure has been taken place.

$$LDH.\ Am^- + X^{n-} \rightarrow LDH.\ (X^{n-})_{m/n} + A^{m-} \text{ or } \ldots\ldots\ldots\ldots\ldots\ldots\ (1)$$

$$LDH.\ Am^- + X^n + mH^{+\ -} \rightarrow LDH.\ (X^{n-})_{m/n} + H_mA \ldots\ldots\ldots..\ldots.(2)$$

The monovalent anions in the precursor solution have a weak electrostatic affinity with the cationic brucite layer in the first step of the synthesis procedure. The precursor solution, on the other hand, contains anions (CO_3^{2-}) that are vulnerable to acid attack in the next phase. This phenomenon explores the anion exchange of the drug molecule with the interlayer anions (Bish, 1980). Although there are many research articles demonstrates the mechanism of the anion exchange technique and the kinetics, till date the explanations are not satisfactory. Further it is very troublesome to estimate the anion

in each individual cases as there are still scarcity is this area owing to unavailability of the reliable technique. In this scenario, most of the research group depends on the basal reflections of the nanoparticle and from that value computation has been made to identify the percentages of anion exchange in the layered structure. Due to this unique property, many charge balancing anions including succinate, or malate, carboxylate or pharmaceutical drugs including antibiotics, analgesics, anticancer and inorganic anions have been incorporated into the interlayer space of the LDH nanoparticle. In this technique, anion exchange capacity is highly dependent on the electrostatic interaction between the cationic nanosheet and anions that are going to be exchanged. Moreover, considering from the thermodynamics point of view, another important factor is the amount of free energy that are involved in the hydration changes. As evident the anion exchange capacity depends based on the electrochemical series.

$$NO_3^- < Br^- < Cl^- < F^- < OH^- < SO_4^{2-} < CrO_4^{2-} < HAsO_4^{2-} < HPO_4^{2-} < CO_3^{2-}$$

The most import factors that influence the anion exchange capacity in LDH structure are given below

a) The anion exchange capability of the incoming anions increases upon increasing the charge and decreasing the ionic radius of the molecule owing to the strong bond strength and increase in electrostatic attraction with the host layer of the nanosheet. Further insertion of a second molecule into the same structure does not have any effect in the anion exchange (Xu et al., 2010).

b) The swelling property and exchange behaviour of the LDH nanoparticle are favoured by the solvents used.

c) The arrangement of host layers significantly influences the anion exchange capacity and pH value of > 4, helps to preserve the hydroxyl layer of the LDH against any damages.

d) In general, high temperature helps in anion exchange process. In case of thermal decomposition, basicity of the LDH is enhanced owing to growth of metal oxides. This also allows for facile acidic anion intercalation, making the layered substance acidic or basic in nature. When pH will be at around 11, the bulky drug molecule can easily accommodate in the interlayer structure of the LDH owing to get more open space in basic condition accordingly (Li et al., 2006b). In one research study reconstitution technique has been taken into consideration for the intercalation of the antibiotic drug namely phenoxy methyl penicillin in the interlayer space of MgAl-LDH and the superiority has been observed against the conventional anion exchange method in drug delivery application (Li et al., 2006b). Moreover, various categories of drugs have been successfully intercalated in LDH and their controlled drug release behaviour has been explored too (Rives et al., 2014). Further the property of the exchangeable anion has its role in the intercalation into the layered structure. It has been observed that hydrophobic drugs need to be solubilized prior to insertion in the layered space whereas hydrophilic one can directly inserted into the interlayer space of the nanoparticle (Trikeriotis and Ghanotakis, 2007). Apart from earlier mentioned category, several antibiotic drugs, antibacterial, anti-inflammatory as well as antifibrinolytic drugs have been incorporated into LDH structure (Costantino et al., 2012, Wang and Zhang, 2012;). In terms of anticancer drugs including 5-fluorouracil (5-FU) (Wang et al., 2005), methotrexate (MTX) (Chakraborty et al., 2011b), etoposide and cisplation(Qin et al., 2013, Qin et al., 2010), have been intercalated into different metal containing LDHs for controlled release of the drug from the nanoconjugate. It has also been discovered that

the co-precipitation technique has a major impact on the drug molecule's functionality (Kim et al., 2007; Kim et al., 2014a, Chakraborty et al., 2012). Camptothecin, a quinolone group of alkaloids has been incorporated in an anionic micelle to impart negative charge that leads to charge constructed intercalation however direct insertion in the interlayer space of LDH has also reported (Tyner et al., 2004),

In another study hydrophobic anticancer drug has been intercalated into ZnAl-LDH via a 'secondary intercalation' technique that can protect the biomolecule (Pang et al., 2013). Moreover, to reduce the toxicity profile of 5-Fluorouracil (5-FU), it has been intercalated in MgAl-LDH via anion exchange technique. It was also observed that the delivery mechanism lowered immunogenicity and had a low integration capacity (Choi et al., 2010). Anion exchange was used to include Vitamer (Choy and Son, 2004b), where methotrexate and floxuridine (FUDR) were intercalated in Mg Al containing LDH via a straightforward co-precipitation approach (Xu et al., 2010; Chakraborty et al., 2010a, Xu et al., 2006a,).

Another set of researchers created surfactant modified ifosfamide (IFO), which was then anion exchanged into the interlayer area of MgAl-LDH (Nie and Hou, 2012). Co-precipitation was used to intercalate the anticancer medication podophyllotoxin (PPT), which was then anion exchanged in MgAl-LDH (Qin et al., 2010). Apart from anticancer drugs NSAIDs including DIC and IBU, naproxen was incorporated into MgAl-LDH (Ambrogi et al., 2001, Khan et al., 2001). Further in another work hypolipidemic drugs including Simvastatin and Fluvastatin were incorporated in MgAl-LDH by coprecipitation technique (Panda et al., 2009). Moreover, antifibrinolytic drug trans-4-(aminomethyl) cyclohexanecarboxylate (traexamic anion) was intercalated into the polymer (ε-polycaprolactone) encoated Mg-Al-LDH (Tammaro et al., 2009). Moreover, co-intercalation of IFO and SDS based surfactants were inserted into the

layered structure of MgAl-LDH by simple anion exchange technique (Nie and Hou, 2012). Further, angiotensin converting enzyme (ACE) inhibitor captopril (CPT) was intercalated in MgAl-LDH by co-precipitation technique (Zhang et al., 2006). Surprisingly, phospholipid bilayers covering lipophilic drugs were contained within the MgAl-LDH interlayer gap (Begu et al., 2009) Anion exchange and co-precipitation procedures have been used to intercalate numerous osteoporotic, anticoagulant, and antimycotic drugs in the same vehicle (Lee et al., 2005). Incorporation of SiO_2 (Bao et al.,2011) or organic functional groups altered the characteristics of the resulting drug-LDH nanohybrids (Alcantara et al., 2010; Miao et al., 2012).

MgAl-LDH has also been utilised to transfer genes into cortical neurons, including SiRNA, as a potential treatment technique for neurological disorders caused by single gene mutations, such as Huntington's disease (Wong et al., 2010).

Further ACE inhibitors including perindopril erbumine (PER) or chloramphenicol (CAM) have been intercalated into ZnAl-LDH, via simple co-precipitation and anion exchange technique (San Roman et al., 2012, Ali et al., 2012;). Many vitamin molecules including L-tyrosine and phenylalanine, have been inserted in to the ZnAl-LDH as well (Fudala et al., 1999a, 1999b, Hwang et al., 2001). Furthermore, rather than using a co-precipitation process in an inert atmosphere, the antibiotic molecule cefazolin (CFZ) was intercalated into ZnAl-LDH via an anion exchange technique (Ryu et al., 2010). An anion exchange approach was used to intercalate polyoxovanadate and 5-aminosalicylate ions into the structure of ZnAl-LDH at various pH levels. It was also discovered that increasing the pH of the reaction mixture resulted in the formation of vanadate ions (Barriga et al., 1998; Zou et al., 2007). Co-precipitation and anion exchange approaches have been used to intercalate enalapril (ENP), lisinopril (LIS), and other antihypertensive medicines in ZnAl-LDH (Xia et al., 2008). ZnAl-LDH

nanosheet was synthesized by a single step technique in room temperature followed by which hydrothermal treatment on sputtered substances (Scarpellini et al., 2014).

Aside from magnesium and zinc-based LDH, calcium-based LDH has also been found as a potential material. The rehydration of CaAl-LDH (Plank et al., 2006) via hydrothermal and organic-water solution routes (Dutta and Pramanik, 2013, Xu et al., 2011) has also been studied extensively. In this context, Lee et al. (2005) found that non-aqueous solvothermal media is a highly beneficial media for the anion exchange approach incorporating organic acid and maintaining the crystallinity of the structure at pH 7.4 (Lee et al., 2005). Another study recently reported intercalation of methotrexate (MTX) using a simple anion exchange approach, with the drug loading percent found to be 53.3 weight% (Saha et al., 2016)

2.2.7. Characterization of metal ion (MgAl, ZnAl and CaAl) containing LDHs

All the LDH molecules have been characterized structurally and compositionally by different sophisticated analytical techniques including X-ray diffraction (XRD), scanning electron microscopy (SEM), Fourier transform infrared spectroscopy (FTIR), dynamic light scattering (DLS), Thermogravimetry Analysis TG-DTA and carbon hydrogen nitrogen analysis (CHN) etc. (Plank et al., 2006; Choi et al., 2008). In a research study, citrate anion was incorporated into MgAl-LDH which was synthesized by simple coprecipitation followed by vacuum drying in one part and the other was treated hydrothermally. It has been noticed from basal reflections (00l) that citrate ion was intercalated into MgAl-LDH and a very well-organized lattice structure was observed in case of hydrothermally treated part that is having a d spacing of 12.0 Å and FTIR study exhibits an intense band at around 3410 cm^{-1} accredited to the presence of hydroxyl ions and water molecules attached to it. Whereas 2-thiophenecarboxylate

anions was incorporated into MgAl-LDH followed by hydrothermal treatment. It has been observed that there was not much variation in the crystalline lattice structure (d spacing) in the nanoparticle (Tronto et al., 2004). Upon heating at 500 °C for 4 h, the layered structure was destroyed thereby indicating the absence of the characteristic pattern in (003) and (006) reflections. Incorporating an anticancer medication, 5-fluorouracil (5-FU), into the MgAl-LDH results in an increase in basal spacing in XRD data, which varies with ageing time. Furthermore, at a wavelength of roughly 1300–1400 cm^{-1}, the FTIR pattern of the nanoparticle indicates total elimination of the nitrate peak that was detected in the naked LDH structure (Wang et al., 2005). Further, the folate antagonist drug methotrexate, as well as vitamins such as ascorbic acid and topopherol acid succinate, were successfully incorporated into the interlayer spaces of MgAl-LDH and ZnAl-LDH, with XRD and FTIR data indicating successful intercalation of the biomolecule in the aforementioned LDH (Choy et al., 2004a; Choy and Son, 2004b; Chakraborty et al., 2013a, 2013b). The basal spacing has been increased from 7.7 Å to 21.3 Å on insertion of the drug MTX into the interlayer space of ZnAl-LDH (Chakraborty et al., 2011b). Significant increase in the (003), (006) and (009) plane on insertion of the SDS in MgAl-LDH. The basal spacing at 003 plane was found to be 20 Å on insertion of SDS anion into it (Zhang et al., 2015). Further the basal spacing of MgAl-LDH was increased significantly from 7.9 Å upon intercalation of the drug molecule into the structure (Mallakpour et al., 2013a, b). Moreover, characteristic diffraction pattern of MgAl-LDH have been observed via a series of reflection in the XRD analysis at a 110 and 113 plane respectively (Zhang et al., 2008a, 2008b). Exfoliated ZnAl-LDH nanoparticles were effectively produced using an emulsion polymerization process, resulting in particles with a width of 50-70 nm and an overall thickness of 1 mm that could be easily disseminated in a polystyrene matrix

(Ding and Qu, 2005). However, ZnAl-LDH nanoparticles have been successfully synthesized via simple coprecipitation technique which yields a basal spacing of 7.69 Å. Further calcined at 450°C causes the layered structure to disintegrate and the oxide structure of ZnAl(O) to develop, which can be rehydrated with Cr (III) complex, resulting in a move of the peak position corresponds to (003) and (006), to a lower value (Sahu et al., 2012).

Lattice constant of the hexagonal structure at 110 plane was found to be 0.3081 nm and the molar ratio of the bivalent and trivalent metal ions was 4:1 (Salak et al., 2012, Newman et al., 2001). Another investigation found two separate peaks of ZnAl-LDH film after 15 minutes of immersion in hot water at 100 °C. The spacing was found to be 7.61 Å which corroborates the literature published earlier elsewhere on ZnAlLDH-CO_3^{2-} system (Yamaguchi et al., 2006). During the intercalation of methacrylic acid into the MgAl-LDH and ZnAl-LDH exhibiting an substantial increase in basal spacing from 8.8 Å to 13.3 Å for MgAl-LDH and from for ZnAl-LDH the spacing was increased from 8.7 Å to 13.8 Å respectively (Kovanda et al., 2009). It is further evident that incorporation of a macromolecule inside the layered structure leads to increase in basal spacing in MgAl-LDH/ZnAl-LDH (Roto and Tahir, 2007, Roto and Villemure, 2002,). When fluorophosphate was added to the ZnAl-LDH by a simple anion exchange technique, however, the crystallinity of the nanohybrid was found to be lower than that of the bare counterpart (Elkhattabi et al., 2012). On the other hand, Nshuti et al. reported that greater crystal size has been obtained during incorporation of Oleate into ZnAl and MgAl-LDHs (Nshuti et al., 2009) synthesised using co-precipitation method as in the case of CaAl-LDH, with a basal spacing of 7.87 (Tóth et al., 2014; Kim et al., 2014b). In a research study podophyllotoxin was successfully intercalated into MgAl-LDH-NO_3 and the particle size and a zeta value were found to be 80-90 nm and 20.3mV

respectively (Qin et al., 2010) whereas the same comprising Cl^- ion and CO_3^{2-} ion exhibits a zeta potential value of 41 mV and 34 mV respectively (Xu et al., 2008a) which indicates a good stability with less tendency of agglomeration. Fluorescein isothiocyanate (FITC) containing MgAl-LDH nanohybrid has been prepared, with a width of 50– 150 nm and a thickness of 10–20 nm respectively and on the other hand rod shaped particles have been prepared with a dimension of 30–60 nm and 100–200 nm respectively. It was detected that successful insertion has been achieved into different mammalian cells (Xu et al., 2008b). CaAl-LDH with particle sizes of 48.4 and 52.6 nm was also synthesised, though after coating in it, the size was reduced to 45.8 and 48.3 nm, respectively, owing to disintegration of nanoparticle during the coating process (Kim et al., 2014b). Moreover, there was deviation in the particle size in the size range of 65–105 nm exhibited by poly-butyl methacrylate containing ZnAl-LDH (Kovanda et al., 2009), whereas, after pamino benzoic acid insertion on the LDH, it exhibits a size in the range of 100– 200 nm, (Roto and Tahir, 2007). Furthermore, diclofenac has been introduced into the layered structure of MgAl-LDH using a hydrothermal technique, resulting in the size range of 194 to 332 nm versus the same without hydrothermally treated (Olfs et al., 2009). This phenomenon is attributed to the hydrothermal technique that results in agglomeration in between the LDH nanoparticles as well (Gu et al., 2014).

Nitrate containing CaAl-LDH was successfully synthesized via coprecipitation technique (Figure. 2.2.). Further hydrothermal treatment was used to adjust particle size in the lateral dimension, which was in the range of 10 nm–2.5 μm (Shafiei et al., 2013). Incidentally, the peak position was found to be at par about the coating and non-coating counterpart as well. The two unique phases (002) and (020) of the naked and its polymer coated counterpart were taken into consideration for estimating the crystallite size,

which was determined to be 48-57 nm, to estimate the crystallinity (Kim et al., 2014b). Because of intercalation of methotrexate drug into CaAl-LDH by anion exchange technique the basal spacing of the nanoconjugate increased significantly from 8.75 Å to 19.17 Å. Furthermore, the increase in MTX breakdown temperature from 290 to 380 degrees Celsius indicates that the nanoconjugate's thermal stability has improved (Chakraborty et al., 2016). Basal spacing of 9.8 Å demonstrates a perpendicular orientation of vitamin C in CaAl-LDH synthesized via simple co-precipitation technique and the drug loading was found to be 36.4 % (Gao et al., 2014). Further structural analysis of CaFe-LDH and CaAl-LDH revealed that calcium is heptacoordinated and the trivalent metal ion is hexacoordinated, as well as that the basal spacing was found to be 8.61 and 8.60, respectively (Kim et al., 2012). TGA also exhibits various valuable database for the bare LDH and drug conjugate nanoconjugate as well. Herein nitrate containing CaAl-LDH loses its 10% mass at around 280 °C due to loss of interlayer water molecule, 15% at 500 °C owing to dihydroxylation of inorganic layer and subsequent loss of 5% at 600 °C is due to destruction of the layered structure of the LDH (Plank et al., 2006). Moreover, TG and DSC studies of preheated (to 100 °C) E-coated and pristine CaAl-LDH exhibits a similar mechanism of mass loss although the reason differs significantly (Kim et al., 2014b). Further the thermal behaviour of the PE intercalated MgAl-LDH was analysed by TG-DTA. It has been observed that two main thermal events occurred in between 90 °C–192 °C. The sharp peak at around 157 °C is attributed to the softening of PE, with a 24.1% mass loss. Further the decomposition at in between 192 °C and 312 °C is owing to breakdown of PE, that corresponds to a sharp peak at around 276 °C with a mass loss of 81.2% (Ali et al., 2012). The thermal degradation profile of SDS intercalated MgAl-LDH has been studied extensively which reveals the mass loss at two remarkable steps which includes

desorption of the water molecules that are physically adsorbed on the surface of the nanoparticle, along with the removal of water molecule in the interlayer space. The dehydroxylation of the brucite layers and the loss of the interlayer SDS molecule are clearly visible in the later stage, with a mass loss of 48.5 percent (Venugopal and Rajamathi, 2011). FESEM images of LDH molecules significantly exhibits the proper structure and surface morphology and particle size. Herewith chiral PAI modified MgAl-LDH nanohybrids shows a plate like crystals that exhibit a size range of 20–50 nm (Mallakpour and Dinari, 2013a). A particle size of 100-300nm has been found in case of ZnAl-LDH nanohybrids and the XRD pattern exhibits an increase in basal spacing after insertion of the MTX into the interlayer space. Moreover, the result was corroborated by the TEM micrograph in which the basal spacing was increased from 8.9°A to 21.3°A. (Chakraborty et al., 2011a, 2011b). Further variation in particle size of MgAl-LDH nanoparticles has been observed while changes in the pH of the synthesis medium that in turn confirmed via XRD and SAED patterns (Chakraborty et al., 2011a, 2011b).

2.2.8. *In vitro* release study of drugs from nanocnjugates

Drug release characteristics refer to the process by which the drug molecule migrates from its original place in the delivery matrices to the outer surface before being released into the medium (Ray et al., 2015a, 2015b). This release process of a biomolecule depends on several intrinsic and extrinsic factors including physicochemical properties of the biomolecule/drug, the structural features of the device, pH of the medium and above all, interrelation between all the parameters (Fu and Kao, 2010). In terms of drug delivery from the nanoconjugate all the above-mentioned parameters have a significant role in the release kinetics. There is no variation in the release property between the hollow nanosphere and nanoplates of MgAl-LDH-IBU nanoparticle at a pH of 7 (Li

and He, 2008). Further numerous release mechanisms have been reported in case of ibuprofen (IBU) or flurbiprofen (FBP) in MgAl-LDH (Perioli et al., 2011, Huang et al., 2011;). Further intercalation of DIC into MgAl-LDH matrix exhibits that drug release profile was modified. In this case it was observed that the drug release from the nanoconjugate was significantly slower compared to the physical mixture of LDH and biomolecule. Moreover, the release analysis exhibits diffusion mechanism that controls the release of drug (Ambrogi et al., 2001). On contrary, at pH 7 almost 60% of the drug was released at once followed by a sustained release upto a period of 200 min respectively (Gunawan and Xu, 2009). In general, many factors are responsible for the release mechanism of the drug molecule from the nanoconjugate in general (Gou et al., 2013). In another study, fenbufen was released in a sustained manner from MgAl-LDH nanoconjugate at a pH of 7.8 (Li et al., 2004) whereas upon lowering the pH of the medium, no release was observed as such (del Arco et al., 2010; Rojas et al., 2012). The below correlation following level A (Figure. 2.3.) according to Drewe and Guitard (1993).

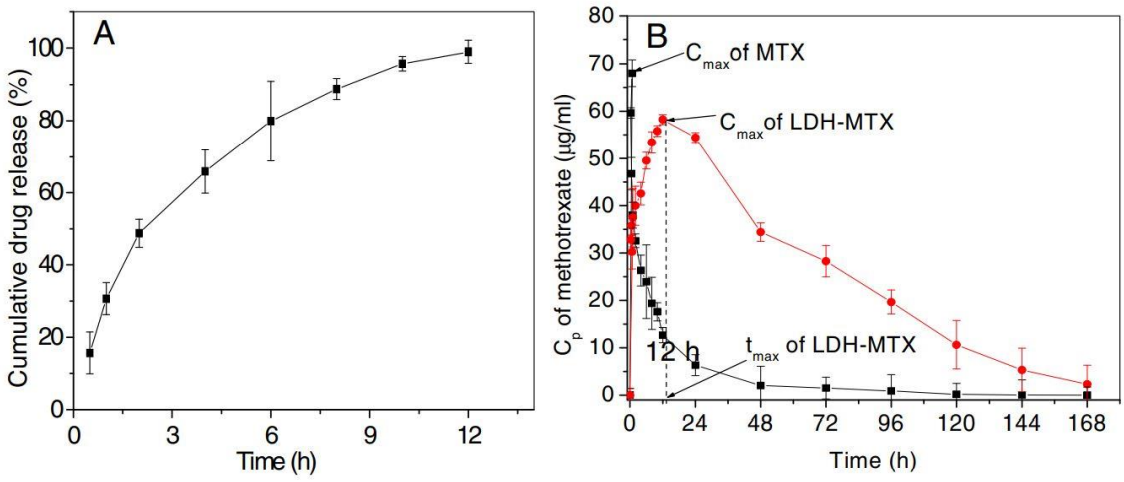

Figure. 2.3. In vitro MTX release profile from MgAl-LDH nanohybrid (B) after oral administration of MTX, the plasma drug concentration is shown.

Further ASA (acetyl salicylic acid) release from MgAl-LDH was studied at pH 7.5 in PBS solution, and it was discovered that the burst release of the ASA conjugated nanohybrid was higher within 4 minutes than the dextran coated counterpart, owing to delamination of the uncoated MgAl-LDH structure (Dong et al., 2013). Furthermore, at pH 7.4, the release pattern of fluvastatin and pravastatin from the MgAl-LDH nanohybrid is monophasic, but as the medium concentration changes, the release pattern changes as well (Panda et al., 2009). It was discovered that the particle size and the drug's release behaviour had a strong relationship. It is clear from this study that increasing particle size and crystallinity causes the drug release from the matrix system to be delayed (Gu et al., 2014). Anticoagulant low molecular weight heparin (LMWH) was released *in vitro* from a MgAl-LDH matrix that exhibits a progressive and biphasic release characteristic with an initial fast release followed by a slower release pattern (Gu et al., 2008). Anticancer drugs exhibit a prolonged release pattern upon insertion into LDH nanoparticles (Chakraborty et al. 2011a, 2011b). It has been observed that MTX was released via diffusion-controlled process from MgAl and ZnAl-LDH matrices at a pH 7.4 (Chakraborty et al., 2011a, 2011b; Ray et al., 2015a, 2015b). Electrostatic interaction between the NP anion and the LDH layer leads to changes in the release pattern of NP (Hou and Jin, 2007). It was further observed that the release of 5-FU was faster at a pH of 7.2 than 4.8 from carboxymethyl modified β cyclodextrin conjugated ZnAl-LDH matrix and follows Korsmeyer Peppas release kinetics (Jin et al., 2010). The greater aqueous solubility and dissolution rate could explain this phenomenon (Kavitha et al., 2013). Although the in-situ co-precipitation technique produced good crystallinity, the anion exchange technique produced a better in vitro release profile, confirming its superiority. In a study, the sustained release of MTX was

observed upto 60h from CaAl-LDH in pH 7.4 that suggests Koresmeyers and Peppas model of release kinetics (Chakraborty et al., 2016).

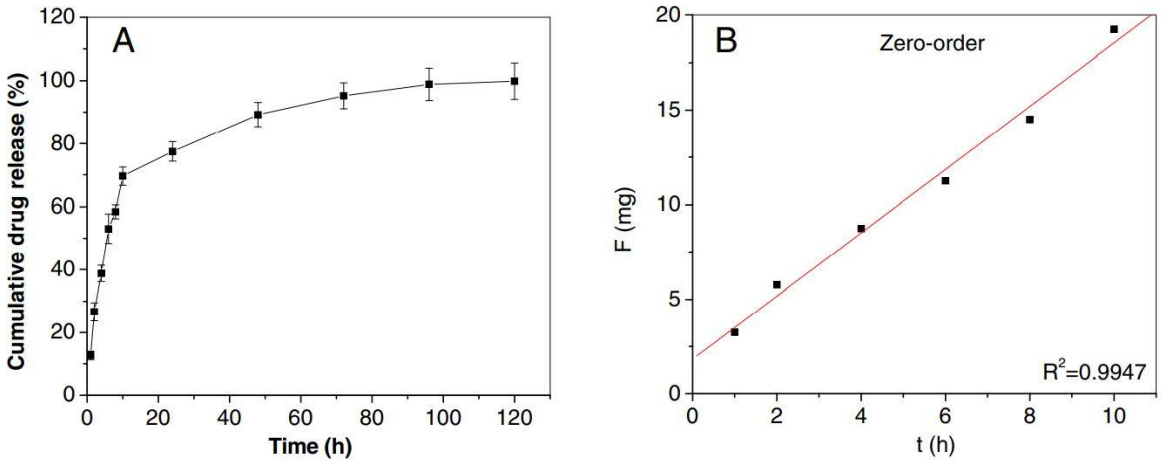

Figure. 2.4. The in vitro release profile of 5-FU from the nanohybrid and the fitting curve

2.2.9. Drug/biomolecule intercalated MgAl, ZnAl, or CaAl-LDH cellular absorption *in vitro*

Because of the clathrin-mediated endocytosis (Figure 2.5) mechanism, nanoparticle uptake is largely dependent on particle size in the 40–100 nm range (Dong et al., 2015).

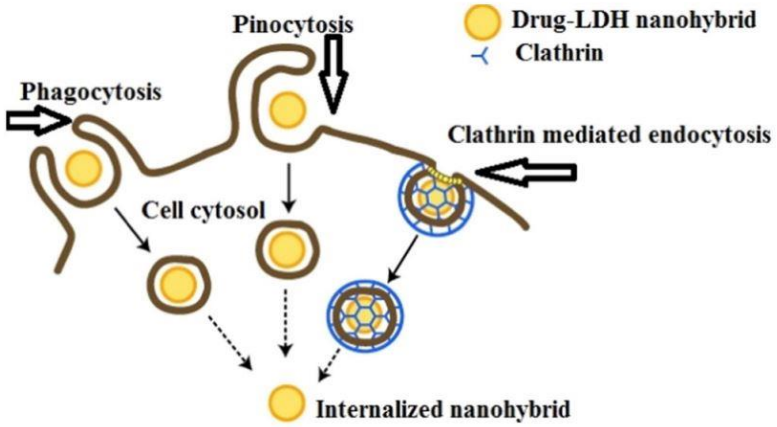

Figure. 2.5. Cellular uptake mechanism of drug-incorporated MgAl-LDH nanohybrid (Saha et al., 2016, Appl. Clay Sci)

In this regard, it is evident that successful insertion of the drug molecule with a particle size of 50-200nm to the cell is based on the concentration dependent manner while a particle size of 350 nm, does not show a concentration dependent uptake (Oh et al., 2006b). Herein, in vitro and in vivo cellular uptake study was further evaluated from the MgAl-LDH nanoparticle that provides a unique strategy to increase the biomolecular delivery efficiency to the cells (Choi and Choy, 2011a, 2011b). It has been further established that the cellular uptake of the drug molecule depends on the concentration of the nanoconjugate. The uptake of nanoparticles into the mouse motor neuron (NSC 34) cell line was determined in a concentration and size dependent manner, which was further confirmed by TEM and confocal microscopy, revealing that LDHs nanoparticles with particle sizes of 20 nm enter the nucleus and cytoplasm, whereas those with particle sizes greater than 20 nm can only be found in the cytoplasm (Li et al., 2013). Further it has been observed that the cellular uptake in case of MTX-LDH nanoconjugate was much higher compared to the bare drug which leads to a lower IC_{50} value for LDH-MTX nanoconjugate (Oh et al., 2006a, 2006b). Another study exhibits that ATP-MgAl-LDH nanohybrid has been successfully uptakes by eukaryotic cells based on incubation time. Further it was also found that after 2h of incubation, the cellular transport efficiency was found to be increase in around 25-folds (Nalawade et al., 2009). The successful uptake of low molecular weight heparin (LMWH) in MgAl-LDH nanohybrid was measured via flow cytometry and it was found that the uptake was almost ten times higher than the LMWH alone (Z. Gu et al., 2008). Further surface modification of a nanoconjugate showed a greater prospect in terms of cellular internalization of the same. Herein MgAl-LDH surface was successfully modified by folic acid (FA) which is a cancer cell specific ligand (Oh et al., 2006a, b; Oh et al., 2009). It was evident that the uptake of the ligand modified nanoparticle was much

higher compared to the bare nanoparticle. The internalisation of the biomolecule coupled LDH in human pancreatic cancer (BxPC3) cells, exhibits energy-dependent cellular uptake which was assessed using fluorescence tagging (Nagaraj et al., 2015). The below schematic representation exhibits the combinational treatment in drug targeting (**Figure 2.6).**

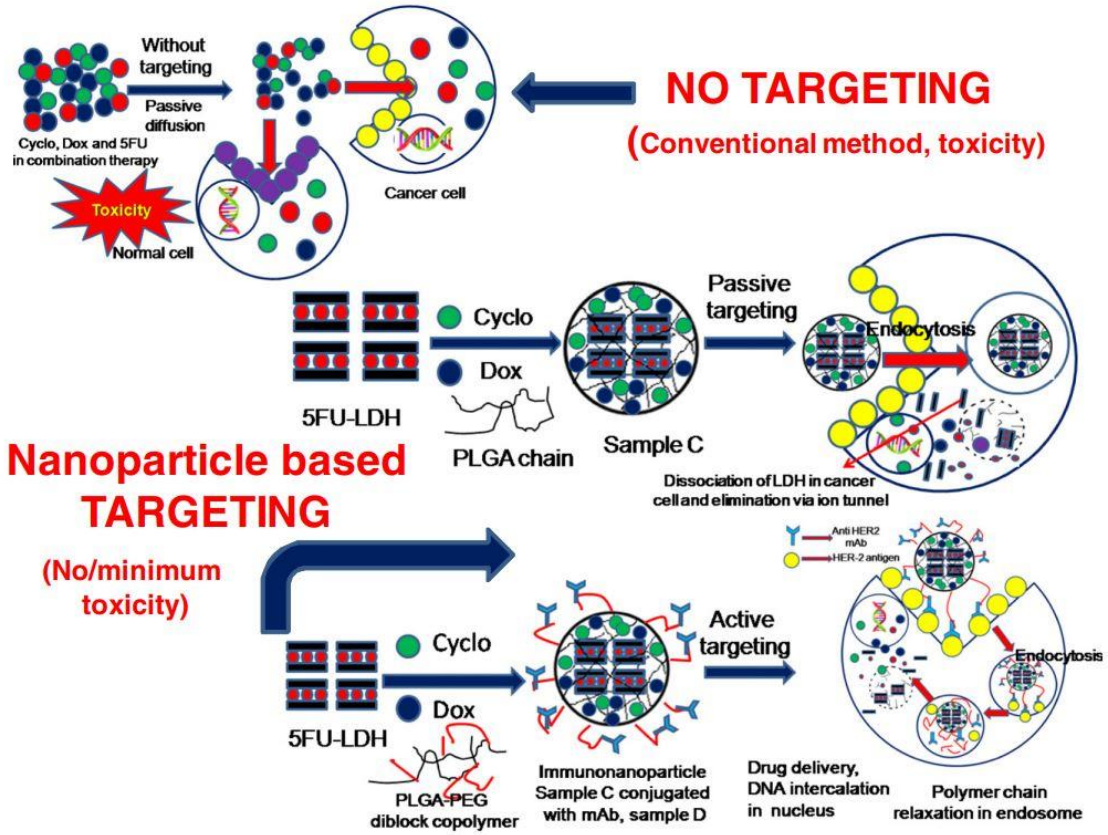

Figure 2.6. MgAl-LDH nanoparticles were used to target anticancer medications such as cyclophosphamide, doxorubicin, and 5-fluorouracil as part of a combination therapy (Saha et al., 2016)

2.2.10. Mg/Zn/CaAl-LDHdrug/biomolecule nanohybrids: in vitro cytotoxicity and in vivo toxicity studies

There is a lot of evidence that drug intercalated MgAl-LDH nanohybrids have lower toxicity than the naked drug, which has been tested using cell lines (Saifullah and

Hussein, 2015). As previously stated, the antihypertensive drug PE incorporated MgAl-LDH generated using Co-precipitation method followed by ex situ anion exchange has no harmful effect on Chang cell line viability (Ali et al., 2012). Moreover, enhancement in efficacy of MTX-LDH nanohybrid has been observed on human colorectal carcinoma (HCT-116) cell line, as evident from the IC_{50} value of the same within 48h in case of nanoconjugate in comparison with bare MTX which attained the IC_{50} value at 72 h respectively (Chakraborty et al., 2013b). In vitro cytotoxicity tests were performed on the HEK293 cell line, HepG2 cell line, and cervical cancer (HeLa) cell line. Except for HepG2 cells, MgAl and ZnAl-LDH were shown to have lower levels of cytotoxicity in all cell lines (Balcomb et al., 2015). On the pheochromocytoma (PC12) neuronal cell line and the mouse fibroblast (NIH 3T3) cell line, levodopa containing ZnAl-LDH nanohybrid demonstrates an improved cytotoxic impact compared to the bare L-DOPA medication (Kura et al., 2014a). In the gastric epithelial (GES1) cell line, there was no significant cytotoxicity difference were observed in case of bare folic acid (FA) and FA incorporated MgAl-LDH nanoparticle (Qin et al., 2014). In the human breast cancer (MCF7) cell line, significant cytotoxic potential has been discovered (Choi and Choy, 2011a, 2011b). A mouse fibroblast cell line (L929) was employed in another investigation to investigate the cytotoxicity of CaAl-LDH nanoparticles. It was observed that significant cytotoxic potential of the nanoparticle was found while incubation for higher time (Shafiei et al., 2013). In a recent study human osteosarcoma cell line (MG-63) was used to assess the cytotoxic potential and the results exhibited that the cancer cell inhibition was approximately two-fold higher compared to bare drug (Chakraborty et al., 2016).

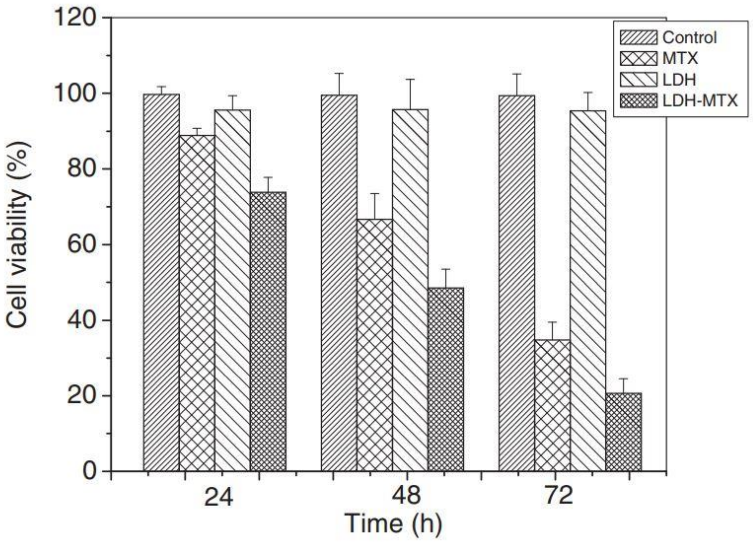

Figure 2.7. Shows the in vitro cell viability of LDH-MTX nanohybrid in a time dependent manner.

2.2.11. Other application of layered double hydroxide

Apart from the biological/pharmaceutical applications, there are many other applications associated with the LDH nanoparticles. Some of these applications include polymer composites, as catalysts, adsorbents and used in environment remediation.

2.2.11.1. LDH nanoparticles as catalysts

Many research study suggests that LDH powder, films or rehydrated LDHs can be used as solid catalysts. Cu^{2+} based LDH powder has been synthesized and used as a catalyst for wet oxidation technique (Zhang et al, 2008). Moreover, activated MgAl-LDH film has proven to be a suitable material for synthesising monolithic catalysts for the acetone aldol condensation reaction and other base catalysis reactions. Further, LDHs have been used in case of waste water treatment, catalysts, additives and flame retardants, medical imaging etc.

2.2.11.2. Water Treatment

In recent days, LDHs have been used for wastewater treatment to remove oxyanions such as F^{-}, PO_4^{3-}, Cl^{-}, Br^{-} which are present in wastewater and have potential harmful effects in human and wildlife. Calcinated LDH powder has potential capability to remove these anions from the contaminated water by incorporating the anions into the LDH by anion exchange method (Lv et al., 2008; Lv et al., 2009).

2.2.11.3. LDH based modified electrodes and biosensors

LDH based biosensors are also currently under development that can be able to detect haemoglobin, urea, glucose level, phenol etc. LDH based biosensor for detection of glucose is already developed by research team (Shan et al., 2007).

2.2.11.4. Carbonated LDH nanoparticles as antacid

It is already evident that LDH has potential antacid activity. It is already well evident that carbonated LDH (MgAl–CO_3–LDH) have pH dependent biodegradability. This LDH has good acid neutralizing capacity, prolonged buffering action and cytoprotective in nature. Owing to this property, it was used as an antacid molecule by trade name Talcid, manufactured by M/s Beyer Pharmaceuticals for the treatment of hyperacidity and for ulcers (Rives, 2001; Evans, and Duan, 2006; He et al., 2006). The basic mechanism of these property includes slow degradation of the molecule in the gastrointestinal pH. In particular the market available antacid formulations are based on the combination of magnesium hydroxide and aluminium hydroxide, which neutralize gastric hydrochloric acid by forming salt and water thus decreases amount of secreted gastric pH and enhance the pH of stomach to 4-6 significantly.

2.2.12. Prospect of the different metal containing LDH in future medicine

Due to their interesting properties, includes ease of synthesis, ability to incorporate anions, thermal stability, and biocompatibility, the anionic clay mineral hydrotalcite has emerged as a single material with multiple medicinal uses, including gene transport (Ladewig et al., 2010) and drug delivery (Tarnawski et al., 2000). Aside from these, the material has low toxicity, high-drug loading capacity with increased drug stability, targeting function, and better cellular penetration into cells that helps overcome multiple drug resistance in certain instances, including cancer (Nalawade et al., 2009). The active pharmaceutical ingredient of two commercially marketed antacid medications, TALCID ™ and ALTACITE ™, contains hydrotalcite. (Playle et al., 1974; Tarnawski et al., 2000). Owing to the intercalating properties of LDHs by different anions, negatively charged oligonucleotides such as small interfering plasmid DNA, RNA (siRNA and shRNA), and microRNA (miRNA) can easily be intercalated using an ex situ anion exchange technique in Alzheimer's or other neurological disorder, cancer, acquired immune deficiency syndrome (AIDS) or other deadly diseases. Gene silencing is a popular strategy in this regard, in addition to being explored internationally for inhibiting the specific genetic expression that is the core cause of the aforesaid illnesses to a significant level. When anionic molecules are incorporated into LDHs, an electrostatic association occurs, followed by facile cellular internalisation of the same in the diseased cell via pinocytosis and drug delivery, resulting in significantly higher efficacy and fewer adverse effects than conventional therapies (Ben-Shushan et al., 2014). DNA/siRNA degradation seems to happen owing to naked gene delivery thus LDH incorporated gene can effectively penetrate the cell membrane and release nucleotides, resulting in high transfection efficiency and protect the DNA/siRNA molecules from systemic degradation. Choy et al. were the first to

illustrate the uptake of 150 nm LDH nanoparticles, introduced into cells via clathrin-mediated endocytosis which is energy-dependent (Choy et al., 2000). 6 to 8 hours after LDH-mediated cell transfection suggests that targeted gene silencing occurred that the LDH host may be capable of successfully releasing the DNA/siRNA molecule (Desigaux et al., 2006; Li et al., 2011). Chronic otitis media is characterised by recurrent bacterial infections that damage the middle ear bones. MgAl-LDH was used to create a dental material that may release fluoride ions in a time-dependent manner without causing toxicity (Tammaro et al., 2014).

Chapter 3

Aims & Objectives

3. Aims & Objectives of the present study

Nano-drug delivery is one of the most challenging approaches towards the treatment of cancer that overcomes several drawbacks of the conventional drug delivery, like uncontrolled release, fluctuation of plasma drug level, poor aqueous solubility etc. Herein, Etoposide been widely used as single or in combination as a first line drug in the treatment of lung cancer, though the side effects associated with the drug including schedule dependency and poor stability and less bioavailability often restricts it to exert the desired therapeutic action. To overcome these drawbacks an attempt has been made to develop a novel nanosized layered double hydroxide ceramic based extended-release drug delivery formulation encapsulating anticancer drug etoposide for the treatment of lung carcinoma.

The specific objective of the present study includes

1. The first objective was to synthesize a novel ceramic based CaAl-layered double hydroxides nanocarrier at varying pH condition and optimization of the same by different sophisticated analytical technique with extensive characterization (XRD, FTIR, FESEM, TEM, particle size, ion chromatography for carbonate estimation, in vitro cytotoxicity).
2. Second objective was to evaluate the anticancer potential of the synthesized nanocarriers at varying pH condition in colon cancer (HCT116), breast cancer (MCF7) and normal human osteoblast precursor (MC3T3) cell line. The motivation was to assess the optimized nanocarrier as a synergistic agent with the encapsulated drug molecule in cancer therapy.
3. The third objective was to encapsulate the drug etoposide in the optimized CaAl-LDH nanocarrier, extensive characterization followed by evaluating the

synergistic anticancer potential of the nanoconjugate in lung cancer by cellular internalization of the nanoconjugate in the non-small cell lung carcinoma (A549) cell line.

The working hypothesis is that the etoposide encapsulated CaAl-LDH ceramic nanoparticles/nanohybrid formulation could have the potential anticancer property with reduced side effects and protects the healthy or normal tissues from the harmful toxicity of the bare drug.

Chapter 4

Experimental procedures

4. Experimental procedures

4.1.Materials

Deionised and decarbonated ultrapure water (Millipore, specific resistivity: 18 MΩ) has been utilized for all the experimental preparations and all chemicals were used in this study as received without undergoing further purification process.

4.2.Reagent list:

1. Calcium nitrate hexahydrate $Ca(NO_3)_2.6H_2O$ Sigma Aldrich, USA 99.0%
2. Aluminium nitrate nonahydrate $Al(NO_3)_3.9H_2O$ Sigma Aldrich, USA 99.0%
3. Sodium hydroxide (pellets) NaOH Sigma Aldrich, USA 99.0%
4. Ammonium hydroxide NH_4OH Sigma Aldrich, USA 99.5%
5. Etoposide drug., Jiangsu Hengrui Medicine Co. Ltd. 99%
6. Tris hydrochloride $C_4H_{11}NO_3.HCl$ Invitrogen, Carlsbad, USA. 99.0%
7. Acetonitrile CH_3CN E-Merck, Germany 99.5%
8. Methanol CH_3OH E-Merck, Germany 99.7%
9. Dimethyl sulfoxide (bioreagent) C2H6OS Sigma Aldrich, USA 99.9%
10. Dimethyl sulfoxide (GR grade) C2H6OS E-Merck, Germany 99.5%
11. Dulbecco's Modification of Eagle's Medium (DMEM) Invitrogen, Carlsbad, USA. 99.0%
12. Phosphate-buffered saline – Sigma Aldrich,USA 99.9%
13. 1X Tripsin-EDTA solution- Sigma Aldrich,USA 99.9%
14. Gentamycin sulfate – Invitrogen, Carlsbad, USA. 99.0%
15. Penicillin- streptomycin – Invitrogen, Carlsbad, USA. 99.0%
16. FBS (Fetal bovine serum) – Invitrogen, Carlsbad, USA. 99.0%
17. Filter (0.2 μm) sterilised – Millipore, USA

18. MTT powder (thiazolyl blue tetrazolium bromide) 3-(4,5 dimethylthiazol e-2-yl)-2,5- phenyltetrazoliu m bromide, $C_{18}H_{18}BrN_5S$ Sigma Aldrich,USA 97.5%
19. Human CAMKII∞ (Calcium/Calmodulin-dependent protein kinase II Alpha) ELISA kit- Elabscience, Texas, U.S.A.
20. Superoxide Dismutase (SOD) assay kit Elabscience, Texas, U.S.A.
21. Nitrogen gas of XL grade 99.99%

3.2 Sample Preparation

The detailed synthesis of samples and experimental procedures are described below

Experimental: Part 1

4.3.Synthesis of pristine bare CaAl-LDH at three pH conditions

CaAl-LDHs were effectively produced by dissolving 32 mmol $Ca(NO_3)_2.4H_2O$ and 16 mmol Al $(NO_3)_3.9H_2O$ in decarbonated water under inert atmosphere (XL grade, 99.99 percent pure) nitrogen gas. Addition of 0.5 mol L^{-1} NaOH solution leads to achieve final pH of the solution to 8.5, 10.5 and 12.5. The resultant white gelatinous precipitate was aged for 24 hours at room temperature under continuous nitrogen purging followed by collection and centrifugation for 5 minutes at around 5000 g (Heal Force, Neofuge 15R, China) to separate the precipitate, washed under running decarbonated water and freeze dried the resultant (EYEL4, FDU2200, Japan) to get nanocrystalline LDH powder. Sample A was the end product (LDH powder) obtained at pH 8.5, sample B obtained at pH 10.5 and sample C obtained at pH 12.5 respectively. CaAl-LDHs were manufactured using the same process as before, but at pH values ranging from 8 to 13, with (pH 8.5, 10.5, and 12.5) serving as representative instances.

4.4. **Characterization techniques**

4.4.1. **Powder X-ray diffraction (PXRD) of all the samples (A, B and C)**

The XRD of CaAl-LDH synthesized at three different pH condition were obtained using a Panalytical X'Pert Pro MPD diffractometer (Almelo, Netherlands) with silicone as a reference material (RM) and radiation level at 40 mA, 40 kV. All three samples were analyzed in the 2ɵ range between 5^0 and 70^0. At each point, the step size was 0.03, and the count time was 2s. Using Bragg's equation, the XRD peak at (002 and 004) of all LDHs were used to detect the basal spacing.

4.4.2. Fourier transform infrared (FTIR)

The spectra from the powder samples were recorded on a F Varian 3600 (USA) spectrometer at room temperature (25^0 C) using the KBr (Sigma Aldrich, 99 percent) pellet technique at a ratio of sample: KBr = 1:100) in the wavelength of 400-4000 cm^{-1} with a scan of 50.

4.4.3. **Determination of particle size and morphology**

Using a Carl Zeiss SMT AG SUPRA 35VP (Germany) field-emission scanning electron microscope (FESEM) and an FEI Tecnai 30G2 S-Twin (Netherlands) transmission electron microscope, the particle size of all CaAl-LDH was studied. The energy dispersive spectroscopy (EDS) equipment linked to the FESEM was used to evaluate the elemental composition of all the LDH samples. A Zetasizer Nano ZS (M/s Malvern, Worcs, UK) based on the quasi-elastic light scattering technique was used to evaluate the particle size, zeta potential, and polydispersity index (PDI) of the synthesised LDH.

4.4.4. **Assessment of trace level carbonate ion (ppm) in all the samples including purged water**

Ion chromatography (792 Basic IC, Metrohm AG, Herisau, Switzerland) and a Metrosep Organic Acids-250 (6.1005.200), Metrohm, Switzerland, separation column was used to measure trace level carbonate ion in all the samples (A, B, and C) as well as nitrogen gas purged aqueous medium. (Chakraborty et al., 2012). To detect trace level ions in the analyte, a thermostatic conductivity detector was attached to the ion chromatography, with a cell volume of 1.5 mL and detecting alternating current in the conductivity range 0-1000 mS cm-1 at 1 kHz. The machine was calibrated by comparing retention time to standard sodium carbonate solutions in the concentration range of 0.5-20 ppm, yielding a calibration generated from chromatograms **(Figure 5.6 A).** 10 mg of each sample (accurately weighed) was dissolved in 20 mL 0.001 mol L-1 HCl solution to make the test solutions for Samples A, B, and C. The solutions, along with a known volume of purged water (XL grade nitrogen gas purged ultrapure water), were then filtered and injected into the chromatograph's injection valve (injection volume: 20 L) using a 10 mL luer lock syringe (SGE Analytical Science, Australia). The retention duration of carbonate anion in the above-mentioned column was then compared to the conductivity of the same in the analyte.

4.4.5. ***In vitro*** **dissolution study of Ca^{2+} ion in simulated body fluid (SBF)**

Using simulated bodily fluid (SBF) at plasma pH of 7.4 and 37°C, an in vitro dissolution study of Ca^{2+} from pure CaAl-LDH was examined. The investigation used a USP type II apparatus (Electrolab TDT-08L dissolution tester) and followed the USP NF 2010 specification. Samples A, B, and C were accurately weighed and

immersed in 1 mg mL^{-1} SBF solution while being constantly stirred. The inductively coupled plasma-atomic emission spectroscopy (ICP-AES) method was used to quantify the amount of Ca^{2+} leached in the SBF solution. Aliquots were extracted at intervals of 0.5, 1, 2, 4, 6, 8, 16, and up to 72 hours, with the solution being supplied at the same time.

4.4.6. *In vitro* anticancer activity of the samples A, B and C

4.4.6.1. Cell culture

ATCC breast cancer (MCF7), human colon carcinoma (HCT116), and human osteoblast precursor (MC3T3) cells (Rockville, MD, USA) were grown in DMEM medium (Invitrogen, USA) which was supplemented with 10% foetal bovine serum, 1 g mL^{-1} penicillin G, and 1 g mL^{-1} streptomycin at 37°C with a flow of 5% CO_2 (HF90 Heal Force, China). After the cells had reached 90% confluence, they were sub cultured using trypsin EDTA. All studies were carried out with cells that were within 5 passes of being removed from cryopreservation.

4.4.6.2. *In vitro* cellular viability of all the LDH samples

CaAl-LDH samples precipitated at the three pH values indicated above were tested for anticancer activity using a cytotoxicity analysis at an interval of 24, 48, and 72 hours. For samples A, B, and C, a stock solution of 1 mg mL^{-1} was produced in Dulbecco's Modified Eagle's Medium (DMEM) (GR grade) and incubated at 37°C in a CO_2 incubator for 24 hours. In a 96-well plate, 1×10^4 of MCF7, HCT116, and MC3T3 cells were placed per well. The cells were incubated at 37°C in a CO_2 incubator for 24 hours after adding 200 µL aliquots of all the samples in each well, in triplicate, to allow sufficient cell adhesion, and the incubation period was

continued for 72 hours and at an interval of 24 hours 200 µL aliquots of the samples in each well were added. As a control experiment, cultured cells were used. The MTT experiment was carried out by adding 3-(4,5-dimethylthiazole-2-yl)-2,5-phenyltetrazolium bromide (MTT) reagent at a concentration of 1 mg mL^{-1} (SigmaAldrich, USA) to all the wells in a ratio of 1:9 (MTT:DMEM) and incubating in a dark place for 4 hours at 37°C. After removing the MTT and DMEM media, the reaction was stopped by adding 100 µL DMSO to each well. In an ELISA reader (Bio-Rad, USA), the absorbance was measured at 550 nm, and the related cell viability was computed. The above-mentioned cell viability assay was performed three times at each time point, and the statistical analysis of the data was set at $P<0.05$ with a 95 percent confidence interval (CI).

Experimental:2

4.4.7. Synthesis procedure of phase pure CaAl-LDH (sample A)

Sample A was made by dissolving 32 mmol of [Ca $(NO_3)_2$.4H2O] and 16 mmol of [Al $(NO_3)_3.9H_2O$] in 250 ml of decarbonated water (18.2 M) and stirring continuously under a nitrogen gas stream (XL grade, 99.99 percent pure). To obtain a white gelatinous suspension, by dropwise addition of the pH of the resulting mixed metal solution was M NaOH, the pH was adjusted to 8.5. It was also aged for 24 hours at room temperature with a constant supply of nitrogen gas. The resultant suspension was centrifuged for 10 minutes at 5000g (Heal Force, China) to separate the precipitate, rinsed with decarbonated millipore water and thereafter freeze dried at 82°C and 20 Pa pressure (EYEL4, FDU2200, Japan) (Saha et al., 2016).

4.4.8. Synthesis of the etoposide (ETO) loaded CaAl-LDH nanoparticle (sample B) by anion exchange technique

Sample B was made using a basic anion exchange method (Qin et al., 2010). In a nutshell, around 50 ml of 0.1 M ETO solution was made by mixing ETO with Millipore water (pH was adjusted to 8 by dissolving NaOH pellet). Furthermore, under constant nitrogen purging, the ETO solution was added to a 100 ml aqueous suspension of 1 g (equal to the equivalent quantity of nitrate ions) of sample A and thereafter drop by drop, 0.01 M NaOH was added until the pH was elevated to 10. The entire synthesis procedure was carried out while the reaction vessel was agitated for 48 hours. At 82 ℃ and 10 Pa pressure, the resultant suspension was centrifuged, washed, and freeze dried. Sample B is the name given to this sample (Qin et al., 2010).

4.4.9. Characterization techniques

The X'Pert Pro MPD diffractometer (Panalytical, Almelo, The Netherlands) was used to obtain powder X-ray diffraction patterns of sample A and sample B at CuKa (= 1.5418) radiation at 40 mA, 40 kV. The 2 theta range of 5° to 70° was used to scan the samples. At each point, the step size was 0.03, and the count time was 2 seconds. At room temperature, FTIR spectra of samples A and B were recorded on a F Varian 3600 (USA) spectrometer using the KBr (Sigma Aldrich, 99%) pellet technique (sample: KBr = 1:100) in the range of 400–4000 cm^{-1} with an average scan of 50. Carl Zeiss SMT AG assessed the particle size and shape of each sample. A Carl Zeiss SMT AG SUPRA 35VP field-emission scanning electron microscope was used to examine the size and shape of the particles in both the samples. The size, polydispersity index (PDI), and zeta potential were examined

further using a Zetasizer Nano ZS (M/s Malvern, Worcs, UK) which was based on the theory of quasi-elastic light scattering. A NETZSCH STA 409 CD thermal analyser was used to perform thermo gravimetric analysis (TG-DTA) on both samples. In an inert atmosphere, the tests were performed from ambient temperature to 1000 °C at a heating rate of 10°C min^{-1}. All the preceding experiments were carried out three times to ensure that the results were consistent.

4.4.10. Determination of loading % of ETO in sample B

A standard amount of sample B was placed in 5 ml of 1 M HCl solution to estimate the percent of drug loading. The solution was stirred for several hours before being examined with a UV–Vis spectrophotometer. Monitoring the absorbance at 254 nm against an ETO standard curve (y = 1.26 + 0.1312, R2 = 0.9919) allowed the concentration of ETO to be measured. The following equation was used to calculate the medication loading: (Weight of ETO in sample B / Weight of sample A) × 100 = percent of drug loading (w/w) (Qin and colleagues, 2013).

4.4.11. Determination of *in vitro* release of ETO from sample B

The type-II USP dissolution test apparatus was used to examine the in vitro drug release of ETO from sample B. (Electrolab TDT-146 08 L Mumbai, India). In a nutshell, 0.086 g of etoposide was placed in a dialysis chamber made up of a cellulose membrane bag (14 kDa) (M/s SigmaAldrich, USA) and immersed in 900 ml of phosphate buffered solution (PBS) having a pH 7.4 at 37 °C with stirring at 100rpm (D'Souza, 2014). At specific periods of 0.5, 1, 2, 4, 6, 8, 12, 24, and finally 72 hours, 10 ml of aliquots were removed and immediately replaced with the equal volume of PBS. Furthermore, the aliquots were filtered via a 0.22 mm, 13 mm plastic filter holder (part no. NR 013100, Pall Corporation, USA) using a 10 ml luer

lock syringe. The solution was then fed into the chromatograph's injection valve (injection volume: 20 µl) (HPLC 820 Metrohm AG, Switzerland). The UV–Vis detector (Lambda1010 Bischoff, Switzerland) was used to record the ETO retention time in the column against its absorbance. The mobile phase for the analysis was a 25:75 combination of acetonitrile and buffer, with a 1 ml min1 flow rate at a λ max 254 nm and a 3.9 mm 30 cm column packing L11. The HPLC system was calibrated before the analysis with a standard solution of the drug ETO in the concentration range of 10–100 ppm. Therefore, with five known concentrations of the drug ETO against its corresponding peak area, the calibration curve was generated.

4.4.12. *In vitro* bioassay

4.4.12.1. Cell culture

ATCC provided the human lung cancer (A549) cell line (Rockville, MD, USA). The cell line was routinely grown in a T25 flask in humified atmosphere at 37 °C with 5% CO_2 in an incubator in Dulbecco Modified Eagle Medium (DMEM, Invitrogen, USA) which was supplemented with 10% foetal bovine serum (FBS), 2 mg ml^{-1} $NaHCO_3$, 1 g ml^{-1} penicillin G (HF90 Heal Force). When the cells were 90–95 % confluent, they were subcultured using trypsin–EDTA (Wang et al., 2010). All the experiments were completed within five passages of being resurrected from cryopreservation.

4.4.12.2. Determination of half maximal inhibitory concentration (IC_{50}) of ETO on A549 (lung adenocarcinoma) cell line

From a stock solution of 1 mg ml^{-1} in dimethyl sulfoxide, the IC_{50} of ETO was determined at various concentrations ranging from 5 to 60 g ml^{-1} (DMSO, GR

grade, Merck, India). Inside a 96-well plate, 3× 10^4 A549 cells were sown in each well. The cells were then treated with ETO in varied doses of 5, 10, 20, 40, and 60 g ml^{-1} and incubated for another 72 hours at 37 °C in a CO_2 incubator to ensure sufficient adhesion to the plate. A549 cells were cultured in DMEM media as a control. After 24 hours of incubation, the MTT was carried out by MTT reagent at a concentration of 1 mg ml^{-1} (Sigma-Aldrich, USA) to all wells in a 1: 9 ratio (MTT reagent: DMEM medium) and incubating in the dark for an additional 4 hours at 37 °C After removing the MTT and adding 100 l DMSO to each well, the reaction was stopped. In an ELISA reader (Bio-Rad, USA), the absorbance was measured at 590 nm, the dosage response curve was constructed, and the half maximum inhibitory concentration (IC_{50}) of ETO was determined (Bhattacharjee et al., 2019).

4.4.12.3. Determination of half maximum inhibitory concentration (IC_{50}) of sample B on lung carcinoma cell line (A549)

After a 24 h incubation at 37 °C in a humified environment containing 5% CO_2, 3× 10^4 cells were planted per well in 96 well plates. The cells were treated with sample B for 24 hours to ensure adequate cell adhesion, and then incubated for another 24 hours after being treated with sample B at various concentrations of 50, 75, 100, 150, and 200 µg ml^{-1}. (Considering the % of drug loading and IC_{50} value of bare etoposide, as above). The control group consisted of cells grown in 200 µl culture media (DMEM) containing 5% DMSO. The cell viability of sample B was examined using the MTT assay, as previously described, and the absorbance was measured at 590 nm using an ELISA plate reader to calculate the IC_{50} (Bio-Rad, USA) (Bhattacharjee et al., 2019).

4.4.12.4. On the A549 cell line, evaluation of sample B's time-dependent synergistic activity in comparison to bare ETO and sample A.

After a 24 hour incubation at 37 ℃ in a humidified environment containing 5% CO_2, 3× 10^4 cells were planted per well in 96 well plates. The cells were treated with sample B at a concentration of 200 µg ml^{-1}, bare ETO at a concentration of 56 µg ml^{-1} (equivalent amount of bare ETO contained in sample B), and sample A at a concentration of 143 µg ml^{-1} as previously described (equivalent amount of sample A present in sample B). The concentration of sample B was determined at random to conduct the trial experiment with an equivalent amount of bare ETO and sample A, as described above, for estimating the synergistic efficacy of sample B (ETO-CaAl LDH nanoconjugate) at 24, 48, and 72 hours. To investigate the synergistic anti-cancer potential of sample B, the cell viability was assessed using MTT, as previously described, and the absorbance was recorded at 590 nm using an ELISA reader (Bio-Rad, USA).

4.4.12.5. Cell proliferation/migration assay *invitro* using sample B

To determine the synergistic potential of sample B on the A549 cell line, an in vitro cell proliferation or migration assay was performed. In this study, A549 cells were put in a six-well plate and incubated until the plate was completely confluent. The confluent layer of the cells was then scratched by one linear scratch perpendicular to the indicated line using a 200 µl sterile tip of micro pipette. To remove the dead cells, the wells were washed with PBS solution, and fresh medium was added to the plates. The connected cells were given the identical concentrations of bare ETO, phase pure CaAl-LDH (sample A), and ETO loaded CaAl-LDH (sample B) as in the cytotoxicity assay. Images of the upper and bottom parts of the line, taken

immediately after the scratch and at 24 hours, were used to track cell migration and proliferation (Zhu et al., 2015). The photographs were taken with a digital camera and an inverted microscope. With the Image J 1.48i software, the amount of healing on scratch wounds was determined using the following formula:

Rate of wound healing (%) = $(A_0 - A_t)/A_0 \times 100\%$, where A_0 indicates the original wound area and A_t designates the wound area at time t, respectively.

4.4.12.6. Tagging of fluorescein isothiocyanate (FITC) with sample B

A green, fluorescent dye, fluorescein isothiocyanate (FITC), was tagged with sample B for intracellular tracing. Briefly, in a nutshell, 3 mg ml^{-1} slurry of sample B was prepared followed by addition of aqueous solution of 1 mg mL^{-1} fluorescein isothiocyanate isomer I (FITC), which was then stirred for 1 hour at room temperature (Li et al., 2013).

4.4.12.6.1. Flow cytometry

The A549 cell line was seeded at 1×10^6 cells per well in a six-well plate, then treated with sample B. After incubation for 24, 48, and 72 hours, the cells were rinsed with PBS solution, and after detaching by using trypsin–EDTA (HiMedia) the solution was centrifuged. Further the pellets were resuspended in PBS after the supernatant was discarded. A flow cytometer (Pertec Sysmex India, Cube 1) was used for the analysis, with an excitation wavelength of 482 nm and an emission wavelength of 502 nm (Li et al., 2013).

4.4.12.6.2. Confocal microscopy

Confocal microscopy was used to observe the uptake of sample B by A549 cells. After 72 hours of incubation, the cells were fixed in 4 percent paraformaldehyde

(Sigma-Aldrich) for 10 minutes before being washed in PBS. The cells were then put onto microscope slides using mounting medium containing DAPI (Riviera Cat No-72900135). Thereafter the images were taken of the transfected cells by an Olympus FluoViewTM FV1000 Confocal Microscope, Japan (Li et al., 2013).

4.4.12.7. CaMKIIα expressiom assay of sample B

The expression of CaMKII in the A549 cell line was measured using the SandwichELISA technique. The cells were first plated into 96-well plates with Dulbecco Modified Eagle Medium (DMEM) at 5×10^4 cells in each well and allowed to attach for 24 hours before being treated with sample A (CaAl-LDH, 143 µg ml^{-1}) and sample B (ETO loaded nanoconjugate, 200 µg ml^{-1}) (as described above) for 24 hours. The cells were then washed with PBS before being trypsinized and disturbed by a repeated frozen–thaw cycle. This procedure was repeated three times. The cell lysates were also centrifuged and stored at 20 °C for further analysis. Using the reagent kit (Elabscience Biotechnology Inc., Texas, USA), the expression of CaMKIIα was measured spectrophotometrically at 450 nm (Bhattacharjee et al., 2019).

4.4.12.8. SOD assay of sample B

The oxidative damage caused by sample B was investigated using an intracellular superoxide dismutase (SOD) assay. The assay procedure was the same as the CaMKII assay described above. In a nutshell, A 549 cells were treated with samples A and sample B as described above and cultured for 24 hours. Superoxide dismutase (SOD) was also evaluated spectrophotometrically at 450 nm using reagent kits purchased from Elabscience Biotechnology Inc. in Texas (Bhattacharjee et al., 2019).

Statistical analysis

All of the experiments were repeated three times, and the results were determined using statistical analysis of the data with a P value of < 0.05 and a 95 percent confidence interval (CI).

Chapter 5

Results & Discussion

5. Results & Discussion

Results & Discussion: Part 1

5.1.PXRD analysis of CaAl-LDH (Sample A at pH 8.5, Sample B at pH 10.5 and Sample C at pH 12.5)

Figure 5.1. shows the powder X-ray diffraction (XRD) patterns of virgin CaAl-LDH produced at three distinct pH settings. The XRD pattern of sample A (Figure 5.1) shows a well crystallised hydrotalcite-like phase with typical (00l) reflections for layered clays, indexed to hexagonal lattice with rhombohedral space group. The phase pure CaAl-LDH is confirmed by the basal spacing (d002) of 8.66 A, which corresponds to the (002) peak of CaAl-LDH (JCPDF 01-089-6723). The X'Pert PRO software was used to validate the phases and it was confirmed that Sample A (CaAl-LDH synthesized at pH 8.5) exhibits formation of pure phase. Whereas Sample B, produced a combined phase including both pure CaAl-LDH (63%) and $CaCO_3$ (aragonite and calcite polymorphs) (37%) (JCPDF 00-022-0147). While in sample C, the proportion of $CaCO_3$ was increased to 43%, with both aragonite and calcite polymorphs which was demonstrated by the presence of significant peaks of both crustal lattice in Figure 5.1, panel (C) and the rest (57%) was CaAl-LDH (JCPDF 00001-0628 and 01072-1214 respectively).

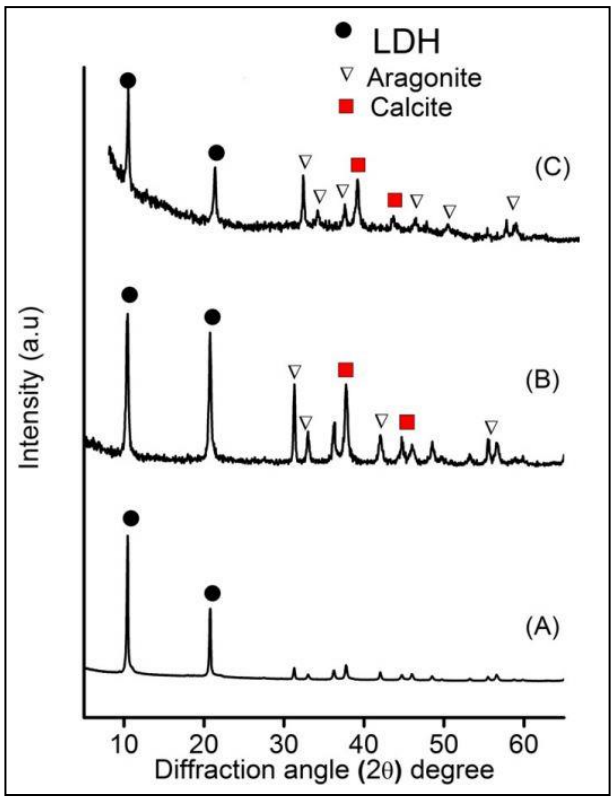

Figure 5.1. The XRD pattern of all the samples (A, B and C) exhibits phase pure and mixed phase containing LDH

The crystal lite size and lattice strain of the precipitated phases were determined using the well-established Scherrer formula from the (002) reflection of all the samples (Table 2) in this investigation

Name	Peak position (2θ)	Crystallite size (nm)	Lattice strain (%)
Sample A	10.20	41.67	0.0098
Sample B	10.26	25.25	0.0160
Sample C	10.09	21.93	0.0188

Table 2: crystal lite size and lattice strain of the precipitated phases from Scherrer formula from the (002) reflection

5.2.FTIR analysis of sample A, B and C

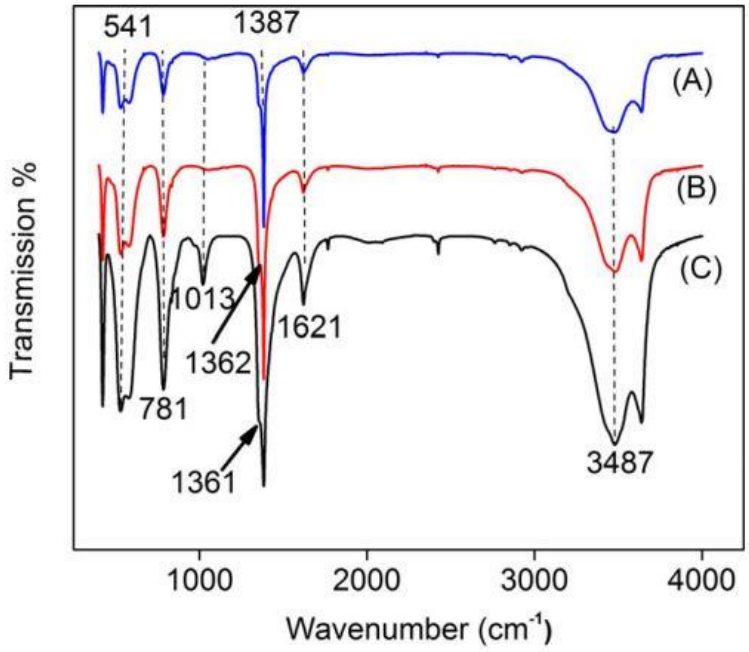

Figure 5.2. The typical vibration bands of (A) sample A, (B) sample B, and (C) sample C in FTIR analysis

The FTIR spectra of virgin CaAl-LDH at three pH settings are shown in Figure 5.2. Stretching vibrations of M–O bonds in the pristine LDH are represented by a couple of low intensity bands about 541 cm^{-1} and 781 cm^{-1}. The stretching vibration of NO_3 anion in sample A is approximately 1385 cm^{-1}, indicating that it is present in the interlayer space, whereas in sample B and C, small notches at 1362 and 1361 cm^{-1} might be attributed owing to the presence of CO_3^{2-}. The stretching vibration of the labile hydroxyl group or physically adsorbed water molecule is represented by the absorption band in the broad range of 3400-3600 cm^{-1} in all three samples A, B, and C.

5.3. Particle size analysis

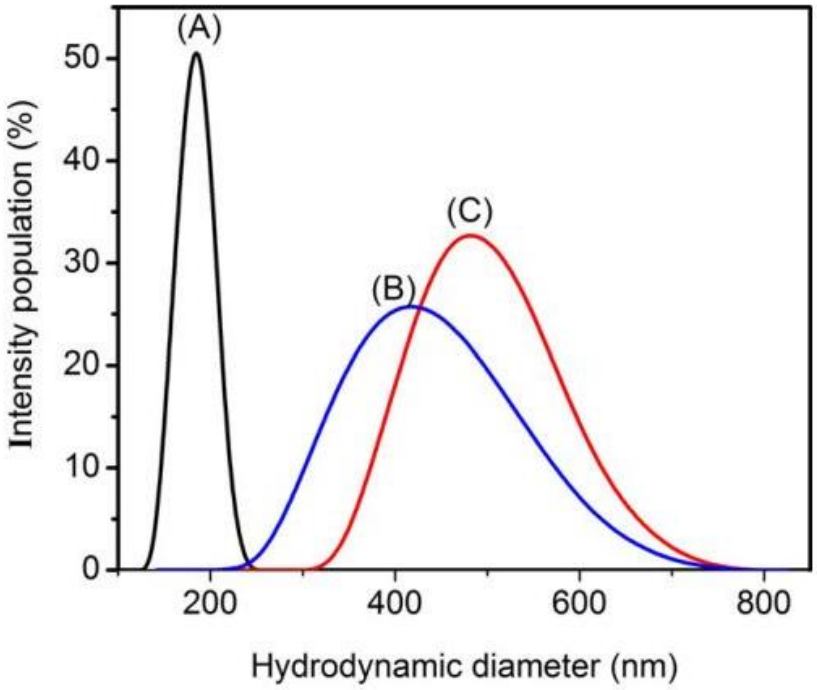

Figure 5.3. Hydrodynamic diameter of all the samples (Sample A,B and C)

The hydrodynamic diameter of CaAl-LDH produced at three distinct pH settings, as evaluated by the dynamic light scattering approach, is shown in Figure 5.3. All of the samples A, B, and C in this investigation have a unimodal size distribution in the 120-800 nm range. Samples A, B, and C have D_{50} values of 184, 414, and 482 nm, respectively, with polydispersity indices (PDI) ranging from 0.20-0.25. Furthermore, sample A's electrokinetic potential of 39.30 mV is moderately stable. In the case of sample B, the particles in the suspension show signs of incipient instability (29.40 mV), while sample C has a much lower value of 5.22 mV.

5.4.Morphological assessments of sample C (pH 12.5)

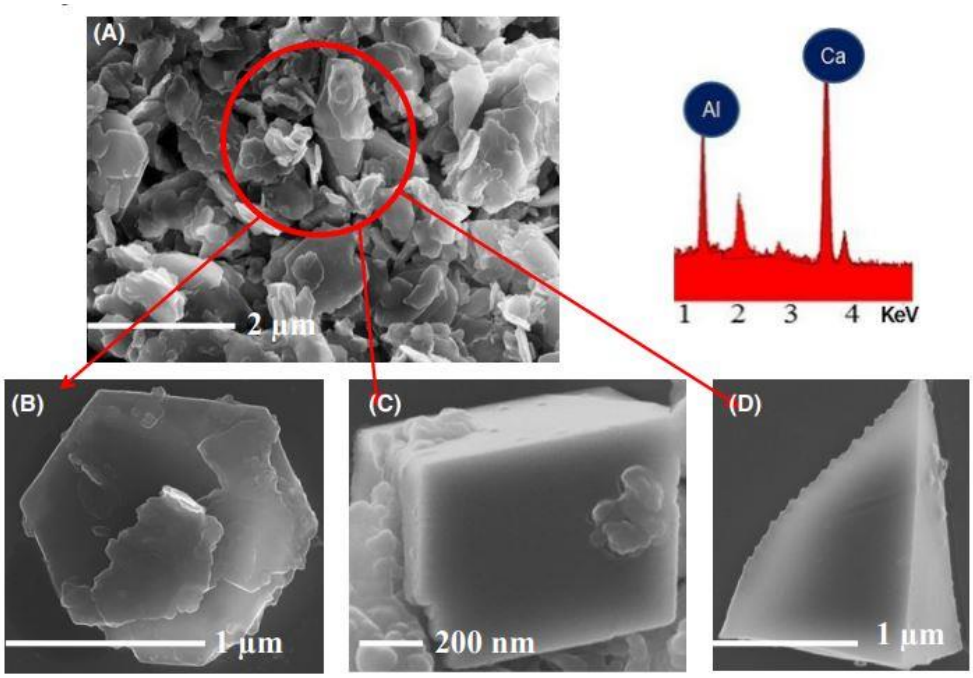

Figure 5.4. FESEM pictures of (A) sample C containing a mixture of CaAl-LDH (B) $CaCO_3$ (C calcite polymorph) and $CaCO_3$ (D aragonite polymorph). (I) EDS (A) of the respective area, with CaAl-LDH as the dominant phase.

As previously indicated and corroborated by the morphological features of the precipitated phase as seen in the FESEM pictures, sample C comprises 43 % $CaCO_3$ (both calcite and aragonite polymorphs) and 57% CaAl-LDH. Figure 5.4A exhibits a variety of morphological traits at low magnification of sample C. At increased magnification, existence of particles of three unique morphologies was found at a specific position designated by a circle; at 5.4 B, a hexagonal platelet is a typical characteristic of LDH usually (CaAl-LDH), A rhombohedron crystal at 5.4 C illustrates the development of calcite polymorph, the most well-known and stable calcium carbonate polymorph. Intriguingly, the presence of the aragonite polymorph could be established in the same precipitated phase, as illustrated in 5.4D, a typical orthorhombic system with a prismatic crystal habit. Figure 5.4 depicts the typical frame area EDAX

design made up of Ca, Al, and other components. Apart from phase pure CaAl-LDH in sample A, which is shown by an arrow.

5.5.TEM analysis of sample A (pH 8.5) and sample C (pH 12.5)

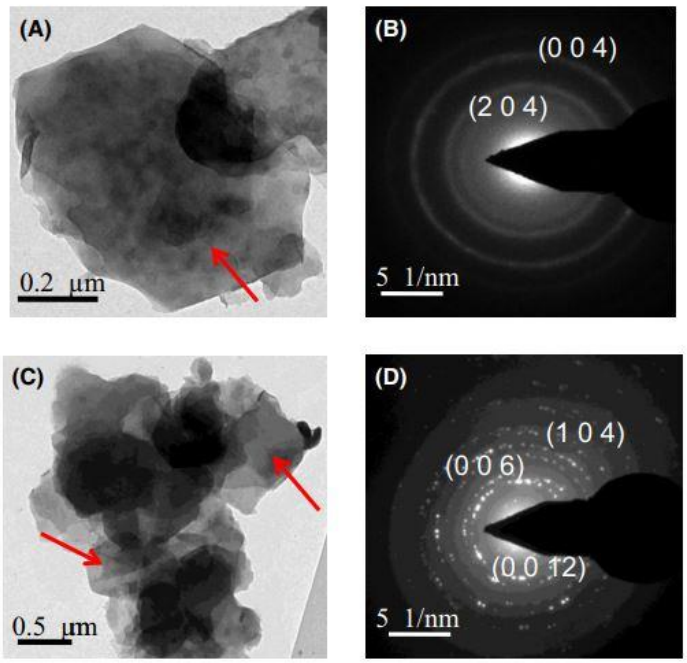

Figure 5.5. TEM images of sample A (A), where the arrow indicates hexagonal platelets (B). Sample C shows the distinctive atomic planes (C) sample C, where the arrow indicates the existence of calcite polymorph (D) sample C's SAED pattern.

TEM pictures confirm the presence of calcite crystals in sample C, as shown by FESEM and XRD data. The atomic planes that correspond to the layered clay structure of CaAl-LDH and $CaCO_3$, as well as the XRD data, has been confirmed by the SAED image (Figure 5.5 B,D).

5.6.Estimation of carbonate ion in all the samples (A, B and C)

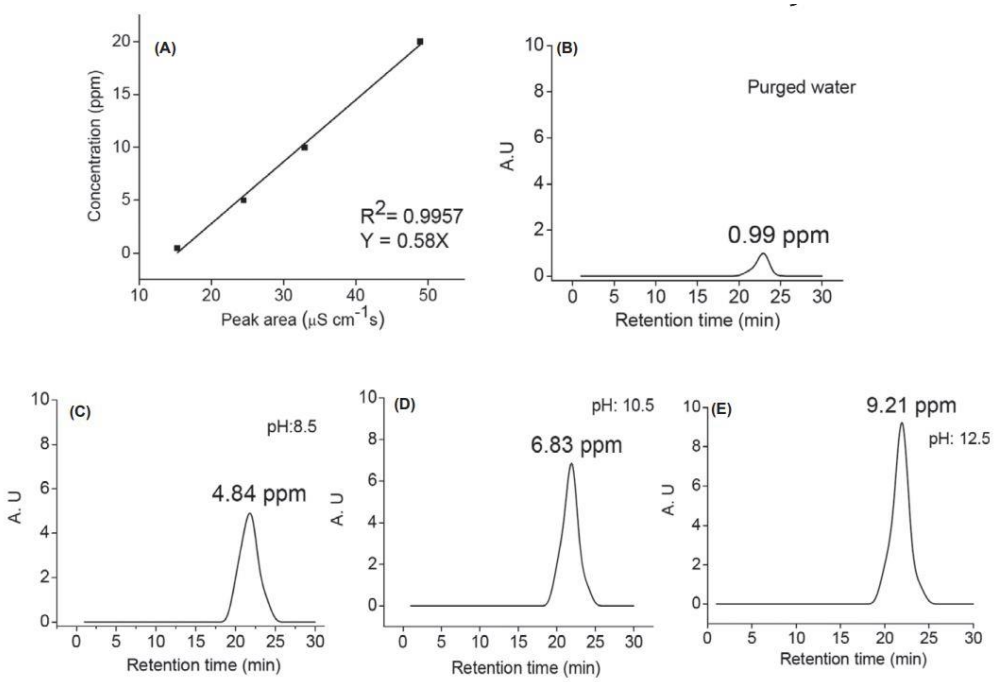

Figure 5.6. Carbonate ion estimation data from ion chromatography (A) calibration curve (B) water purged by nitrogen (C) sample A (D) sample B (E) sample C

At pH levels of 8.5, 10.5, and 12.5, respectively, ion chromatograms of conductivity of the analyte (s) in the test solutions (sample A, B, and C) vs retention time are shown in Figure 5.6, with the carbonate anion having a retention period of 23 minutes. The presence of a trace level carbonate anion in the precipitation medium (nitrogen gas purged ultrapure water) was discovered (Figure 5.6 B). Interestingly, the concentration of the same anion increases with rising pH (sample A is 4.84 ppm whereas sample B is 6.83 ppm) and nearly doubles at pH 12.5 (9.21 ppm) (Figure 5.6 C-E).

5.7.In vitro dissolution study

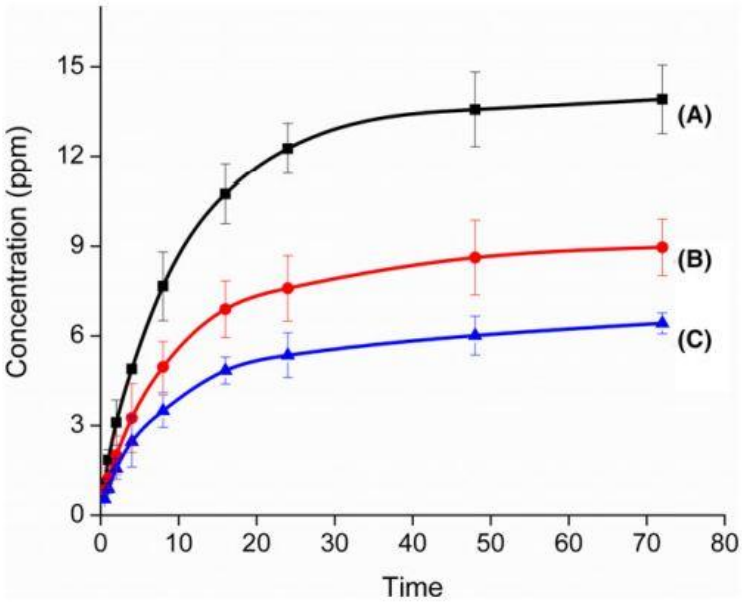

Figure 5.7. The dissolution summary of the Ca^{2+} in SBF solution as a function of time from (A) sample A, (B) sample B, and (C) sample C. (in h)

The time-dependent dissolution profile of Ca^{2+} from samples A, B, and C is shown in Figure 5.7. The amount of $Ca2^{+}$ ion leached in the solution for sample A was found to be 12.26 ppm after 24 hours and 13.91 ppm after 72 hours. In 24 hours, sample B's concentration was lowered to 7.49 ppm, and in 72 hours, it was reduced to 8.96 ppm. This was then reduced to 5.35 ppm and 6.42 ppm at 24 and 72h respectively for sample C (Table 3)

Time (h)	Sample A (ppm)	Sample B (ppm)	Sample C (ppm)
0.5	1.05	0.85	0.54
1	1.85	1.25	0.89
2	3.10	2.01	1.56
4	4.89	3.25	2.46
8	7.66	4.96	3.49
16	10.75	6.89	4.84
24	12.26	7.59	5.35
48	13.57	8.62	6.01
72	13.91	8.96	6.42

Table 3: The time-dependent dissolution profile of Ca_2^+ ion from samples A, B, and C

Assessment of Ca:Al molar ratio

The molar ratio of Ca:Al in all the samples (A, B, and C) were calculated using a conventional method.

5.8.*In vitro* Cell viability study of all the samples (A, B and C)

All three samples (A, B, and C) were examined for cell viability at three different time points (24, 48, and 72 h) using colon and breast cancer cell lines (HCT116 and MCF7) and healthy bone cells (MC3T3) (osteoblast precursor). Part A shows a strong suppression of cell growth (HCT116) to 49.79 % in 24 h for sample A, which increases to 57.64 % at 48 hours, and then to 70.77 percent at 72 hours [Figure 5.8, part A, panel (A)]. For sample A only, panel (B) exhibits a similar tendency (to a lesser extent of 39.38 % within 24 hours, followed by 43.62 % at 48 h, which increases to 46.80% at 72h respectively), However, utilising the cancer cells HCT116 and MCF7, no significant impacts were observed for samples B and C at the above-mentioned time intervals. [Figure 5.8, part A, panel (A) and (B)] Part B of Figure 5.8, panel (C), illustrates that healthy MC3T3 cells have a high vability (95-98%) in the presence of

all three samples A, B, and C, with no inhibitory effect on healthy cells. The software GraphPad PRISM 7.04 (Version) was used to analyse in vitro cytotoxicity data. The significance of the data was determined at a confidence interval (CI) of 95 percent and a value of $P<0.05$.

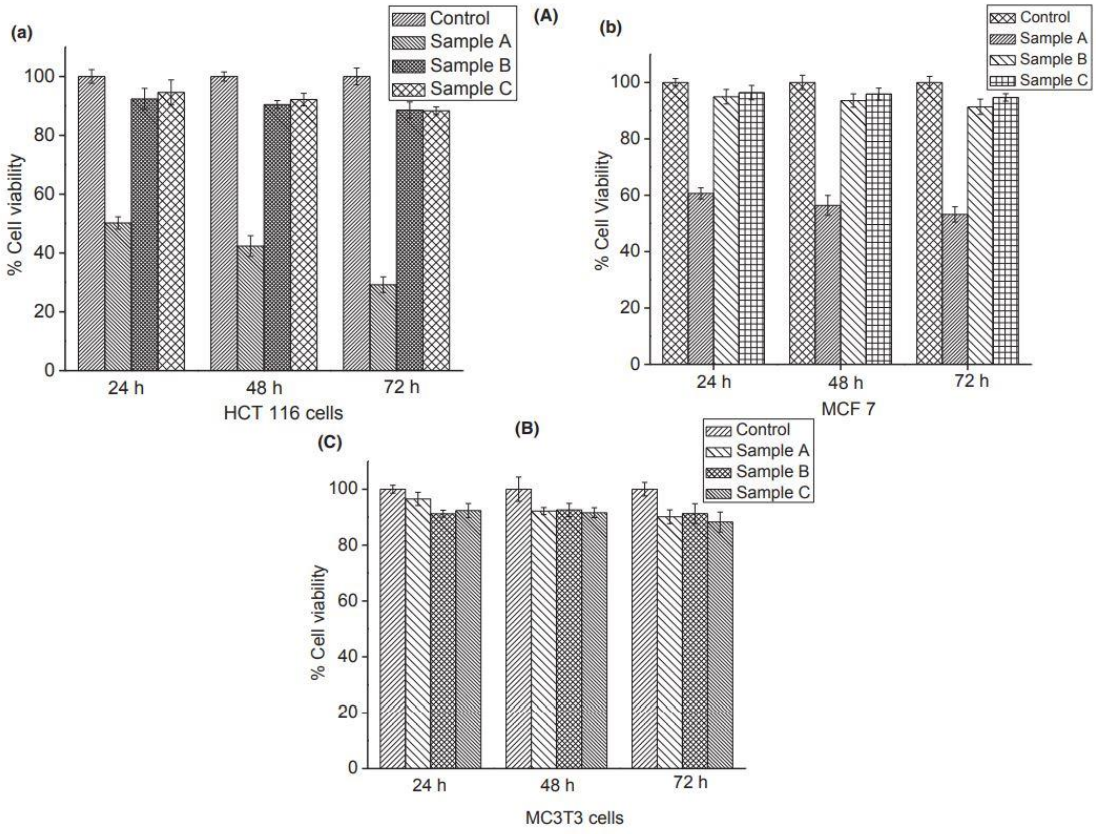

Figure 5.8. Part (A) uses samples A, B, and C to demonstrate the vitality of cancer cells (HCT 116 and MCF7). Part (B) shows the results as in the healthy cell line, MC3T3 osteoblast precursor.

The CaAl-LDHs generated at pHs 9, 10, and 11 followed the same pattern as the CaAl-LDHs discussed previously. It is now well established that the size of the mitochondrial Ca^{2+} pool is maintained under normal conditions, but that under pathological situations, a substantial amount of Ca^{2+} can accumulate in mitochondria, inducing apoptosis. The mechanism discussed as above is shown in Figure 5.9.

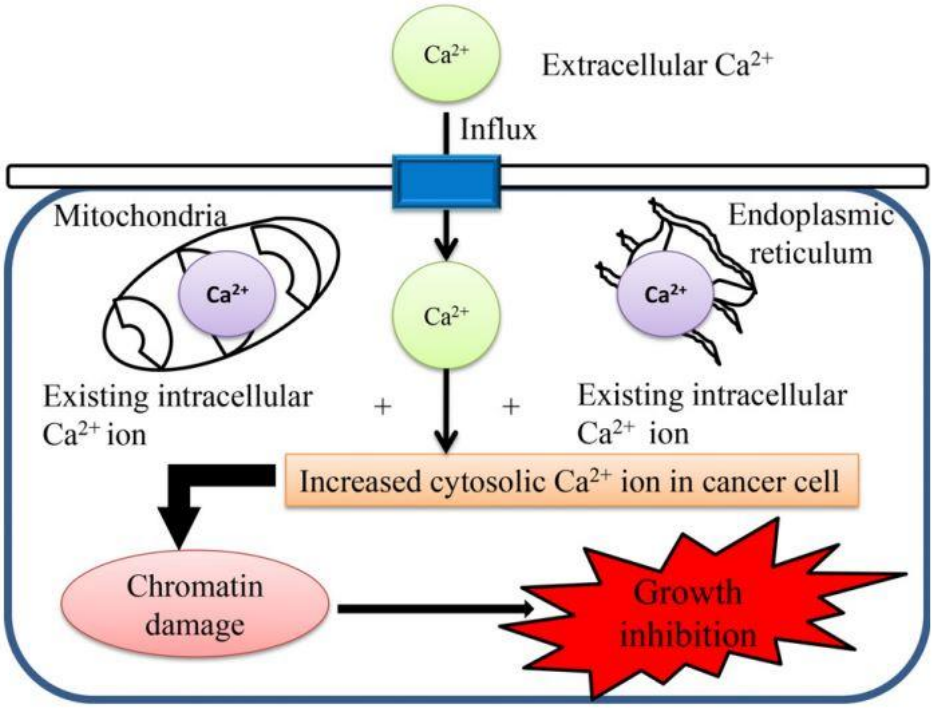

Figure 5.9. The mechanism of cancer cell growth suppression caused by extracellular Ca2+ influx

In the presence of a trace quantity of carbonate anion in the purged OH ions (1 ppm, from adsorbed ambient CO_2). In this case, both the polymorphs (calcite/aragonite) of $CaCO_3$ were precipitated, as well as phase pure CaAl-LDH. In the presence of an insoluble inorganic matrix, the metastable aragonite phase stabilises better than the thermodynamically more stable calcite phase, the impact of the soluble cation has been attributed to this (Sarkar A et al., 2013; Raz S et al., 2000). The microstrain (0.0098%) of the CaAl-LDH lattice, owing to Ca^{2+} ion with a larger ionic radius in the cationic brucite layer that was precipitated at lower pH conditions (pH:8.5) (Milkoff et al., 1992) is greatly enhanced by the heterogeneous nucleation at higher pH conditions (pH:10.5), resulting in precipitation of $CaCO_3$ (aragonite and calcite polymorphs 37%) which helps in variation of the disregistry factors and free energy of nucleation (Lioliou MG et al.,2007; Sun W et al., 2015) often results in increased lattice strain (0.0160%),

compared to the phase pure CaAl-LDH lattice. The precipitation of $CaCO_3$ (calcite and aragonite polymorph, 43 percent, bigger quantity) at pH 12.5, as explained above, causes this to increase to a higher value (0.0188 percent). Ca:Al molar ratio of all the samples confirm the phases from XRD data. Sample A exhibits highest ratio of 2, that decreases in samples B and C respectively as the Ca^{2+} ion precipitates in the form of $CaCO_3$ at higher pH condition lowering the Ca content. Aggregation-free nanoparticles with a D_{50} of 184 nm in the cationic environment of the colloidal dispersion show moderate stability at a higher electrokinetic potential of 39.30 mV for sample A. An incipient instability (29.40 mV) of the suspension is observed in case of sample B,, whereas for sample C, a significantly lower electrokinetic potential of 5.22 mV demonstrates quick coagulation or flocculation, resulting in a large amount of agglomeration. It is clear that as the pH value increases from 8.5 to 12.5, the zeta potential decreases significantly (39.30 mV to 5.22 mV), indicating a significant effect on particle stability in colloidal dispersion, based on size and charge. At higher pH values (10.5-12.5), the cationic CaAl-LDH nanoparticles encounter a higher concentration of [OH] ions in the dispersion medium, gradually approaching the system's isoelectric point (IEP) and thus the environment of maximum instability, causing particle coagulation and flocculation, and tending to form larger particles with sizes in the 400-500 nm range. In the FESEM pictures, the distinctive crystal structure of the phase pure CaAl-LDH and the precipitated $CaCO_3$ could be seen. Samples B and C, that includes $CaCO_3$ of both the aragonite and calcite polymorphs of typical crystal lattice, exhibit the previously observed phenomena of substrate assisted stabilisation of metastable phases under higher pH settings. Aragonite polymorph, for example, is linked to an interfacial host and guest interaction. Furthermore, the role of the soluble bivalent cation (e.g., Mg_2^+) on $CaCO_3$ crystallisation is well known, which supports our

findings in the production of the metastable aragonite polymorph, along with calcite, in samples B and C. Importantly, the SAED pattern produced through TEM investigation confirmed the previous observation. The carbonate anion in the samples A, B, and C were estimated by ion exclusion chromatographic technique (Haddad PR et al., 1990). The analysis was carried out using an inverse chemical suppression technique with 25 mmol L^{-1} LiCl as the regenerating solution, similar to our previous work, because detection of the carbonate anion in the nonsuppressed mode of analysis was impossible due to its weak conductivity (Chakraborty et al., 2013). The incorporation of the carbonate anion via inclusion phenomenon, which could be attributed to the increased order of the carbonate anion concentration (ppm) from samples A to C exhibiting an enhanced concentration, influenced the kinetics of the forward reaction leading to the precipitation of calcium hydroxide and then calcium carbonate, on account of the higher concentration of OH ions at higher pH. The calcium concentration of e.g., sample A ([phase pure, 100 percent CaAl-LDH) > sample B (CaAl-LDH+$CaCO_3$) > sample C (CaAlLDH+$CaCO_3$), determines the dissolution profile of Ca^{2+} at a certain time point (e.g., 24 hours). At pH more than 10, calcium ion creates hydroxide precipitates, and their solubility increases as pH decreases. Because the solubility product of calcium hydroxide Ksp is higher than that of the two crystalline polymorphs of calcium carbonate (aragonite) and (calcite), the dissolution of the Ca^{2+} ion from the hydroxide homologue is significantly greater than that of the carbonate salt. As a result, more Ca^{2+} is collected in the cells of sample A, increasing the cellular Ca^{2+} concentration and limiting cancer cell proliferation. however, in the remaining two situations, for example, samples B and C, where a mixed phase comprising the above-mentioned carbonate salts is present, lesser calcium ion dissolution leads to lower Ca^{2+} buildup in the cancer cell (HCT116 here), which is unable to achieve the inhibitory concentration.

The intracellular Ca^{2+} ion concentration and the expression of many ion channels are known to influence cancer cell death. There's also evidence that a short-lived, high-amplitude Ca^{2+} ion can cause an increase in the same in mitochondria, leading to cell death. The apoptosis pathway in cancer cells requires careful control of Ca^{2+} ion concentration in the endoplasmic reticulum (ER), which necessitates a complex interplay between key receptors such as IP3R, RyR, and SERCA, as well as signalling proteins activated by calcium-sensing G-protein-coupled receptors (GPCR). This observation supports the previous explanation, indicating that an increased amount of intracellular cytosolic Ca^{2+} ion, because of buildup over a 72-hour period, causes the ion to pass through the mitochondria, perhaps inhibiting cell growth (Figure 5.9). In contrast to samples B and C, which have larger particle sizes, sample A (phase pure CaAl-LDH) has a smaller particle size, which allows it to pass into the cancer cell more easily, probably by an endocytosis mechanism. Further the rate of growth inhibition of MCF7 cells is substantially lower than that of the above cell line, and this is due to a special property of MCF7 breast cancer cells that overexpresses the isoforms of both specific Ca^{2+} inflow and Ca^{2+} sequestering channel or efflux pumps. They also have a Ca^{2+} eflux mechanism that corresponds to the Ca^{2+} channel influx channel expression. As a result, as the MCF7 cell's ability to efflux Ca2+ ion increases, the likelihood of growth inhibition in MCF7 cells decreases, as shown in Figure 5.8, part A, panel (B). At a 95 % confidence range (CI), a significant statistical difference ($P<0.05$) was found in the in vitro cytotoxicity assay of sample A. value results in less calcium ion dissolution, which leads to less calcium ion accumulation in cancer cells (HCT116 and MCF7), which gradually reduces anticancer efficacy, as discussed above, based on intracellular calcium ion concentration and its influence on cancer cell apoptosis.

Results: Part 2

5.9. PXRD analysis sample A (phase pure CaAl-LDH) and sample B (ETO incorporated CaAl-LDH)

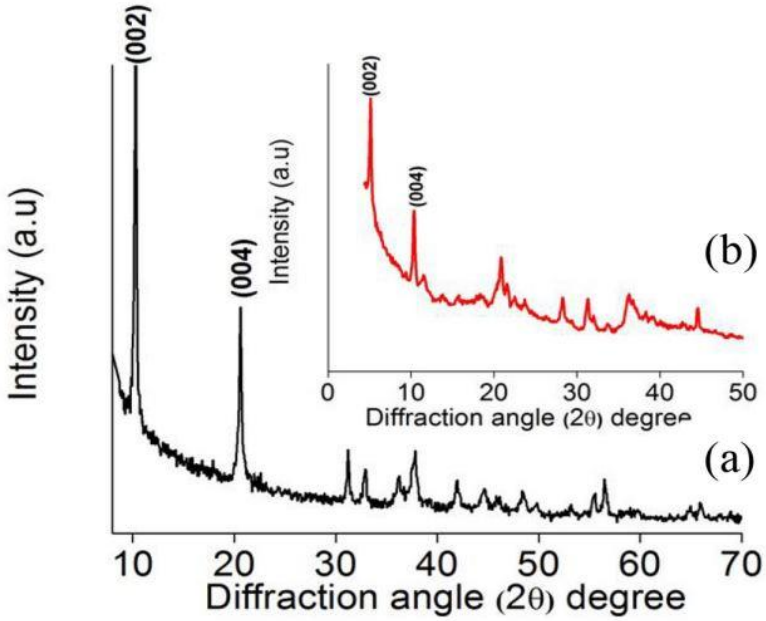

Figure 5.9. Powder X-ray diffraction patterns of (a) sample A (phase pure CaAl-LDH) (b) sample B (ETO incorporated CaAl-LDH).

Figure 5.9. shows the powder X-ray diffraction (XRD) patterns of samples A and B. For layered clay materials, almost all the characteristic planes show a fine crystalline hydrotalcite-like phase with characteristic (00l) reflections that are precisely indexed to hexagonal lattice structure with rhombohedra group (Chakraborty et al., 2013). As shown in Figure 5.9, the basal spacing (d002) of 8.5764 corresponds to the (002) diffraction peak of sample A (JCPDF 01-089-6723), which rose to 17.18 in sample B as the corresponding peak (002) migrated from $2\theta = 10.31$ to $2\theta = 5.14$. This is owing to the enlargement of the interlayer space caused by the drug ETO being inserted into sample A along the z-axis, which represents the layer stacking direction in the nanoconjugate. The (hkl) indexing was used to assess the lattice parameters along the

c axis in the hexagonal crystal structure for Sample A and Sample B. For Sample A and Sample B, the c value increased from 17.14 to 34.36, respectively (Kim et al., 2012). We used the well-known Scherrer formula (Scherrer, 1918) to assess the size of the crystallite and strain of the precipitated phases by single profile analysis from the same plane in this study:

Crystallite size $K\gamma = B \cos \theta$

(%) Lattice strain$= B/(4 \tan \theta)$

Lattice strain is the force created when an atom is displaced from its normal lattice location, which is most caused by crystal defects. The initial residual strain of the hexagonal lattice structure of Sample A is larger due to a micro-strain presumably related to lattice deformation, as shown by the above data (Table 4).

Table: 4 The crystallite size and lattice strain of sample A (Bare phase pure LDH) and sample B (Nanoconjugate) along (002) plane from single profile analysis using Scherrer formula.

Sample name	**Peak position (002) 2Ɵ**	**Crystallite size (nm)**	**Lattice strain (%)**
Sample A	10.31	10.31	0.0194
Sample B	5.14	41.55	0.011

To compensate for the inherent strain, this event may result in an increased force of repulsion between the cationic layers. Furthermore, the strain was reduced because of the insertion of ETO with an anionic side, which aids in imparting an interaction between the layers, lowering the strain. This observation corroborated the preceding

findings (Chakraborty et al., 2016). Figure 5.10 A shows the FT-IR spectra of sample A and sample B. The stretching vibration of metal oxygen (M-O) bonds may be responsible for a few of low intensity bands in the region of 500 cm^{-1} to 750 cm^{-1} (Chakraborty et al., 2011; Chakraborty et al., 2012; Alexa et al., 2013). Furthermore, the stretching vibration at around 1388 cm^{-1} corresponds to NO ions in sample A, but it was found to be less intense at the same place in sample B, indicating a reduction in NO_3 ions in the interlayer region due to an anion exchange process with ETO.

5.10. FTIR analysis of Sample A, Sample B and Etoposide

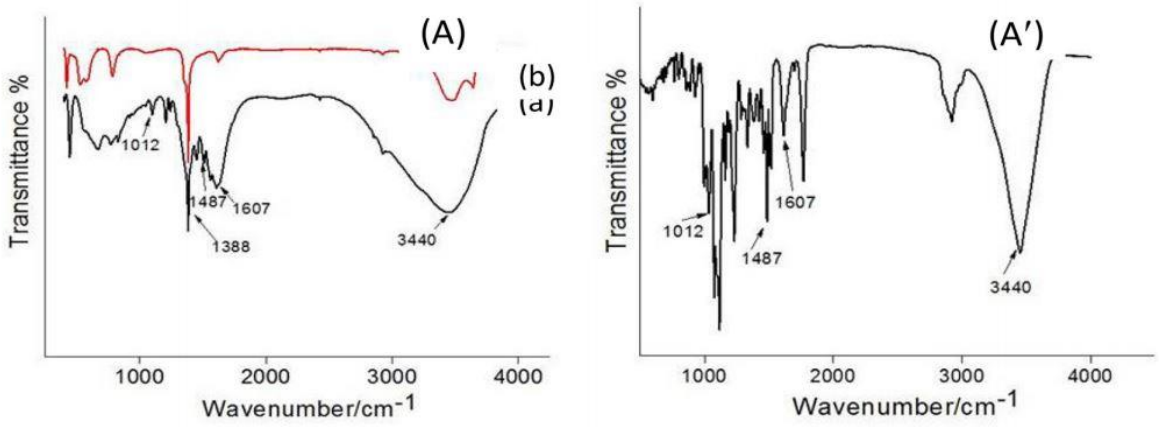

Figure 5.10. (A) FT-IR spectra of (a) sample A (b) sample B (A') FT-IR spectrum of bare ETO drug showing the characteristic vibration bands.

In both samples, the absence of a vibration peak about 1362 cm^{-1} indicates the absence of CO_3^{2-} anion in the interlayer space. The presence of (C-O stretch of carboxyl methyl) bonds in the ETO structure could explain the stretching vibration at 1610 cm^{-1}. In addition, the bands at 1012 cm^{-1} and 1487 cm^{-1} in Sample B could be attributable to the existence of aromatic $–OCH_3$ and C-C stretching vibrations. The stretching vibration of the labile hydroxyl (O-H) group in both samples is represented by the absorption band at roughly 3440 cm^{-1} (Wang et al., 2018).

5.11. Hydrodynamic diameter of Sample A and Sample B

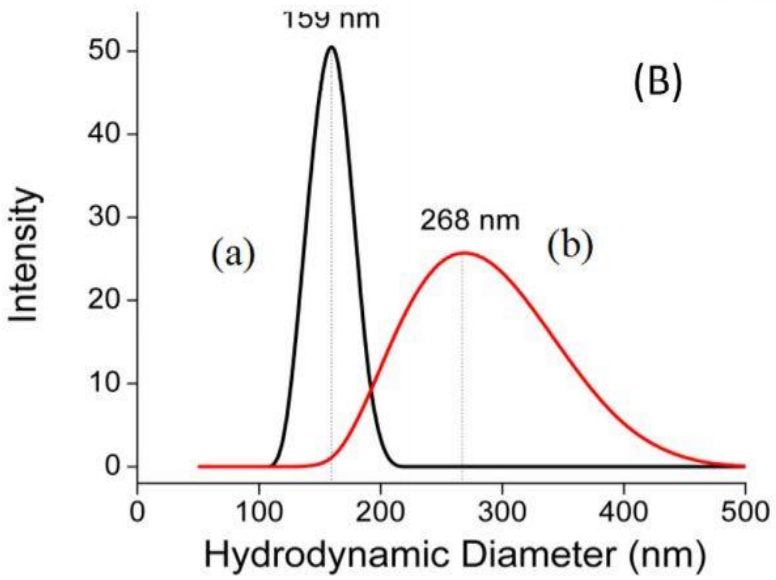

Figure 5.11. (B) Hydrodynamic diameter of (a) sample A (b) sample B.

The hydrodynamic diameter of sample A and sample B, as measured by dynamic light scattering (DLS), is shown in Figure 5.11. Both samples have a unimodal size distribution in the range of 130–200 nm and 210–330 nm, respectively, with a polydispersity index (PDI) in the range of 0.15–0.20 in the current investigation. Sample A has a D_{50} of 159 nm, while sample B has a D_{50} of 268 nm. Furthermore, the electro kinetic potential of sample A is 37.30 mV, indicating moderate stability, and stability has been marginally lowered to 27.2 mV after intercalation of the drug molecule (Sample B). This could be due to nanoparticle agglomeration, which eventually leads to flocculation of the particle in suspension near the isoelectric point (Rahaman et al., 2019).

5.12. Morphological assessment of Sample A and Sample B

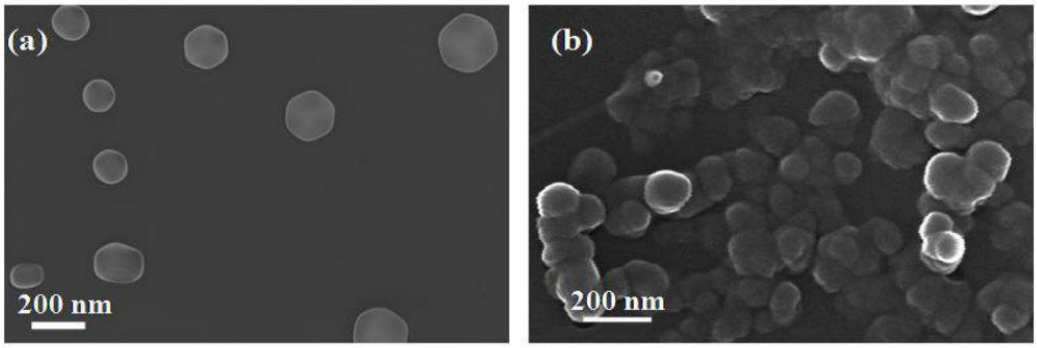

Figure 5.12. FESEM image of (a) sample A (b) sample B.

FESEM pictures of sample A show well dispersed CaAl-LDH nanoparticles with virtually hexagonal morphology of the layered double hydroxide, whereas particle size was increased in sample B due to mild agglomeration, which had a substantial impact on sample B's stability (Figure 5.12.).

5.13. Thermogravimetric assessment of bare drug (ETO), sample A and B

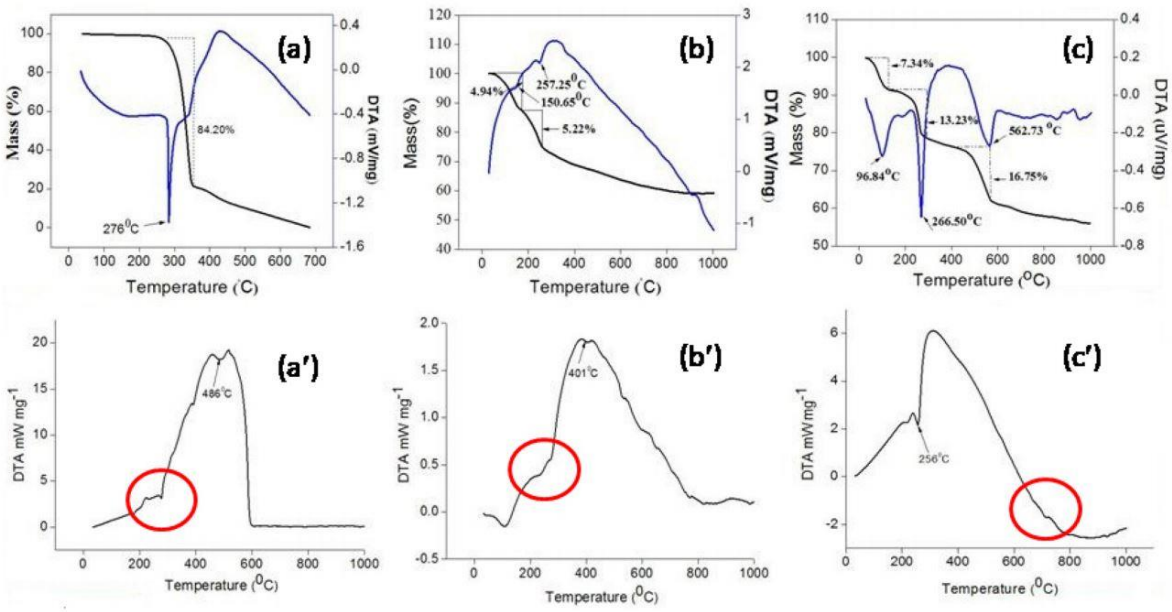

Figure 5.13. Thermogravimetric analysis (TG-DTA) and DSC of (a, a') ETO (b,b') sample A and (c,c') sample B.

When heated to 1000 °C, both samples (A and B) lose 41.5 percent and 47 percent of their total weight, respectively, whereas the naked ETO drug loses nearly 99 percent of its mass when heated to 700 °C. A deep endotherm for raw ETO drug in Figure 5.13 (a) (arrow highlighted) correlates to the start of the decomposition process, which lasted until 450 °C, as evidenced by DSC data in Figure 5.13 (a). Due to breakdown of organic and inorganic anions, mass loss of sample A and sample B happened largely at two temperature areas about 150 °C and 266 °C (arrow marked). Dehydroxylation was responsible for nearly 10.26% mass loss in sample A and 20.57% mass loss in sample B when heated to 235 °C. This further increased to 36% on heating at 650 °C owing to breakdown of interlayer anions, in sample A whereas sample B exhibited a mass loss of 41.23% owing to decarboxylation of ETO and decomposition of remaining nitrate and other charge balancing anions. The rest of 6% weight loss in sample B is due to dehydroxylation from the layered double hydroxide and oxide-based lattice structure when heated to roughly 800 °C. The comparable DSC patterns, shown in panels (b') and (c'), support and connect the preceding data (marked by red circle). Finally, the naked drug (ETO) showed significant mass loss of over 80% up to around 400 °C, as seen by the TG-DTA plot [Figure 5.13 a]. At the same temperature, the mass loss of the bare LDH (sample A) was only around 30%, as shown in Figure 5.13 (b), which can be attributed to the bare LDH system's typical thermal deterioration trend (Mahjoubi et al., 2017) whereas, the same for sample B was found to be around 25% (Figure 5.13 (c), demonstrates the increased thermal stability of the encapsulated ETO in the LDH nanoparticles which is self-explanatory to conclude that there is almost no mass loss corresponding to the intercalated ETO drug. The UV-VIS spectroscopy calibration curve of etoposide standard yielded in vitro drug loading of 27.72 percent in sample B.

5.14. *In vitro* drug release kinetics from sample B and physical mixture

To suit the in vitro ETO release from sample B, different release kinetics models were used. The dialysis membrane diffusion technique was used to investigate the in vitro ETO release from sample B and a physical mixing of the two (ETO and sample A) (Ray et al., 2015). The dialysis chamber kept both samples and allowed the medication to diffuse into the receiver compartment right away. In phosphate buffered solution at pH 7.4, the release profiles of ETO from sample B and physically mixed powder (ETO and sample A) are shown in Figure. 5.14 (c–f). Result suggested that due to the lack of drug and nanocarrier interaction in the physical mixture almost complete (99.5%) release in the former case, within 12 h whereas in case of nanohybrid, the cumulative release of ETO from sample B exhibits an initial burst release of nearly 40% from the within the first 2 h owing to the loosely bound drug on the surface of the nanoparticle. The leftover drug, intercalated within the nanoparticle's interlayer space, follows ETO's prolonged release for up to 72 hours, which could be due to ETO's slow diffusion from the interlayer space of sample B (Ray et al., 2015).

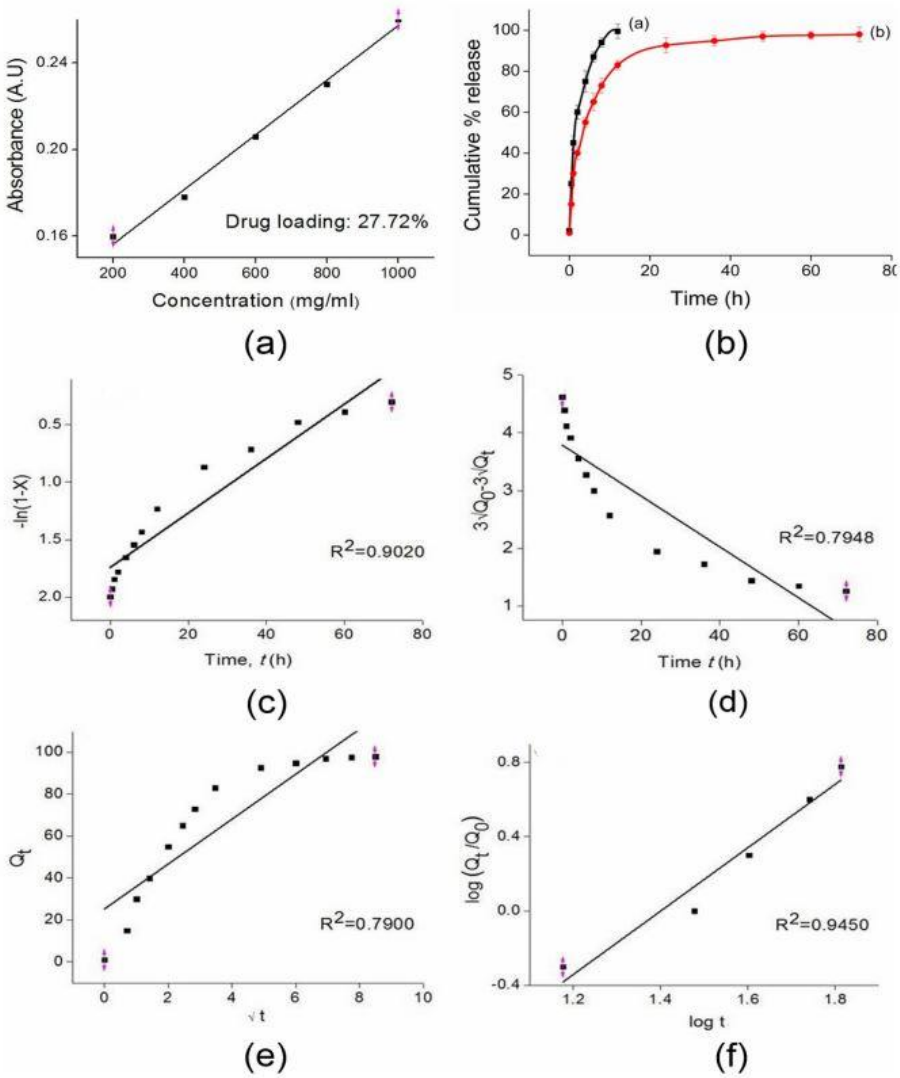

Figure. 5.14 (a) Calibration curve of etoposide gained from UV-VIS spectroscopy; (b) In vitro release of ETO from (a) Physical mixture of sample A and ETO (1:1, w/w) (b) sample B in phosphate buffer saline at pH 7.4; (c)-(f) Release kinetics models (a) First-order model; (b) Hixon Crowel model; (c) Higuchi model (d) Korsmeyer-Peppas model.

The above mentioned release kinetic models were fitted to the above-mentioned in vitro release data: The correlation coefficients for the first order, Higuchi model, Hixon-Crawel equation, and Korsmeyer–Peppas models were determined (Figure. 5.14) (Peppas, 1985; Dash et al., 2010; Bhaskar et al., 1986) (Table 5).

Kinetic Model	Mathematical equation	Parameter (R^2)
First order	$Q_t = Q_0 e^{-Kt}$	0.9020
Hixon Crowel	$3\sqrt{Q_0} - 3\sqrt{Q_t} = K_{HC}.t$	0.7948
Higuchi	$Q_t = K_H\, t^{1/2}$	0.7900
Korsmeyer–Peppas	$F = (Q_t / Q_0) = K_m\, t^n$	0.9450

Table 5: The correlation coefficients for the first order, Higuchi model, Hixon-Crawel equation, and Korsmeyer–Peppas models

Importantly, based on the obtained correlation coefficient (R2) value 0.9450, the Korsmeyer-peppas model is proposed for the release of ETO from sample B. Furthermore, the kinetic exponent 'n' for sample B was 0.107, showing that the drug was released from the matrix in a regulated manner following a quasi-Fickian diffusion phenomena (Sahoo et al., 2012).

5.15. Assessment of IC_{50} of bare drug (ETO) and Sample B

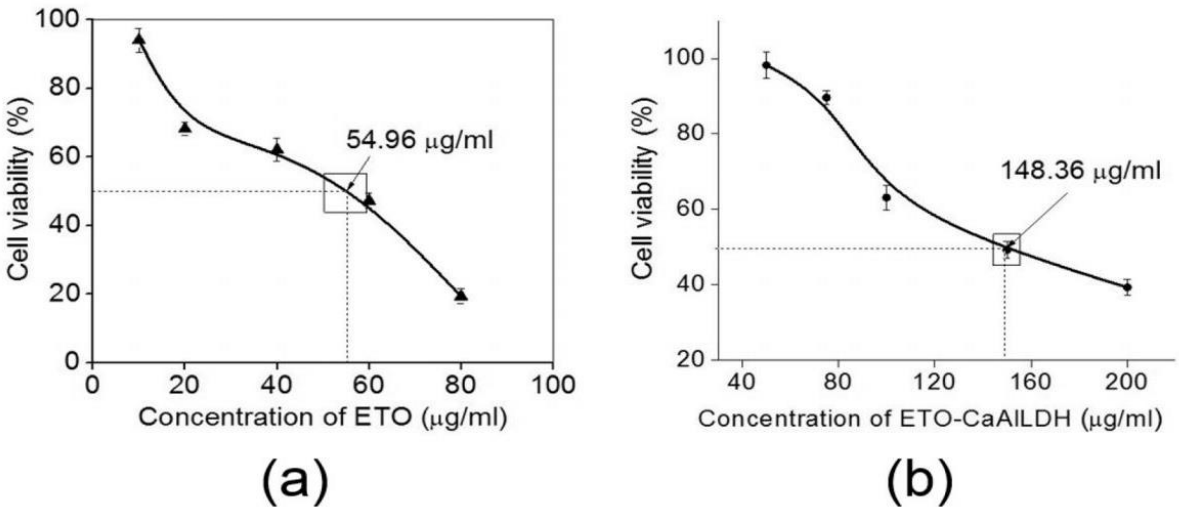

Figure 5.15. The half maximal inhibitory (IC_{50}) concentration of (a) ETO treated on A549 cell line (b) sample B treated on A549 cell line

The half maximum inhibitory concentration (IC_{50}) is a measure of a drug's potency, and it indicates the concentration required to inhibit a biological or biochemical function to its 50%. To assess ETO's efficacy in reducing the proliferation of the human adenocarcinoma (A549) cell line, the IC_{50} was measured (Saha et al., 2020). For this, an ETO stock solution (1mg ml^{-1}) was made in DMEM by dissolving ETO in it. ETO's IC50 was determined at five distinct doses (5, 10, 20, 40, and 60 µg ml^{-1}). The IC_{50} value of ETO was 54.96 µg ml^{-1} as shown in Figure 5.15 a, with a substantial dose-dependent response profile lasting up to 24 hours. Further, the IC_{50} value of sample B was evaluated at 24 hours after the A549 cells were treated with sample B to the amount of 50, 75, 100, 150, and 200 µg ml^{-1}, considering the drug loading percent (27.72%) and the IC_{50} value of ETO, as previously described. The IC_{50} value of sample B was 148.36 µg ml^{-1} after 24 hours, indicating that sample B has a significant synergistic anticancer potential when compared to bare ETO, as the drug concentration decreased from 54.96 µg ml^{-1} to 41.12 µg ml^{-1} (based on the percent drug loading in sample B, 27.72 percent) in this case.

5.16. *In vitro* cell viability and cell migration assay of ETO, sample A and B

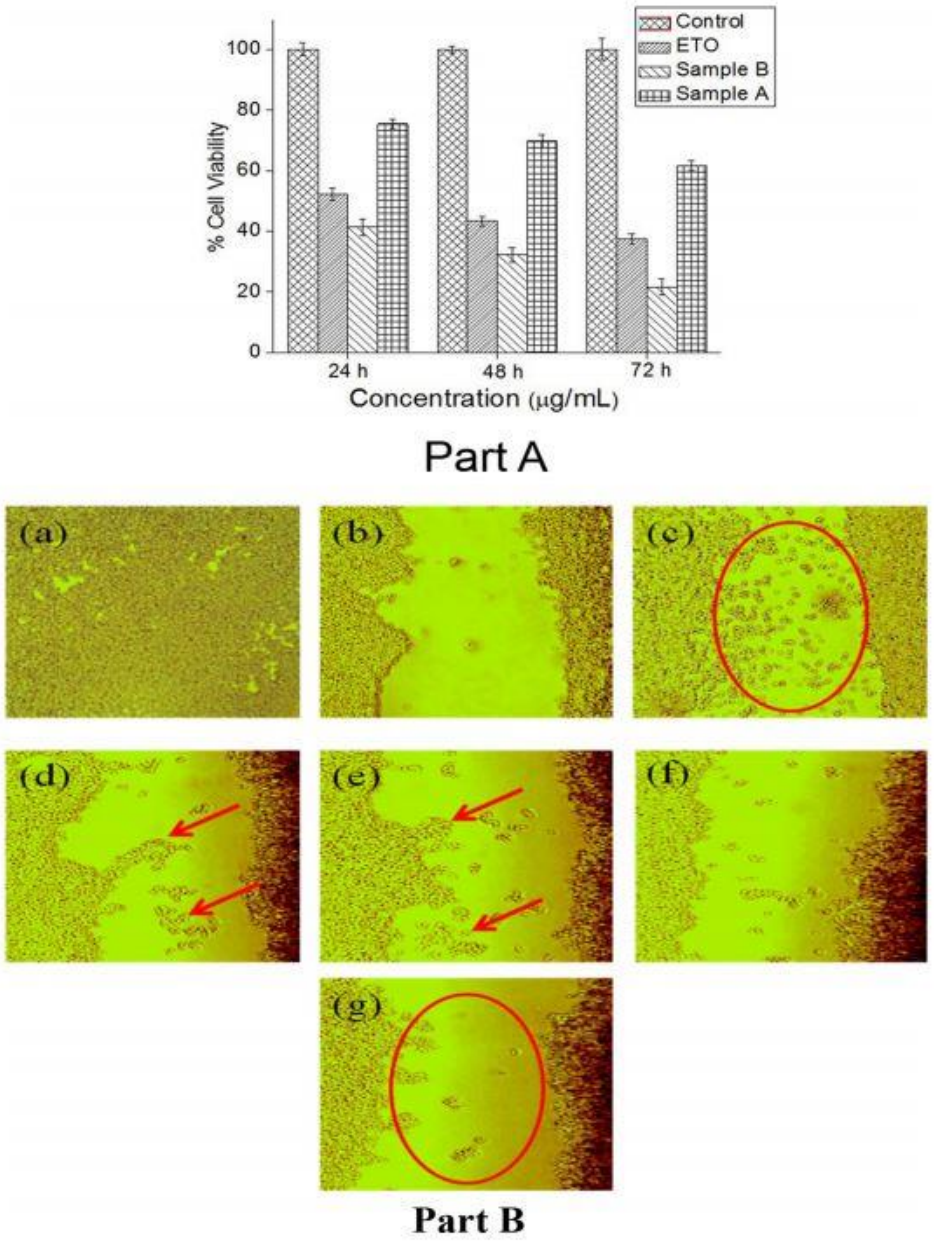

Figure 5.16. (A) In vitro cell viability study of the ETO, sample A and sample B on A549 cell line in varying time including 24, 48 and 72 h respectively; (B) In vitro cell migration assay shows (a) Confluent cells in 6 well plate (b) scratch by micropipette on the confluent plate (c) A549 cells without treatment (d) Cells treated with sample A (e)

Cells treated with ETO (f) A549 cell treated with physical mixture (1:1, w/w) (g) Cells treated with Sample B

To test the synergistic anti-cancer potential of sample B, an in vitro cell viability investigation (Figure 5.16. A) was performed on the A549 cell line. Sample B's cell viability was reduced to 21.56 % after 72 hours when compared to bare ETO and sample A which showed a viability of 37.45 % and 61.85 %, respectively ($P<0.05$). This is due to the cells' selectivity and the induction of mitochondrial apoptosis in cancer cells by disrupting the cellular membrane, that depends on ROS generation, which plays a crucial role in disrupting mitochondrial function and leading to apoptosis (Maiyo and Singh, 2017). Furthermore, the intracellular Ca^{2+} concentration is important in controlling the apoptotic pathway in the endoplasmic reticulum (ER), which involves a delicate interplay between several receptors, including IP3R, RyR, and SERCA, as well as various signalling proteins, all of which are activated by the calcium-sensing G-protein-coupled receptor (GPCR). This apoptotic mechanism backs up the previous findings (Saha et al., 2018). The proliferation/migration assay of the A549 cell line is shown in Figure 5.15**.**B after treatment with sample A, bare ETO, physical mixure of CaAl-LDH and ETO in (1:1 w/w ratio), and sample B. We found that sample A treated cells proliferate at 48.70 % compared to 59.34 % in control cells, indicating anti-cancer action similar to that previously reported by our study group (Bhattacharjee et al., 2019). Further, proliferation was much lower in sample B (18.62%) compared to bare ETO (37.89%), and physical mixure of CaAl-LDH and ETO in (1:1 w/w ratio) was 34.66 % ($P<0.05$), indicating sample B's synergistic anticancer potential (ETO intercalated in sample A). Due to the failure to give the drug with a prolonged release effect from the nanoconjugate, the physical mixture did not show substantial cytotoxicity when compared to Sample B. It is clear that cell proliferation/migration is

a multi-step, extremely complex process that is predominantly influenced by membrane flow model (Bretscher, 1983) in which a component integrin is very much required which attaches the cells to surface that helps in proliferation of the cells. Furthermore, the rise in intracellular Ca^{2+} ion concentration is required for cancer cell death (Bose et al., 2015). Furthermore, the anti-cancer medicine etoposide works by inhibiting the enzyme topoisomerase II, which causes DNA damage that leads to apoptosis (Maanen et al., 1988). The synergistic anti-cancer potential of sample B (ETO intercalated CaAlLDH) could be linked to the apoptotic pathway mechanism described above. The cellular absorption of sample B in the A549 cell line, which was expressed by Fluorescein isothiocyanate, was measured by flow cytometry (FITC).

5.17. Cellular uptake study of Sample B into A549 cell line

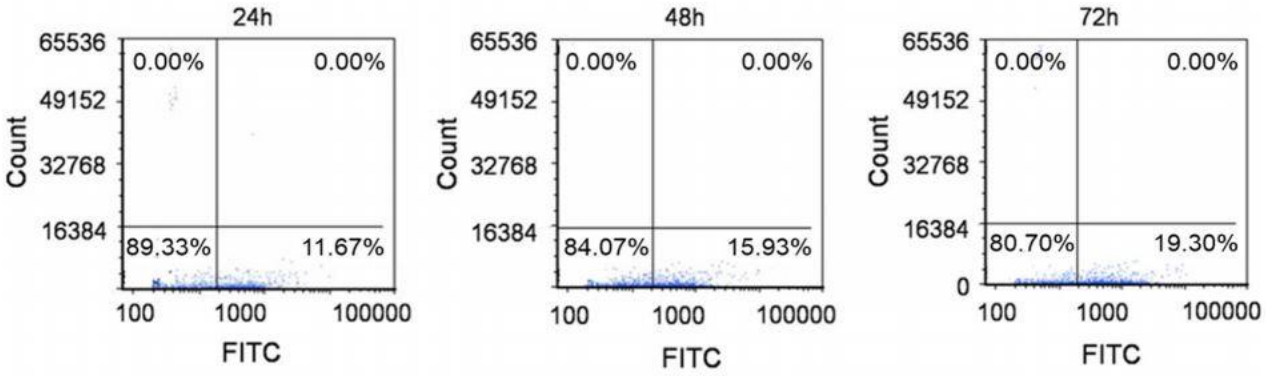

Figure 5.17 exhibits uptake of FITC tagged sample B into A549 cell line, showing internalization of the nanoconjugate into the cell (sample B);

Figure 5.17 shows conventional FACS profiles, which shows a strong uptake profile of sample B in a time-dependent manner. The cellular absorption was determined to be 11.67 % after 24 hours and rose to 19.30 % after 72 hours of incubation. This finding backs with evidence from an in vitro cytotoxicity study, which implies that sample B has a synergistic anti-cancer effect.

5.18. Cellular internalization of sample B in A549 cell line

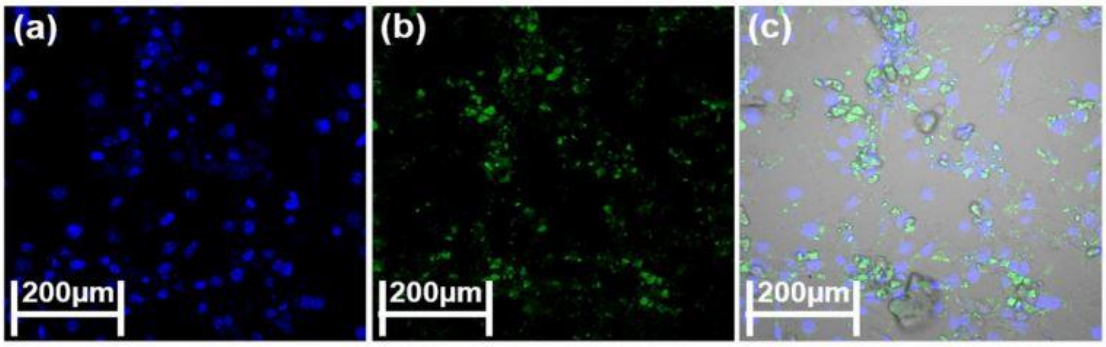

Figure 5.18. Confocal image of (a) DAPI image (b) FITC image (c) superimposed image.

Confocal laser scanning microscopy (CLSM) pictures, displayed in Figure 5.18, corresponding to 24 hours of incubation time, confirmed the above observation of cellular uptake of the FITC tagged sample B employing A549 cells. The presence of FITC-tagged sample B in the intracellular matrix indicated that sample B had successfully internalised the matrix, which was confirmed by nuclei stained by DAPI. Because an elevated quantity of Ca^{2+}/calmodulin protein kinase II (CAMKII) was expressed in cancer cell proliferation and migration, sample A and sample B were employed to modulate cellular function in this investigation.

5.19. Protein expression assay of sample B

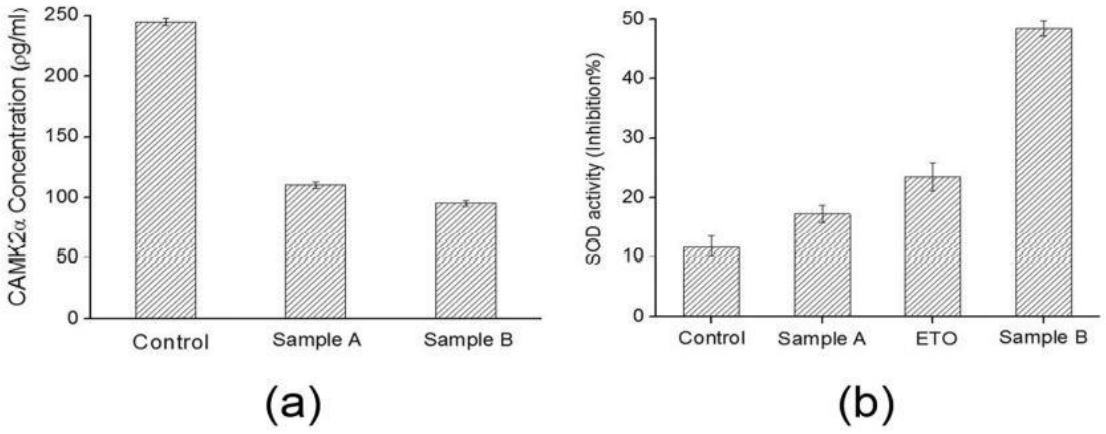

Figure 5.19. exhibits (a) CAMKIIα expression assay; (b) SOD expression assay.

After 24 hours of incubation in the CAMKII expression experiment, this specific protein was found to be 244.78 pg/ml in the A549 cell line whereas in case of sample A and B treated sample CAMKIIα was reduced to 110.52 pg/ml and 95.14 pg/ml respectively ($P>0.05$) Figure 5.19. Furthermore, self-associative / changeable domains control (Evans and Shea, 2009) the interaction of CaMKII enzyme with calcium and calmodulin, and an increase in calcium and calmodulin concentration causes inactivation of this specific enzyme (Yamagata et al., 2006). By lowering superoxide dismutase (SOD) enzyme activity, CAMKII regulates the formation of reactive oxygen species (ROS). Furthermore, a normal SOD level is required for the cells' intrinsic function to be maintained (Zhou et al., 2014). The calcium content of samples A and B has a direct effect on Ca^{2+}/calmodulin protein kinase II (CAMKII). As a result, we observed a similar modulatory impact of CAMKII after treating both samples. Etoposide is well recognised for increasing the production of reactive oxygen species (ROS), which causes cancer cells to die (Conklin, 2004).

According to the results of the experiment, etoposide reduces SOD enzyme activity, which increases ROS production, which is essential for cancer cell apoptosis. Because of the presence of the drug Etoposide in sample B only, the difference in modulation of SOD activity by sample A and sample B is significant, as mentioned above. To measure SOD activity, A549 cells were subjected to sample A and sample B in this investigation. Sample B showed a substantial suppression of SOD activity when compared to the control ($P < 0.05$) (See Fig. 5.19 b) The synergistic anticancer potential of sample B is understood due to the major participation of Ca^{2+} ion in both CAMKII and SOD activity at the cellular level, which is in conformity with all the preceding results.

Chapter 6

Conclusion

Conclusion

The study demonstrates a pH-dependent synthesis of CaAl-LDH by a straightforward coprecipitation approach technique (at pH 8.5, pH 10.5, and pH 12.5). Surprisingly, phase pure CaAl-LDH was generated at a lower pH 8.5 but an increase in pH results in the development of $CaCO_3$ (both aragonite and calcite polymorphs) (pH 10.5 and 12.5), as well as CaAl-LDH. In Sample A, XRD data revealed the characteristic planes of phase pure CaAl-LDH, however in the case of the mixed phases, the signature peaks of both aragonite and calcite could be detected. The SAED pattern of TEM, in turn, confirmed the observation. Based on the varied pH of the precipitation, the particle size was discovered to be in the range of 150-500 nm. Further the in vitro cytotoxicity study using human colon cancer cell line (HCT116) revealed growth suppression using sample A after 24 hours, which increased to 70.77 percent after 72 hours, showing substantial anticancer efficacy. For obvious reasons, this was not particularly efficient (46.80% after 72 hours) in the instance of breast cancer cells (MCF7). Healthy bone cells (MC3T3) were used to confirm the findings, and all three samples showed good vitality (95-98%). In this part the present study opens a new avenue for using phase pure (100%) CaAl-LDH as an active anticancer agent. Moreover, anti-cancer drug etoposide was intercalated into the phase pure LDH. When comparing the CaAl-LDH-ETO nanoconjugate (sample B) to bare CaAl-LDH (sample A) and the etoposide drug, the synergistic anti-cancer capability of the CaAl-LDH-ETO nanoconjugate (sample B) was discovered. The etoposide drug was successfully intercalated into the interlayer space of the bare phase pure sample A (CaAl-LDH at a pH 8.5) after an increase in basal spacing (d002) from 8.5764 to 17.18 Å. Particle size increased from 120 to 200 nm in bare phase pure CaAl-LDH nanoparticles to 230–320nm in etoposide intercalated CaAl-LDH that was attributed to flocculation/agglomeration of CaAl-LDH-ETO

nanoconjugates on intercalation. At pH 7.4, the etoposide release investigation revealed that the release kinetics follows a quasi Fickian diffusion phenomenon (Korsmeyer-Peppas model). Further the in vitro cell viability on A549 (human lung adenocarcinoma) cells showed considerable growth inhibition (21.56 percent in 72 hours) when sample B (ETO loaded nanoconjugate) was used, which was subsequently investigated as corroborated by cell proliferation/migration assay. The cellular absorption in the A549 cell line was reported to be 11.67 percent after 24 hours and increased to 19.30 percent after 72 hours of incubation. After 24 hours of incubation, CAMKIIα expression in the A549 cell line was determined to be 244.78 pg/ml, which was reduced to 110.52 pg/ml and 95.14 pg/ml in samples A and B, respectively. SOD gene activity was downregulated up to fourfold in sample B compared to control and twofold compared to bare ETO in the SOD assay.

In conclusion, this study uncovers a novel element of synergism for etoposide a well-known anticancer drug and a suitable delivery carrier (phase pure CaAl-LDH) which provides a new route for its application in a more effective way in the management of lung carcinoma.

Chapter 7

Bibliography

References

Aabid Shalla, Mushtaq Bhat, Chapter Twelve - Smart polymer composites in drug delivery, Editor(s): Showkat Ahmad Bhawani, Anish Khan, Mohammad Jawaid, In Woodhead Publishing Series in Composites Science and Engineering, Smart Polymer Nanocomposites, Woodhead Publishing, 2021, Pages 261-294, ISBN 9780128199619.

Aisawa, S., Sasaki, S., Takahashi, S., Hirahara, H., Nakayama, H., Narita, E., 2006. Intercalation of amino acids and oligopeptides into Zn–Al layered double hydroxide by coprecipitation reaction. J. Phys. Chem. Solids 67, 920-925.

Aisner, J., Lee, E.J., 1991. Etoposide current and future status. Cancer 67 (1), 215–219.

Alexa, I.F., Pastravanu, C.G., Ignat, M., Popovici, E., 2013. A comparative study on longterm MTX controlled release from intercalated nanocomposites for nanomedicine applications. 106, 135–139.

Alcantara, A.C.S., Aranda, P., Darder, M., Ruiz-Hitzky, E., 2010. Bionanocomposites based on alginate-zein/layered double hydroxide materials as drug delivery systems. J. Mater. Chem. 20, 9495-9504.

Ali, S.H.H.A., Al-Qubaisi, M., Hussein, M.Z., Zainal, Z., Hakim, M.N., 2011. Preparation of hippurate-zinc layered hydroxide nanohybrid and its synergistic effect with tamoxifen on HepG2 cell lines. Int. J. Nanomedicine. 6, 3099-3111.

Ambrogi, V., Fardella, G., Grandolini, G., Perioli, L., 2001. Intercalation compounds of hydrotalcite-like anionic clays with antiinflammatory agents--I. Intercalation and in vitro release of ibuprofen. Int. J. Pharm. 220, 23-32.

Aramendı, x, a, M., x, a, A., Borau, V., Jiménez, C., Marinas, J.M., Ruiz, J.R., Urbano, F.J., 2002. Comparative Study of Mg/M(III) (M=Al, Ga, In) Layered Double

Hydroxides Obtained by Coprecipitation and the Sol–Gel Method. J. Solid State Chem. 168, 156-161.

Arriagada, R., Bergman, B., Dunant, A., 2004. The international adjuvant lung cancer trial collaborative group. Cisplatin-based adjuvant chemotherapy in patients with completely resected non-small cell lung cancer. N. Engl. J. Med. 350, 351–360.

Ay, A.N., Zümreoglu-Karan, B., Temel, A., Rives, V., 2009. Bioinorganic Magnetic Core−Shell Nanocomposites Carrying Antiarthritic Agents: Intercalation of Ibuprofen and Glucuronic Acid into Mg−Al−Layered Double Hydroxides Supported on Magnesium Ferrite. Inorg. Chem. 48, 8871-8877.

Babakhani, S., Talib, Z.A., Hussein, M.Z., Ahmed, A.A.A., 2014. Optical and Thermal Properties of Zn/Al-Layered Double Hydroxide Nanocomposite Intercalated with Sodium Dodecyl Sulfate. J. Spectrosc. 2014, 1-10.

Bajpai, P.K., Benghuzzi, H.A., 1988. Ceramic systems for long-term delivery of chemicals and biologicals. J Biomed. Mater. Res. 22, 1245-1266.

Bajpai, P.K., Graves, G.A., 1980. Porous ceramic carriers for controlled release of proteins, polypeptides, hormones and other substances within human and mammalian species, US. Patent No. 4218255.

Balcomb, B., Singh, M., Singh, S., 2015. Synthesis and Characterization of Layered Double Hydroxides and Their Potential as Nonviral Gene Delivery Vehicles. Chem. Open. 4, 137-145.

Bao, H., Yang, J., Huang, Y., Xu, Z.P., Hao, N., Wu, Z., Lu, G.Q., Zhao, D., 2011. Synthesis of well-dispersed layered double hydroxide core@ordered mesoporous silica

shell nanostructure (LDH@mSiO(2)) and its application in drug delivery. Nanoscale. 3, 4069-4073.

Barahuie, F., Hussein, M., Fakurazi, S., Zainal, Z., 2014a. Development of Drug Delivery Systems Based on Layered Hydroxides for Nanomedicine. Int. J. Mol. Sci. 15, 7750.

Barahuie, F., Hussein, M.Z., Arulselvan, P., Fakurazi, S., Zainal, Z., 2014b. Drug delivery system for an anticancer agent, chlorogenate-Zn/Al-layered double hydroxide nanohybrid synthesised using direct co-precipitation and ion exchange methods. J. Solid State Chem.217, 31-41.

Barriga, C., Jones, W., Malet, P., Rives, V., Ulibarri, M.A., 1998. Synthesis and Characterization of Polyoxovanadate-Pillared Zn−Al Layered Double Hydroxides: An X-ray Absorption and Diffraction Study. Inorg. Chem. 37, 1812-1820.

Bechet, D., Couleaud, P., Frochot, C., Viriot, M.L., Guillemin, F., Barberi-Heyob, M., 2008. Nanoparticles as vehicles for delivery of photodynamic therapy agents. Trends Biotechnol. 26, 612-621.

Bégu, S., Aubert-Pouëssel, A., Polexe, R., Leitmanova, E., Lerner, D.A., Devoisselle, J.-M., Tichit, D., 2009. New Layered Double Hydroxides/Phospholipid Bilayer Hybrid Material with Strong Potential for Sustained Drug Delivery System. Chem. Mater. 21, 2679-2687.

Ben-Shushan, D., Markovsky, E., Gibori, H., Tiram, G., Scomparin, A., Satchi-Fainaro, R., 2014. Overcoming obstacles in microRNA delivery towards improved cancer therapy. Drug. Deliv. Transl. Res. 4, 38-49.

Berridge, M.J., Lipp, P., Bootman, M.D., 2000. The versatility and universality of calcium signaling. Nat. Rev. Mol. Cell Biol. 1, 11–21.

Bhaskar, R., Murthy, S.R.S., Miglani, B.D., Viswanathan, K., 1986. Novel method to evaluate diffusion controlled release of drug from resinate. Int. J. Pharm. 28 (1), 59–66.

Bhattacharjee, A., Rahaman, S.H., Saha, S., Chakraborty, M., Chakraborty, J., 2019. Determination of half maximal inhibitory concentration of CaAl layered double hydroxide on cancer cells and its role in the apoptotic pathway. Appl. Clay Sci. 168, 31–35.

Biondi, M., Ungaro, F., Quaglia, F., Netti, P.A., 2008. Controlled drug delivery in tissue engineering. Adv. Drug Deliv. Rev. 60, 229-242.

Bish D.L., 1980. Anion-exchange in takovite: applications to other hydroxide minerals. Bull. Mineral. 103, 170-175.

Bolognini, M., Cavani, F., Scagliarini, D., Flego, C., Perego, C., Saba, M., 2003. Mg/Al mixed oxides prepared by coprecipitation and sol–gel routes: a comparison of their physico-chemical features and performances in m-cresol methylation. Micropor Mesopor Mat. 66, 77-89.

Bose, T., Cieslar-Pobuda, A., Wiechec, E., 2015. Role of ion channels in regulating Ca2+ homeostasis during the interplay between immune and cancer cells. Cell Death Dis. 6, 1648–1659.

Braterman, P.S., Xu, Z.P., Yarberry, F, Auerbach, S.M., Carrado, K.A., Dutta, P.K. 2004. Handbook of Layered materials: Layered Double Hydroxides. Marcel Dekker Inc., New York, 373-474.

Bretscher, M.S., 1983. Distribution of receptors for transferrin and low-density lipoprotein on the surface of giant HeLa cells. Proc. Natl. Acad. Sci. 80 (2), 454–458.

Cai, A., Xu, X., Pan, H., Tao, J., Liu, R., Tang, R., Cho, K., 2008. Direct Synthesis of Hollow Vaterite Nanospheres from Amorphous Calcium Carbonate Nanoparticles via Phase Transformation. J. Phys. Chem. C. 112, 11324-11330.

Cai, Y., Pan, H., Xu, X., Hu, Q., Li, L., Tang, R., 2007. Ultrasonic Controlled Morphology Transformation of Hollow Calcium Phosphate Nanospheres: A Smart and Biocompatible Drug Release System. Chem. Mater. 19, 3081-3083.

Cai, Y., Tang, R., 2008. Calcium phosphate nanoparticles in biomineralization and biomaterials.J. Mater Chem. 18, 3775-3787.

Cao, F., Wang, Y., Ping, Q., Liao, Z., 2011. Zn-Al-NO(3)-layered double hydroxides with intercalated diclofenac for ocular delivery. Int. J. Pharm. 404, 250-256.

Carretero, M.I., 2002. Clay minerals and their beneficial effects upon human health. A review. Appl. Clay Sci. 21, 155-163.

Chakraborty, J., Chakraborty, M., Ghosh, S., Mitra, M.K., 2013. Drug delivery using nanosized layered double hydroxide, an anionic clay. Key Eng. Mater. 571, 133–167.

Chakraborty, J., Daneu, N., Rečnik, A., Chakraborty, M., Dasgupta, S., Ghosh, J., Sengupta, S., Mazumdar, S., Sinha, M.K., Basu, D., 2011a. Stepwise formation of crystalline apatite in the biomimetic coating of surgical grade SS 316L substrate: A TEM analysis. J. Taiwan. Inst. Chem. E. 42, 682-687.

Chakraborty, J., Roychowdhury, S., Sengupta, S., Ghosh, S., 2013b. Mg-Al layered double hydroxide-methotrexate nanohybrid drug delivery system: evaluation of efficacy. Mater. Sci. Eng. C. Mater. Biol. Appl.33, 2168-2174.

Chakraborty, M., Bose, P., Mandal, T., Datta, B., Das, T., Pal, S., Chakraborty, J., Mitra, M., Basu D., 2010a. Effect of Process Variations on Anticancerous Drug Intercalation in Ceramic Based Delivery System. Trans. Ind. Ceram. Soc. 69 (4), 229-234.

Chakraborty, M., Dasgupta, S., Bose, P., Misra, A., Mandal, T.K., Mitra, M., Chakraborty, J., Basu, D., 2011. Layered double hydroxide: Inorganic organic conjugate nanocarrier for methotrexate. J. Phys. Chem. Solids 72 (6), 779–783.

Chakraborty, M., Dasgupta, S., Sengupta, S., Chakraborty, J., Basu, D., 2010b. Layered double hydroxides based ceramic nanocapsules as reservoir and carrier of functional anions. Trans. Ind. Ceram. Soc. 69, 153–163.

Chakraborty, M., Dasgupta, S., Sengupta, S., Chakraborty, J., Ghosh, S., Ghosh, J., Mitra, M.K., Mishra, A., Mandal, T.K., Basu, D., 2012. A facile synthetic strategy for Mg–Al layered double hydroxide material as nanocarrier for methotrexate. Ceram. Int. 38, 941–949.

Chakraborty, M., Dasgupta, S., Soundrapandian, C., Chakraborty, J., Ghosh, S., Mitra, M.K., Basu, D., 2011b. Methotrexate intercalated ZnAl-layered double hydroxide. J. Solid State Chem. 184, 2439-2445.

Chakraborty, M., Ray, S, Saha, S., Ghosh, J., Ghosh, Swapankumar., Mitra, M.K. Chakraborty, Jui., 2016. Adv. Sci. Eng. Med. 8, 450-459.

Chen, H., Zhang, F., Fu, S., Duan, X., 2006. In Situ Microstructure Control of Oriented Layered Double Hydroxide Monolayer Films with Curved Hexagonal Crystals as Superhydrophobic Materials. Adv. Mater. 18, 3089-3093.

Chen, J., Shao, R., Li, L., Xu, Z.P., Gu, W., 2014. Effective inhibition of colon cancer cell growth with MgAl-layered double hydroxide (LDH) loaded 5-FU and PI3K/mTOR dual inhibitor BEZ-235 through apoptotic pathways. Int. J. Nanomedicine 9, 3403-3411.

Cho K.J., Wang X., Nie S.M., Chen Z., Shin D.M., Therapeutic nanoparticles for drug delivery in cancer, Clinical Cancer Research 2008, 14 (5) 1310-1316.

Cho, S., Jung, S.H., Jang, J.W., Oh, E., Lee, K.H., 2008. Simultaneous Synthesis of Al-Doped ZnO Nanoneedles and Zinc Aluminum Hydroxides through use of a seed layer. Cryst. Growth Des. 8, 4553-4558.

Choi, G., Piao, H., Alothman, Z.A., Vinu, A., Yun, C.O., Choy, J.H., 2016. Anionic clay as the drug delivery vehicle: tumor targeting function of layered double hydroxide-methotrexate nanohybrid in C33A orthotopic cervical cancer model. Int. J. Nanomedicine 11, 337-348.

Choi, S.J., Choy, J.H., 2011a. Effect of physico-chemical parameters on the toxicity of inorganic nanoparticles. J. Mater. Chem. 21, 5547-5554.

Choi, S.J., Choy, J.H., 2011b. Layered double hydroxide nanoparticles as target-specific delivery carriers: uptake mechanism and toxicity. Nanomedicine 6(5), 803-814.

Choi, S.J., Jae-Min, O., Choy, J.H., 2010. Biocompatible nanoparticles intercalated with anticancer drug for target delivery: pharmacokinetic and biodistribution study. J Nanosci. Nanotechnol. 10(4), 2913-2916.

Choi, S.J., Oh, J.M., Choy, J.H., 2008. Anticancer drug-layered hydroxide nanohybrids as potent cancer chemotherapy agents. J. Phys. Chem. Solids 69, 1528-1532.

Choi, S.J., Oh, J.M., Choy, J.H., 2009. Biocompatible ceramic nanocarrier for drug delivery with high efficiency. J. Ceram. Soc. Jpn. 117, 543-549.

Choy, J.H., Choi, S.J., Oh, J.M., Park, T., 2007. Clay minerals and layered double hydroxides for novel biological applications. Appl. Clay Sci. 36, 122-132.

Choy, J.H., Jung, J.S., Oh, J.M., Park, M., Jeong, J., Kang, Y.K., Han, O.J., 2004a. Layered double hydroxide as an efficient drug reservoir for folate derivatives. Biomaterials 25, 3059-3064.

Choy, J.H., Kwak, S.Y., Jeong, Y.J., Park, J.S., 2000. Inorganic Layered Double Hydroxides as Nonviral Vectors.Angewandte Chemie. 39, 4041-4045.

Choy, J.H., Kwak, S.Y., Park, J.S., Jeong, Y.J., Portier, J., 1999. Intercalative Nanohybrids of Nucleoside Monophosphates and DNA in Layered Metal Hydroxide. J. Am. Ceram. Soc. 121, 1399-1400.

Choy, J.H., Son, Y.H., 2004b. Intercalation of vitamer into LDH and their controlled release properties. Bull. Korean Chem. Soc. 25, 122–126.

Conklin, K.A., 2004. Chemotherapy-associated oxidative stress: impact on chemotherapeutic effectiveness. Integrative Cancer Therapies 3 (4), 294–300.

Constantino, V.R.L., Pinnavaia, T.J., 1995. Basic Properties of Mg2+1-xAl3+x Layered Double Hydroxides Intercalated by Carbonate, Hydroxide, Chloride, and Sulfate Anions. Inorg. Chem. 34, 883-892.

Cooper GM. The Cell: A Molecular Approach. 2nd edition. Sunderland (MA): Sinauer Associates; 2000. The Development and Causes of Cancer. Available from: https://www.ncbi.nlm.nih.gov/books/NBK9963/

Costantino, U., Nocchetti, M., Tammaro, L., Vittoria, V., 2012. Modified Hydrotalcite-Like Compounds as Active Fillers of Biodegradable Polymers for Drug Release and Food Packaging Applications. Recent Pat. Nanotechnol. 6, 218-230.

D'Souza, S., 2014. A review of in vitro drug release test methods for nano-sized dosage forms. Adv. Pharm. 304757, 1–12.

Dai, X., Shivkumar, S., 2008. Hybrid analogs for the production of porous calcium phosphate scaffolds. Mater. Sci. Eng. C 28, 336-340.

Dash, S., Murthy, P.N., Nath, L.N., Chowdhury, P., 2010. Kinetic modeling on drug release from controlled drug delivery systems. Acta Pol. Pharm. 67 (3), 217–223.

del Arco, M., Fernández, A., Martín, C., Rives, V., 2010. Solubility and release of fenbufen intercalated in Mg, Al and Mg, Al, Fe layered double hydroxides (LDH): The effect of Eudragit® S 100 covering. J. Solid State Chem. 183, 3002-3009.

Desigaux, L., Belkacem, M.B., Richard, P., Cellier, J., Léone, P., Cario, L., Leroux, F., Taviot-Guého, C., Pitard, B., 2006. Self-Assembly and Characterization of Layered Double Hydroxide/DNA Hybrids. Nano Lett. 6, 199-204.

Ding, P., Qu, B., 2005. Synthesis and characterization of exfoliated polystyrene/ZnAl layered double hydroxide nanocomposite via emulsion polymerization. J. Colloid Interface Sci. 291, 13-18.

Dong, H., Chen, M., Rahman, S., Parekh, H.S., Cooper, H.M., Xu, Z.P., 2014. Engineering small MgAl-layered double hydroxide nanoparticles for enhanced gene delivery. Appl. Clay Sci. 100, 66-75.

Dong, H., Parekh, H.S., Xu, Z.P., 2015. Particle size- and number-dependent delivery to cells by layered double hydroxide nanoparticles. J Colloid Interface Sci. 437, 10-16.

Dong, L.e., Gou, G., Jiao, L., 2013. Characterization of a dextran–coated layered double hydroxide acetylsalicylic acid delivery system and its pharmacokinetics in rabbit. Acta Pharm. Sin. B 3, 400-407.

Drewe, J., Guitard, P., 1993. In vitro-in vivo correlation for modified-release formulations. J. Pharm. Sci. 82, 132-137.

Du, L.C., Qu, B.J., 2006. Preparation of LLDPE/MgAl-LDH Exfoliation Nanocomposites with Enhanced Thermal Properties by melt intercalation. Chin. J. Chem. 24, 1342-1345.

Du, Y., Hu, G., O'Hare, D., 2009. Nucleation and growth of oriented layered hydroxides on polymer resin beads. J. Mater. Chem. 19, 1160-1165.

Dutta, K., Pramanik, A., 2013. Synthesis of a novel cone-shaped CaAl-layered double hydroxide (LDH): its potential use as a reversible oil sorbent. Chem. Commun. 49, 6427-6429.

Elkhattabi, E.H., Badreddine, M., Berraho, M., Legrouri, A., 2012. Incorporation of fluorophosphate into zinc–aluminium–nitrate layered double hydroxide by ion exchange. Bull. Mater. Sci. 35, 693-700.

Evans, T.I.A., Shea, M.A., 2009. Energetics of calmodulin domain interactions with the calmodulin binding domain of CaMKII. Proteins. 76, 47–61.

FDA Guidance for Industry, 1999, Waiver of in vivo bioavailability and bioequivalence studies for immediate release solid oral dosage forms containing certain active moieties/active ingredients based on biopharmaceutics classification system, U.S. Department of Health and Human Services Food and Drug Administration Center for Drug Evaluation and Research (CDER).

Flesken-Nikitin, A., Toshkov, I., Naskar, J., Tyner, K.M., Williams, R.M., Zipfel, W.R., Giannelis, E.P., Nikitin, A.Y., 2007. Toxicity and biomedical imaging of layered nanohybrids in the mouse. Toxicol. Pathol. 35, 806-812.

Fornasari, G., Gazzano, M., Matteuzzi, D., Trifirò, F., Vaccari, A., 1995. Synthesis and Application of Anionic ClaysStructure and reactivity of high-surface-area Ni/Mg/Al mixed oxides. Appl. Clay Sci. 10, 69-82.

Fu, Y., Kao, W.J., 2010. Drug release kinetics and transport mechanisms of non-degradable and degradable polymeric delivery systems. Expert Opin Drug Deliv 7, 429-444.

Fudala, Å., Pálinkó, I., Hrivnák, B., Kiricsi, I., 1999a. Amino Acid-Pillared Layered Double Hydroxide and Montmorillonite Thermal Characteristics. J. Therm. Anal. Calorim. 56, 317-322.

Fudala, A.A., Palinko, I.I., Kiricsi, I., 1999b. Preparation and Characterization of Hybrid Organic-Inorganic Composite Materials Using the Amphoteric Property of Amino Acids: Amino Acid Intercalated Layered Double Hydroxide and Montmorillonite. Inorg. Chem. 38, 4653-4658.

Gao, X., Chen, L., Xie, J., Yin, Y., Chang, T., Duan, Y., Jiang, N., 2014. In vitro controlled release of vitamin C from Ca/Al layered double hydroxide drug delivery system. Mater. Sci. Eng. C 39, 56-60.

Gao, Y.F., Nagai, M., Masuda, Y., Sato, F., Seo, W.S., Koumoto, K., 2006. Surface Precipitation of Highly Porous Hydrotalcite-like Film on Al from a Zinc Aqueous Solution. Langmuir 22, 3521-3527.

Goffin, J., Lacchetti, C., Ellis, P.M., Ung, Y.C., Evans, W.K., 2010. First-line systemic chemotherapy in the treatment of advanced non-small cell lung cancer: a systematic review. J.Thorac. Oncol. 5 (2), 260–274.

Gou, G., Dong, L, Bao, F.J., Wang, Z.Y., Jiao L., Huang, J., Sun, Y., Xue, B., 2013. A Review on Research of the Sustained Release Drug Delivery System Based on Magnesium Aluminate Layered Double Hydroxide. Appl. Mech. Mater. 320, 495-504.

Gryparis, E.C., Hatziapostolou, M., Papadimitriou, E., Avgoustakis, K., 2007. Anticancer activity of cisplatin-loaded PLGA-mPEG nanoparticles on LNCaP prostate cancer cells. Eur. J. Pharm. Biopharm. 67, 1-8.

Gu, Z., Rolfe, B.E., Thomas, A.C., Campbell, J.H., Lu, G.Q., Xu, Z.P., 2011. Cellular trafficking of low molecular weight heparin incorporated in layered double hydroxide nanoparticles in rat vascular smooth muscle cells. Biomaterials 32, 7234-7240.

Gu, Z., Thomas, A.C., Xu, Z.P., Campbell, J.H., Lu, G.Q., 2008. In Vitro Sustained Release of LMWH from MgAl-layered Double Hydroxide Nanohybrids. Chem. Mater. 20, 3715-3722.

Gu, Z., Wu, A., Li, L., Xu, Z., 2014. Influence of Hydrothermal Treatment on Physicochemical Properties and Drug Release of Anti-Inflammatory Drugs of Intercalated Layered Double Hydroxide Nanoparticles. Pharmaceutics 6(2), 235-248.

Gunawan, P., Xu, R., 2008. Synthesis of unusual coral-like layered double hydroxide microspheres in a nonaqueous polar solvent/surfactant system. J. Mater. Chem. 18, 2112-2120.

Gunawan, P., Xu, R., 2009. Direct Assembly of Anisotropic Layered Double Hydroxide (LDH) Nanocrystals on Spherical Template for Fabrication of Drug-LDH Hollow Nanospheres. Chem. Mater. 21, 781-783.

Guo, X., Xu, S., Zhao, L., Lu, W., Zhang, F., Evans, D.G., Duan, X., 2009a. One-Step Hydrothermal Crystallization of a Layered Double Hydroxide/Alumina Bilayer Film on Aluminum and Its Corrosion Resistance Properties. Langmuir 25, 9894-9897.

Guo, X., Zhang, F., Xu, S., Evans, D.G., Duan, X., 2009b. Preparation of layered double hydroxide films with different orientations on the opposite sides of a glass substrate by in situ hydrothermal crystallization. Chem. Commun. 44, 6836-6838.

Gursky, J.A., Blough, S.D., Luna, C., Gomez, C., Luevano, A.N., Gardner, E.A., 2006. Particle−Particle Interactions between Layered Double Hydroxide Nanoparticles. J. Am. Chem. Soc. 128, 8376-8377.

Haddad PR, Jackson PE. Ion Chromatography – Principles and Applications, 1st ed. Amsterdam: Elsevier Verlag; 1990.

Hasan, S., Ali, H.A., Al-Qubaisi, M., Hussein, M.Z., Ismail, M., Zainal, Z., Hakim, M.N., 2012. Controlled-release formulation of antihistamine based on cetirizine zinc-layered hydroxide nanocomposites and its effect on histamine release from basophilic leukemia (RBL-2H3) cells. Int. J. Nanomedicine 7, 3351-3363.

Hassan, Saad & Kamel, Ayman & Maher, Heba. (2020). Drug delivery systems between metal, liposome, and polymer-based nanomedicine: a review. European Chemical Bulletin. 9. 91-102.

He, J., Wei, M., Li, B., Kang, Y., Evans, D.G., Duan, X., 2006. Preparation of Layered Double Hydroxides, in: Duan, X., Evans, D.G. (Eds.), Layered Double Hydroxides. Springer Berlin Heidelberg, Berlin, Heidelberg, pp. 89-119.

Hesse, D., Badar, M., Bleich, A., Smoczek, A., Glage, S., Kieke, M., Behrens, P., Muller, P.P., Esser, K.H., Stieve, M., Prenzler, N.K., 2013. Layered double hydroxides as efficient drug delivery system of ciprofloxacin in the middle ear: an animal study in rabbits. J. Mater. Sci. Mater. Med. 24, 129-136.

Hnatyszyn, H.J., Kossovsky, N., Gelman, A., Sponsler, E., 1994. Drug delivery systems for the future. PDA J. Pharm. Sci. Technol. 48, 247-254.

Hou, W.G., Jin, Z.L., 2007. Synthesis and characterization of Naproxen intercalated Zn–Al layered double hydroxides. Colloid. Polym. Sci. 285, 1449-1454.

Hu, G., O'Hare, D., 2005. Unique Layered Double Hydroxide Morphologies Using Reverse Microemulsion Synthesis. J. Am. Chem. Soc. 127, 17808-17813.

Hu, G., Wang, N., O'Hare, D., Davis, J., 2006. One-step synthesis and AFM imaging of hydrophobic LDH monolayers. Chem. Commun. 3, 287-289.

Huang, S.S., Fan, Y., Cheng, Z.Y., Kong, D.Y., Yang, P.P., Quan, Z.W., Zhang, C.M., Lin, J., 2009. Magnetic mesoporous silica spheres for drug targeting and controlled release. J. Phys. Chem. C 113, 1775–1784.

Huang, W., Zhang, H., Pan, D., 2011. Study on the release behavior and mechanism by monitoring the morphology changes of the large-sized drug-LDH nanohybrids. AlChE J. 57, 1936-1946.

Hussein Al Ali, S.H., Al-Qubaisi, M., Hussein, M.Z., Ismail, M., Zainal, Z., Hakim, M.N., 2012. Controlled release and angiotensin-converting enzyme inhibition

properties of an antihypertensive drug based on a perindopril erbumine-layered double hydroxide nanocomposite. Int. J. Nanomedicine 7, 2129-2141.

Hwang, S.H., Han, Y.S., Choy, J.H., 2001. Intercalation of functional organic molecules with pharmaceutical, cosmeceutical and nutraceutical functions into layered double hydroxides and zinc basic salts. Bull. Korean Chem. Soc. 22, 1019–2021.

Jeffery, G.H., Bassett. J., Mendham, J., Denney, R.C., 1980. Vogel Textbook of Quantitative Chemical fifth ed. John Wiley & Sons Inc. New York

Jiang, H., Geng, D., Liu, H., Li, Z., Cao, J., 2016. Co-delivery of etoposide and curcumin by lipid nanoparticulate drug delivery system for the treatment of gastric tumors. Drug Deliv 23 (9), 3665–3673.

Jin, L., Liu, Q., Sun, Z., Ni, X., Wei, M., 2010. Preparation of 5-Fluorouracil/β-Cyclodextrin Complex Intercalated in Layered Double Hydroxide and the Controlled Drug Release Properties. Ind. Eng. Chem. Res. 49, 11176-11181.

Joel, S.P., Clark, P., Heap, L., 1995. Pharmacological attempts to improve the bioavailability of oral etoposide. Cancer Chemother. Pharmacol. 37 (1–2), 125–133.

Kamaly, N., Yameen, B., Wu, J., & Farokhzad, O. C. (2016). Degradable Controlled-Release Polymers and Polymeric Nanoparticles: Mechanisms of Controlling Drug Release. *Chemical reviews*, *116*(4), 2602–2663. https://doi.org/10.1021/acs.chemrev.5b00346

Kavitha, K., Rao, S., Nalini, C.N., 2013. An Investigation on Enhancement of Solubility of 5 Fluorouracil by Applying Complexation Technique- Characterization, Dissolution and Molecular-Modeling Studies. J. App. Pharm. Sci. 3 (03), 162-166

Kedar, U., Phutane, P., Shidhaye, S., Kadam, V., 2010. Advances in polymeric micelles for drug delivery and tumor targeting. Nanomedicine 6, 714-729.

Khan, A.I., Lei, L., Norquist, A.J., O'Hare, D., 2001. Intercalation and controlled release of pharmaceutically active compounds from a layered double hydroxide. Chem. Commun. 22, 2342-2343.

Khan, A.I., O'Hare, D., 2002. Intercalation chemistry of layered double hydroxides: recent developments and applications. J. Mater. Chem. 12, 3191-3198.

Kim T.H., Heo, I.I., Paek, S.M., Park, C.B., Choi, A.J., Lee, S.H., Choy, J.H., Oh, J.M., 2012. Layered Metal Hydroxides Containing Calcium and Their Structural Analysis. Bull. Korean Chem. Soc. 33(6), 1845-1850

Kim, J.Y., Choi, S.J., Oh, J.M., Park, T., Choy, J.H., 2007. Anticancer drug-inorganic nanohybrid and its cellular interaction.J. Nanosci. Nanotechnol. 7, 3700-3705.

Kim, T.H., Kim, H.J., Jae-Min, O., 2012. Interlayer structure of bioactive molecule, 2-aminoethane sulfonate, intercalated into calcium-containing layered double hydroxides. J. Nanomater. 2012, 1–7 987938.

Kim, T.H., Lee, J.A., Choi, S.J., Oh, J.M., 2014. Polymer coated CaAl-layered double hydroxide nanomaterials for potential calcium supplement. Int. J. Mol. Sci. 15, 22563-22579.

Klemkaite, K., Prosycevas, I., Taraskevicius, R., Khinsky, A., Kareiva, A., 2011. Synthesis and characterization of layered double hydroxides with different cations (Mg, Co, Ni, Al), decomposition and reformation of mixed metal oxides to layered structures. Cent. Eur. J. Chem. 9, 275-282.

Koch, G., Walz, A., Lahu, G., Schropp, J., 2009. Modeling of tumor growth and anticancer effects of combination therapy. J. Pharmacokinet. Pharmacodyn. 36 (2), 179–187.

Kovanda, F., Jindova, E., Dousova, B., Kolousek, D., Plestil, J., Sedlakova, Z., 2009. layered double hydroxides intercalated with organic anions and their application in preparation of ldh/polymer nanocomposites. Acta Geodyn. Geomater. 61 (153), 111–119.

Kriven, W.M., Kwak, S.Y., Wallig, M.A., 2004. Bio-resorbable nanoceramics for gene and drug delivery. MRS Bulletin. 29, 33–37.

Kuang, Y., Zhao, L., Zhang, S., Zhang, F., Dong, M., Xu, S., 2010. Morphologies, Preparations and Applications of Layered Double Hydroxide Micro-/Nanostructures. Materials 3(12), 5220-5235.

Kuo, Y.M., Kuthati, Y., Kankala, R.K., Wei, P.R., Weng, C.F., Liu, C.L., Sung, P.J., Mou, C.Y., Lee, C.H., 2015. Layered double hydroxide nanoparticles to enhance organ-specific targeting and the anti-proliferative effect of cisplatin. J. Mater. Chem. B 3, 3447-3458.

Kura, A.U., Ain, N.M., Hussein, M.Z., Fakurazi, S., Hussein-Al-Ali, S.H., 2014a. Toxicity and metabolism of layered double hydroxide intercalated with levodopa in a Parkinson's disease model. Int. J. Mol. Sci. 15, 5916-5927.

Kura, A.U., Hussein, M.Z., Fakurazi, S., Arulselvan, P., 2014b. Layered double hydroxide nanocomposite for drug delivery systems; bio-distribution, toxicity and drug activity enhancement. Chem. Cent. J. 8, 1-8.

Kura, A.U., Saifullah, B., Cheah, P.-S., Hussein, M.Z., Azmi, N., Fakurazi, S., 2015. Acute oral toxicity and biodistribution study of zinc-aluminium-levodopa nanocomposite. Nanoscale Res. Lett. 10, 1-11.

Kwak, S.Y., Jeong, Y.J., Park, J.S., Choy, J.H., 2002. Bio-LDH nanohybrid for gene therapy. Solid State Ionics 151, 229-234.

Kwak, S.Y., Kriven, W.M., Wallig, M.A., Choy, J.H., 2004. Inorganic delivery vector for intravenous injection. Biomaterials 25, 5995-6001.

L. Crepaldi, E., C. Pavan, P., B. Valim, J., 1999. A new method of intercalation by anion exchange in layered double hydroxides. Chem. Commun.2, 155-156.

Ladewig, K., Niebert, M., Xu, Z.P., Gray, P.P., Lu, G.Q.M., 2010. Efficient siRNA delivery to mammalian cells using layered double hydroxide nanoparticles. Biomaterials 31, 1821-1829.

Ladewig, K., Xu, Z.P., Lu, G.Q., 2009. Layered double hydroxide nanoparticles in gene and drug delivery. Expert Opin. Drug. Del. 6, 907-922.

Lee, J.H., Rhee, S.W., Jung, D.Y., 2005. Step-wise Anion-Exchange in LDH using Solvothermal Treatment. Bull. Korean Chem. Soc. 26 (2), 248-252.

Lee, J.H., Rhee, S.W., Nam, H.J., Jung, D.Y., 2009. Surface selective deposition of PMMA on layered double hydroxide nanocrystals immobilized on solid substrates. Adv. Mater. 21, 546–549.

Li, A., Qin, L., Wang, W., Zhu, R., Yu, Y., Liu, H., Wang, S., 2011. The use of layered double hydroxides as DNA vaccine delivery vector for enhancement of anti-melanoma immune response. Biomaterials 32, 469-477.

Li, B., He, J., 2008. Multiple Effects of Dodecanesulfonate in the Crystal Growth Control and Morphosynthesis of Layered Double Hydroxides. J. Phys. Chem. C 112, 10909-10917.

Li, B., He, J., G. Evans, D., Duan, X., 2004. Inorganic layered double hydroxides as a drug delivery system—intercalation and in vitro release of fenbufen. Appl. Clay Sci. 27, 199-207.

Li, L., Feng, Y., Li, Y., Zhao, W., Shi, J., 2009. Fe3O4 Core/Layered Double Hydroxide Shell Nanocomposite: Versatile Magnetic Matrix for Anionic Functional Materials. Angew. Chem. Int. Ed. 48, 5888-5892.

Li, L., Gu, Z., Gu, W., Liu, J., Xu, Z.P., 2016. Efficient drug delivery using SiO2-layered double hydroxide nanocomposites. J. Colloid Interface Sci. 470, 47-55.

Li, L., Ma, R., Iyi, N., Ebina, Y., Takada, K., Sasaki, T., 2006a. Hollow nanoshell of layered double hydroxide. Chem. Commun. 29, 3125-3127.

Li, S., Li, J., Wang, C.J., Wang, Q., Cader, M.Z., Lu, J., Evans, D.G., Duan, X., O'Hare, D., 2013. Cellular uptake and gene delivery using layered double hydroxide nanoparticles. J. Mater. Chem. B1, 61-68.

Li, S., Shen, Y., Xiao, M., Liu, D., Fan, L., 2015. Synthesis and controlled release properties of β-naphthoxyacetic acid intercalated Mg–Al layered double hydroxides nanohybrids. Arab. J. Chem. http://dx.doi.org/10.1016/j.arabjc.2015.04.034

Li, W.Z., Lu, J., Chen, J.S., Li, G.D., Jiang, Y.S., Li, L.S., Huang, B.Q., 2006b. Phenoxymethylpenicillin–intercalated hydrotalcite as a bacteria inhibitor. J. Chem. Technol. Biotechnol. 81, 89-93.

Li, Y., Xu, J., Zhang, S.J., Li, D.X., Zheng, B., Hou W.G.., 2009. Synthesis and characterization of floxuridine-LDH nanohybrid. Chin. J. Inorg. Chem. 25, 2124–2128.

Liu, C., Hou, W., Li, L., Li, Y., Liu, S., 2008a. Synthesis and characterization of 5-fluorocytosine intercalated Zn–Al layered double hydroxide. J. Solid State Chem. 181, 1792-1797.

Liu, J., Huang, X., Li, Y., Sulieman, K.M., He, X., Sun, F., 2006. Facile and large-scale production of ZnO/Zn-Al layered double hydroxide hierarchical heterostructures. J. Phys. Chem. B 110, 21865-21872.

Liu, J., Li, Y., Huang, X., Li, G., Li, Z., 2008b. Layered Double Hydroxide Nano- and Microstructures Grown Directly on Metal Substrates and Their Calcined Products for Application as Li-Ion Battery Electrodes. Adv. Funct. Mater. 18, 1448-1458.

Lorico, A., Rappa, G., Finch, R.A., Yang, D., Flavell, R.A., Sartorelli, A.C., 1997. Disruption of the murine MRP (multidrug resistance protein) gene leads to increased sensitivity to etoposide (VP-16) and increased levels of glutathione. Cancer Res. 57 (23), 5238–5242.

Lü, Z., Zhang, F., Lei, X., Yang, L., Xu, S., Duan, X., 2008. In situ growth of layered double hydroxide films on anodic aluminum oxide/aluminum and its catalytic feature in aldol condensation of acetone. Chem. Eng. Sci. 63, 4055-4062.

Maanen, J.M., Retèl, J., de Vries, J., Pinedo, H.M., 1988. Mechanism of action of antitumor drug etoposide: a review. J. Natl. Cancer Inst. 80 (19), 1526–1533.

Maeda H, Khatami M. Analyses of repeated failures in cancer therapy for solid tumors: poor tumor-selective drug delivery, low therapeutic efficacy and unsustainable costs. Clin Transl Med. 2018 Mar 1;7(1):11.

Mahaney, W.C., Hancock, R.G.V., Aufreiter, S., Huffman, M.A., 1996. Geochemistry and clay mineralogy of termite mound soil and the role of geophagy in chimpanzees of the Mahale Mountains, Tanzania. Primates 37, 121-134.

Mahjoubi, F.Z., Khalidi, A., Abdennouri, M., Barka, N., 2017. Zn–Al layered double hydroxides intercalated with carbonate, nitrate, chloride and sulphate ions: Synthesis, characterisation and dye removal properties. J. Taibah Univ. Sci. 11 (1), 90–100.

Maiyo, F., Singh, M., 2017. Selenium nanoparticles: potential in cancer gene and drug delivery. Nanomedicine (London) 12 (9), 1075–1089.

Mallakpour, S., Dinari, M., 2013a. Facile synthesis of nanocomposite materials by intercalating an optically active poly(amide-imide) enclosing (L)-isoleucine moieties and azobenzene side groups into a chiral layered double hydroxide. Polymer 54, 2907-2916.

Mallakpour, S., Dinari, M., 2014. Structural Characterization and Thermal Properties of Chiral Poly(amide-imide)/Modified MgAl Layered Double Hydroxide Nanocomposites Prepared via Solution Intercalation. Polym. Plast. Technol. Eng. 53, 1047-1055.

Mallakpour, S., Dinari, M., Behranvand, V., 2013b. Ultrasonic-assisted synthesis and characterization of layered double hydroxides intercalated with bioactive N,N[prime or minute]-(pyromellitoyl)-bis-l-[small alpha]-amino acids. RSC Adv. 3, 23303-23308.

Manhire A, Charig M, Clelland C, et al., 2003, Guidelines for radiologically guided lung biopsy Thorax, 58:920-936.

Martínez-Ortiz, M.d.J., Lima, E., Lara, V., Vivar, J.M., 2008. Structural and Textural Evolution during Folding of Layers of Layered Double Hydroxides. Langmuir 24, 8904-8911.

Masarudin, M.J., Yusoff, K., Rahim, R.A., Hussein, M.Z., 2009. Successful transfer of plasmid DNA into in vitro cells transfected with an inorganic plasmid-Mg/Al-LDH nanobiocomposite material as a vector for gene expression. Nanotechnology 20, 045602.

McBain, S.C., Yiu, H.H., Dobson, J., 2008. Magnetic nanoparticles for gene and drug delivery. Int. J. Nanomedicine 3 (2), 169–180. Med. Oncol. 1 (2), 109–118.

Mendell-Harary, J., Dowell, J., Bigora, S., Piscitelli, D., Butler, J., Farrell, C., Devane, J., Young, D., 1997. Nonlinear in Vitro-in Vivo Correlations, in: Young, D., Devane, J.G., Butler, J. (Eds.), In Vitro-in Vivo Correlations. Springer US, Boston, MA, 199-206.

Meyn, M., Beneke, K., Lagaly, G., 1993. Anion-exchange reactions of hydroxy double salts. Inorg. Chem. 32, 1209-1215.

Miao, Y.E., Zhu, H., Chen, D., Wang, R., Tjiu, W.W., Liu, T., 2012. Electrospun fibers of layered double hydroxide/biopolymer nanocomposites as effective drug delivery systems.Mater. Chem. Phys. 134, 623-630.

Minkoff I. Materials Processes: A Short Introduction. Berlin, Heidelberg: Springer-Verlag; 1992:1.

Mokhtari, R.B., Homayouni, T.S., Baluch, N., Morgatskaya, E., Kumar, S., Das, B., Yeger, H., 2017. Combination therapy in combating cancer. Oncotarget. 8 (23), 38022–38043.

Molina, J.R., Yang, P., Cassivi, S.D., Schild, S.E., Adjei, A.A., 2008. Non-small cell lung cancer: epidemiology, risk factors, treatment, and survivorship. Mayo Clin. Proc. 83 (5), 584–594.

Nagaraj, V.J., Sun, X., Mehta, J., Martin, M., Ngo, T., Dey, S.K., 2015. Synthesis, Characterization, and In Vitro Drug Delivery Capabilities of (Zn, Al)-Based Layered Double Hydroxide Nanoparticles. J. Nanotech. 2015, 1-10.

Nalawade, P., Aware, B., Kadam, V.J., Hirlekar, R.S., 2009. Layered double hydroxides: A review. J. Sci. Ind. Res. 68, 267-272.

Nawroth, T., Rusp, M., May, R.P., 2004. Magnetic liposomes and entrapping : time-resolved neutron scattering TR-SANS and electron microscopy. Physica B 350, E635-E638.

Newman, S., Jones, W., 1998. Synthesis, characterization and applications of layered double hydroxides containing organic guests. New J. Chem. 22, 105-115.

Newman, S.P., Jones, W., Jones, W., Rao, C.N.R., 2001. Layered double hydroxides as templates for the formation of supramolecular structures. In Supramolecular Organization and Materials Design, Ch. 9 Cambridge University Press, 295–331.

Nie, H.Q., Hou, W.G., 2012. Synthesis and Characterization of Ifosfamide Intercalated Layered Double Hydroxides. J. Disper. Sci.Technol. 33, 339-345.

Nshuti, C.M., Songtipya, P., Manias, E., Gasco, M.M.J., Hossenlopp, J.M., Wilkie, C.A., 2009. Polymer nanocomposites using zinc aluminum and magnesium aluminum oleate layered double hydroxides: Effects of the polymeric compatibilizer and of composition on the thermal and fire properties of PP/LDH nanocomposites. Polym. Degrad. Stab. 94, 2042–2054.

Ogawara, K.-i., Un, K., Minato, K., Tanaka, K.-i., Higaki, K., Kimura, T., 2008. Determinants for in vivo anti-tumor effects of PEG liposomal doxorubicin: Importance of vascular permeability within tumors.Int. J. Pharm. 359, 234-240.

Oh, J.M., Choi, S.J., Kim, S.T., Choy, J.H., 2006b. Cellular uptake mechanism of an inorganic nanovehicle and its drug conjugates: Enhanced efficacy due to clathrin-mediated endocytosis. Bioconjug. Chem. 17, 1411-1417.

Oh, J.M., Choi, S.J., Lee, G.E., Han, S.H., Choy, J.H., 2009. Inorganic Drug-Delivery Nanovehicle Conjugated with Cancer-Cell-Specific Ligand. Adv. Funct. Mater. 19, 1617-1624.

Oh, J.M., Park, M., Kim, S.T., Jung, J.Y., Kang, Y.G., Choy, J.H., 2006a. Efficient delivery of anticancer drug MTX through MTX-LDH nanohybrid system. J. Phys. Chem. Solids 67, 1024-1027.

Olfs, H.W., Torres-Dorante, L.O., Eckelt, R., Kosslick, H., 2009. Comparison of different synthesis routes for Mg–Al layered double hydroxides (LDH): Characterization of the structural phases and anion exchange properties. Appl. Clay Sci. 43, 459-464.

Palmer, S.J., Frost, R.L., Nguyen, T., 2009. Hydrotalcites and their role in coordination of anions in Bayer liquors: Anion binding in layered double hydroxides. Coord. Chem. Rev. 253, 250-267.

Pan, D., Zhang, H., Fan, T., Chen, J., Duan, X., 2011. Nearly monodispersed core-shell structural Fe3O4@DFUR-LDH submicro particles for magnetically controlled drug delivery and release. Chem. Commun. 47, 908-910.

Panda, H.S., Bahadur, D., 2012. Study of the preparation, properties and kinetics of anion release in drug intercalated magnetic nanohybrids. Mater. Res. Bull. 47, 571-579.

Panda, H.S., Srivastava, R., Bahadur, D., 2009. In-Vitro Release Kinetics and Stability of Anticardiovascular Drugs-Intercalated Layered Double Hydroxide Nanohybrids. J. Phys. Chem. B 113, 15090-15100.

Pang, X., Ma, X., Li, D., Hou, W., 2013. Synthesis and characterization of 10-hydroxycamptothecin-sebacate-layered double hydroxide nanocomposites. Solid State Sci. 16, 71-75.

Peppas, N.A., 1985. Analysis of Fickian and non-Fickian drug release from polymers. Pharm. Acta Helv. 60 (4), 110–111.

Perioli, L., Ambrogi, V., di Nauta, L., Nocchetti, M., Rossi, C., 2011. Effects of hydrotalcite-like nanostructured compounds on biopharmaceutical properties and release of BCS class II drugs: The case of flurbiprofen. Appl. Clay Sci. 51, 407-413.

Plank, J., Dai, Z., Andres, P.R., 2006. Preparation and characterization of new Ca–Al–polycarboxylate layered double hydroxides. Mater. Lett. 60, 3614-3617.

Playle, A.C., Gunning, S.R., Llewellyn, A.F., 1974. The in vitro antacid and anti-pepsin activity of hydrotalcite. Pharm. Acta. Helv. 49, 298-302.

Prinetto, F., Ghiotti, G., Graffin, P., Tichit, D., 2000. Synthesis and characterization of sol–gel Mg/Al and Ni/Al layered double hydroxides and comparison with co-precipitated samples. Micropor. Mesopor. Mat. 39, 229-247.

Qin, L., Wang, M., Zhu, R., You, S., Zhou, P., Wang, S., 2013. The in vitro sustained release profile and antitumor effect of etoposide-layered double hydroxide nanohybrids. Int. J. Nanomedicine 8, 2053–2064.

Qin, L., Wang, S., Zhang, R., Zhu, R., Sun, X., Yao, S., 2008. Two different approaches to synthesizing Mg–Al-layered double hydroxides as folic acid carriers. J. Phys. Chem. Solids 69(11), 2779-2784.

Qin, L., Wang, W., You, S., Dong, J., Zhou, Y., Wang, J., 2014. In vitro antioxidant activity and in vivo antifatigue effect of layered double hydroxide nanoparticles as delivery vehicles for folic acid. Int.J. Nanomedicine 9, 5701-5710.

Qin, L., Xue, M., Wang, W., Zhu, R., Wang, S., Sun, J., Zhang, R., Sun, X., 2010. The in vitro and in vivo anti-tumor effect of layered double hydroxides nanoparticles as delivery for podophyllotoxin. Int. J. Pharm. 388 (1–2), 223–230.

Rahaman, S., Bhattacharjee, A., Saha, S., Chakraborty, M., Chakraborty, J., 2019. shRNA intercalation in CaAl-LDH nanoparticle synthesized at two different pH conditions and its comparative evaluation. Appl. Clay Sci. 171, 57–64.

Ray, S., Joy, M., Sa, B., Ghosh, S., Chakraborty, J., 2015. pH dependent chemical stability and release of methotrexate from a novel nanoceramic carrier. RSC Adv. 5, 39482–39494.

Ray, S., Mishra, A., Mandal, T.K., Sa, B., Chakraborty, J., 2015b. Optimization of the process parameters for the fabrication of a polymer coated layered double hydroxide-methotrexate nanohybrid for the possible treatment of osteosarcoma. RSC Adv. 5, 102574-102592.

Raz S, Weiner S, Addadi L. Formation of high-magnesian calcite via an amorphous precursor phase: possible biological implications. Adv Mater. 2000;12:38-42.

Reichle, W.T., 1986. Synthesis of anionic clay minerals (mixed metal hydroxides, hydrotalcite). Solid State Ionics 22, 135-141.

Rives, V., del Arco, M., Martín, C., 2014. Intercalation of drugs in layered double hydroxides and their controlled release: A review. Appl. Clay Sci. 88–89, 239-269.

Rocchetti, M., Bene, F.D., Germani, M., Fiorentini, F., Poggesi, I., Pesenti, E., Magni, P., De Nicolao, G., 2009. Testing additivity of anticancer agents in pre-clinical studies: a PK/PD modelling approach. Eur. J. Cancer 45 (18), 3336–3346.

Rojas, R., Palena, M.C., Jimenez-Kairuz, A.F., Manzo, R.H., Giacomelli, C.E., 2012. Modeling drug release from a layered double hydroxide–ibuprofen complex. Appl. Clay Sci. 62–63, 15-20.

Roto, R., Tahir, I., Mustofa, 2007. Zn-Al Layered double hydroxide host material for sunscreen compound of p-aminobenzoic acid. Indo. J. Chem. 7 (1), 1 – 4.

Roto, R., Villemure, G., 2002. Electrochemical impedance spectroscopy of electrodes modified with thin films of Ni□Al□Cl layered double hydroxides. J. Electroanal. Chem. 527, 123-130.

Roy, I., Ohulchanskyy, T.Y., Pudavar, H.E., Bergey, E.J., Oseroff, A.R., Morgan, J., Dougherty, T.J., Prasad, P.N., 2003. Ceramic-Based Nanoparticles Entrapping Water-Insoluble Photosensitizing Anticancer Drugs: A Novel Drug−Carrier System for Photodynamic Therapy. J. Am. Ceram. Soc. 125, 7860-7865.

Ryu, S.J., Jung, H., Oh, J.M., Lee, J.K., Choy, J.H., 2010. Layered double hydroxide as novel antibacterial drug delivery system. J. Phys. Chem. Solids 71, 685-688.

Saha, S., Ray, S., Ghosh, S., Chakraborty, J., 2018. pH-dependent facile synthesis of CaAl layered double hydroxides and its effect on the growth inhibition of cancer cells. J. Am. Ceram. Soc. 101, 3924–3935.

Sahoo, S., Chakraborti, C.K., Behera, P.K., 2012. Development and evaluation of astroretentive controlled release polymeric suspensions containing ciprofloxacin and carbopol polymers. J. Chem. Pharm. Res. 4, 2268–2284.

Sahu, R., Mohanta, B.S., Das, N.N., 2012. Intercalation of biologically important iminodiacetatochromium (III) ion in the interlayer of Zn-Al layered double hydroxide. Ind. J. Chem. 51A, 812-815.

Saifullah, B., Hussein, M.Z., Hussein-Al-Ali, S.H., Arulselvan, P., Fakurazi, S., 2013a. Antituberculosis nanodelivery system with controlled-release properties based on para-amino salicylate–zinc aluminum-layered double-hydroxide nanocomposites. Drug Des. Dev. Ther. 7, 1365-1375.

Saifullah, B., Hussein, M.Z., Hussein-Al-Ali, S.H., Arulselvan, P., Fakurazi, S., 2013b. Sustained release formulation of an anti-tuberculosis drug based on para-amino salicylic acid-zinc layered hydroxide nanocomposite. Chem. Cent. J. 7(1), 72-82.

Saifullah, B., Hussein, M.Z.B., 2015. Inorganic nanolayers: structure, preparation, and biomedical applications. Int. J. Nanomedicine 10, 5609–5633.

Salak, A.N., Tedim, J., Kuznetsova, A.I., Ribeiro, J.L., Vieira, L.G., Zheludkevich, M.L., Ferreira, M.G.S., 2012. Comparative X-ray diffraction and infrared spectroscopy study of Zn–Al layered double hydroxides: Vanadate vs nitrate. Chem. Phys. 397, 102-108.

San Román, M.S., Holgado, M.J., Salinas, B., Rives, V., 2012. Characterisation of Diclofenac, Ketoprofen or Chloramphenicol Succinate encapsulated in layered double hydroxides with the hydrotalcite-type structure. Appl. Clay Sci. 55, 158-163.

Sarkar A, Dutta K, Mahapatra S. Polymorph control of calcium carbonate using insoluble layered double hydroxide. Cryst Growth Des. 2013;13:204-211.

Satheesh, N.J., Busselberg, D., 2015. The role of intracellular calcium for the development and treatment of neuroblastoma. Cancers. 7, 823–848.

Scarpellini, D., Falconi, C., Gaudio, P., Mattoccia, A., Medaglia, P.G., Orsini, A., Pizzoferrato, R., Richetta, M., 2014. Morphology of Zn/Al layered double hydroxide nanosheets grown onto aluminum thin films. Microelectron. Eng. 126, 129-133.

Scherrer, P., 1918. Bestimmung der Gr€oße und der inneren Struktur von Kolloidteilchen mittels Reontgenstrahlen. Nachrichten von der Gesellschaft der Wissenschaften zu G€ottingen. Math. Phys. Klasse. 1918, 98–100.

Shafiei, S.S., Solati-Hashjin, M., Rahim-Zadeh, H., Samadikuchaksaraei, A., 2013. Synthesis and characterisation of nanocrystalline Ca–Al layered double hydroxide {[Ca2Al(OH)6]NO3.nH2O}: in vitro study. Adv. Appl. Ceram. 112, 59-65.

Shen, H., Tan, J., Saltzman, W.M., 2004. Surface-mediated gene transfer from nanocomposites of controlled texture. Nat. Mater. 3, 569-574.

Soumya, R.S., Ghosh, S., Abraham, E.T., 2010. Preparation and characterization of guar gum nanoparticles. Int. J. Biol. Macromol. 46, 267–269.

Sun, H., Chu, Z., Hong, D., Zhang, G., Xie, Y., Li, L., Shi, K., 2016. Three-dimensional hierarchical flower-like Mg–Al-layered double hydroxides: Fabrication, characterization and enhanced sensing properties to NOx at room temperature. J. Alloys Compd. 658, 561-568.

Szabados, M., Mészáros, R., Erdei, S., Kónya, Z., Kukovecz, Á., Sipos, P., Pálinkó, I., 2016. Ultrasonically-enhanced mechanochemical synthesis of CaAl-layered double

hydroxides intercalated by a variety of inorganic anions. Ultrason. Sonochem. 31, 409-416.

Tammaro, L., Costantino, U., Bolognese, A., Sammartino, G., Marenzi, G., Calignano, A., Tetè, S., Mastrangelo, F., Califano, L., Vittoria, V., 2007. Nanohybrids for controlled antibiotic release in topical applications. Int. J. Antimicrob. Agents 29, 417-423.

Tammaro, L., Costantino, U., Nocchetti, M., Vittoria, V., 2009. Incorporation of active nano-hybrids into poly(ε-caprolactone) for local controlled release: Antifibrinolytic drug. Appl. Clay Sci. 43, 350-356.

Tammaro, L., Vittoria, V., Calarco, A., Petillo, O., Riccitiello, F., Peluso, G., 2014. Effect of layered double hydroxide intercalated with fluoride ions on the physical, biological and release properties of a dental composite resin. J. Dent. 42, 60-67.

Tarnawski, A.S., Tomikawa, M., Ohta, M., Sarfeh, I.J., 2000. Antacid talcid activates in gastric mucosa genes encoding for EGF and its receptor. The molecular basis for its ulcer healing action. J. Physiol. Paris 94, 93-98.

Tóth, V., Sipiczki, M., Pallagi, A., Kukovecz, Á., Kónya, Z., Sipos, P., Pálinkó, I., 2014. Synthesis and properties of CaAl-layered double hydroxides of hydrocalumite-type. Chem. Pap. 68, 633-637.

Trikeriotis, M., Ghanotakis, D.F., 2007. Intercalation of hydrophilic and hydrophobic antibiotics in layered double hydroxides. Int. J. Pharm. 332, 176-184.

Tronto, J., Reis, M.J.d., Silvério, F., Balbo, V.R., Marchetti, J.M., Valim, J.B., 2004. In vitro release of citrate anions intercalated in magnesium aluminium layered double hydroxides. J. Phys. Chem. Solids 65, 475-480.

Tyner, K.M., Schiffman, S.R., Giannelis, E.P., 2004. Nanobiohybrids as delivery vehicles for camptothecin. J. Control. Release 95, 501-514.

Venugopal, B.R., Rajamathi, M., 2011. Layer-by-layer composite of anionic and cationic clays by metathesis. J. Colloid Interface Sci. 355, 396-401.

Viseras, C., Lopez-Galindo, A., 1999. Pharmaceutical applications of some spanish clays (sepiolite, palygorskite, bentonite): some preformulation studies. Appl. Clay Sci. 14, 69-82.

Wang, H., Cheng, H., Wang, F., Wei, D., Wang, X., 2010. An improved 3-(4,5- I methylthiazol-2-yl)-2,5-diphenyl tetrazolium bromide (MTT) reduction assay for evaluating the viability of Escherichia coli cells. J. Microbiol. Methods 82, 330–333.

Wang, J., Zhou, J., Li, Z., Song, Y., Liu, Q., Jiang, Z., Zhang, M., 2010. Magnetic, Luminescent Eu-Doped Mg–Al Layered Double Hydroxide and Its Intercalation for Ibuprofen. Chem. Eur. J. 16, 14404-14411.

Wang, Q., O'Hare, D., 2012. Recent Advances in the Synthesis and Application of Layered Double Hydroxide (LDH) Nanosheets. Chem. Rev. 112, 4124-4155.

Wang, Y., Tseng, W.J., 2009. A Novel Technique for Synthesizing Nanoshell Hollow Alumina Particles. J. Am. Ceram. Soc. 92, S32-S37.

Wang, Y., Zhang, D., 2012. Synthesis, characterization, and controlled release antibacterial behavior of antibiotic intercalated Mg–Al layered double hydroxides. Mater. Res. Bull. 47, 3185-3194.

Wang, Y., Zhang, F., Xu, S., Wang, X., Evans, D.G., Duan, X., 2008. Preparation of Layered Double Hydroxide Microspheres by Spray Drying. Ind. Eng. Chem. Res. 47, 5746-5750.

Wang, Z., Liang, P., He, X., Wu, B., Liu, Q., Xu, Z., Wu, H., Liu, Z., Qian, Y., Wang, S., Zhu, R., 2018. Etoposide loaded layered double hydroxide nanoparticles reversing chemoresistance and eradicating human glioma stem cells in vitro and in vivo. Nanoscale 10 (27), 13106–13121.

Wang, Z., Wang, E., Gao, L., Xu, L., 2005. Synthesis and properties of Mg2Al layered double hydroxides containing 5-fluorouracil. J. Solid State Chem. 178, 736-741.

Wong, Y., Cooper, H.M., Zhang, K., Chen, M., Bartlett, P., Xu, Z.P., 2012. Efficiency of layered double hydroxide nanoparticle-mediated delivery of siRNA is determined by nucleotide sequence. J. Colloid Interface Sci. 369, 453-459.

Wong, Y., Markham, K., Xu, Z.P., Chen, M., Lu, G.Q., Bartlett, P.F., Cooper, H.M., 2010. Efficient delivery of siRNA to cortical neurons using layered double hydroxide nanoparticles. Biomaterials 31, 8770-8779.

Woo, M.A., Woo Kim, T., Paek, M.-J., Ha, H.-W., Choy, J.-H., Hwang, S.-J., 2011. Phosphate-intercalated Ca–Fe-layered double hydroxides: Crystal structure, bonding character, and release kinetics of phosphate. J. Solid State Chem. 184, 171-176.

Wozniak, A.Z., 2009. Adjuvant therapy for resected non-small cell lung cancer. Ther. Adv.

Xia, S.J., Ni, Z.M., Xu, Q., Hu, B.X., Hu, J., 2008. Layered double hydroxides as supports for intercalation and sustained release of antihypertensive drugs. J. Solid State Chem. 181, 2610-2619.

Xiaobo, W., Zhimin, B., Zhiyong, H., Qifu, Z., fenling, Q., 2015. The influence of synthesis conditions on the structure of Mg-Al layered double hydroxide, Key Eng. Mater. 655, 267-270.

Xu, R., Pang, W., Huo, Q., 2010. Modern Inorganic Synthetic Chemistry. Elsevier, Edition 1st , Amsterdam.

Xu, S., Zhang, B., Chen, Z., Yu, J., Evans, D.G., Zhang, F., 2011. A General and Scalable Formulation of Pure CaAl-Layered Double Hydroxide via an Organic/Water Solution Route. Ind. Eng. Chem. Res. 50, 6567-6572.

Xu, Z.P., Jin, Y., Liu, S., Hao, Z.P., Lu, G.Q., 2008a. Surface charging of layered double hydroxides during dynamic interactions of anions at the interfaces. J. Colloid Interface Sci. 326, 522-529.

Xu, Z.P., Niebert, M., Porazik, K., Walker, T.L., Cooper, H.M., Middelberg, A.P., Gray, P.P., Bartlett, P.F., Lu, G.Q., 2008b. Subcellular compartment targeting of layered double hydroxide nanoparticles. J. Control. Release 130, 86-94.

Xu, Z.P., Stevenson, G.S., Lu, C.-Q., Lu, G.Q., Bartlett, P.F., Gray, P.P., 2006a. Stable Suspension of Layered Double Hydroxide Nanoparticles in Aqueous Solution. J. Am. Chem. Soc. 128, 36-37.

Xu, Z.P., Zeng, Q.H., Lu, G.Q., Yu, A.B., 2006b. Inorganic nanoparticles as carriers for efficient cellular delivery. Chem. Eng. Sci. 61, 1027-1040.

Yamagata, Y., Imoto, K., Obata, K., 2006. A mechanism for the inactivation of Ca2+/ calmodulin-dependent protein kinase II during prolonged seizure activity and its consequence after the recovery from seizure activity in rats in vivo. Neuroscience. 140, 981–992.

Yamaguchi, N., Nakamura, T., Tadanaga, K., Matsuda, A., Minami, T., Tatsumisago, M., 2006. Direct Formation of Zn−Al Layered Double Hydroxide Films with High

Transparency on Glass Substrate by the Sol−Gel Process with Hot Water Treatment. Cryst. Growth Des. 6, 1726-1729.

Yang, L., 2010. Nanophase Ceramics for Improved Drug Delivery: Current Opportunities and Challenges. Am. Ceram. Soc. Bull. 89 (2), 24-32.

Yang, P.P., Quan, Z.W., Li, C.X., Kang, X.J., Lian, H.Z., Lin, J., 2008. Bioactive, luminescent and mesoporous europium-doped hydroxyapatite as a drug carrier. Biomaterials. 29, 4341–4347.

Yao, C., Webster, T.J., 2009. Prolonged antibiotic delivery from anodized nanotubular titanium using a co-precipitation drug loading method. J. Biomed. Mater. Res. Appl. Biomater 91B, 587-595.

Yu, J., Chung, H.E., Choi, S.J., 2013. Acute Oral Toxicity and Kinetic Behaviors of Inorganic Layered Nanoparticles. J. Nanomater. 2013, 1-8.

Yuan, H., Sun, B., Gao, F., Lan, M., 2016. Synergistic anticancer effects of andrographolide and paclitaxel against A549 NSCLC cells. Pharm. Biol. 54 (11), 2629–2635.

Yun, S.K., Pinnavaia, T.J., 1995. Water Content and Particle Texture of Synthetic Hydrotalcite-like Layered Double Hydroxides. Chem. Mater. 7, 348-354.

Zhang, F., Sun, M., Xu, S., Zhao, L., Zhang, B., 2008a. Fabrication of oriented layered double hydroxide films by spin coating and their use in corrosion protection. Chem. Eng. J. 141, 362-367.

Zhang, F., Zhao, L., Chen, H., Xu, S., Evans, D.G., Duan, X., 2008b. Corrosion Resistance of Superhydrophobic Layered Double Hydroxide Films on Aluminum. Angew. Chem. Int. Ed. 47, 2466-2469.

Zhang, H., Pan, D., Duan, X., 2009a. Synthesis, Characterization, and Magnetically Controlled Release Behavior of Novel Core−Shell Structural Magnetic Ibuprofen-Intercalated LDH Nanohybrids. J. Phys. Chem. C 113, 12140-12148.

Zhang, H., Pan, D., Zou, K., He, J., Duan, X., 2009b. A novel core-shell structured magnetic organic-inorganic nanohybrid involving drug-intercalated layered double hydroxides coated on a magnesium ferrite core for magnetically controlled drug release. J. Mater. Chem. 19, 3069-3077.

Zhang, H., Zou, K., Guo, S., Duan, X., 2006. Nanostructural drug-inorganic clay composites: Structure, thermal property and in vitro release of captopril-intercalated Mg–Al-layered double hydroxides. J. Solid State Chem. 179, 1792-1801.

Zhang, J., Xie, X., Li, C., Wang, H., Wang, L., 2015. The role of soft colloidal templates in the shape evolution of flower-like MgAl-LDH hierarchical microstructures. RSC Adv. 5, 29757-29765.

Zhang, K., Xu, Z., Lu, J., Tang, Z., Zhao, H., Good, D., Wei, M., 2014. Potential for Layered Double Hydroxides-Based, Innovative Drug Delivery Systems. Int. J. Mol. Sci. 15, 7409-7428.

Zhenlan, Q., Heng, Y., Bin Z., Wanguo H., 2009. Synthesis and release behavior of bactericides intercalated Mg–Al layered double hydroxides, Colloids Surf. A 348(1), 164-169.

Zhou, D., Shao, L., Spitz, D.R., 2014. Reactive oxygen species in normal and tumor stem cells. Adv. Cancer Res. 122, 1–67.

Zhu, R., Wang, Q., Zhu, Y., Wang, Z., Zhang, H., Wu, B., Wu, X., Wang, S., 2016. pH sensitive nano layered double hydroxides reduce the hematotoxicity and enhance the

anticancer efficacy of etoposide on non-small cell lung cancer. Acta Biomater. 29, 320-332.

Zhu, Y., Wu, Y., Zhang, H., Wang, Z., Wang, S., Qian, Y., Zhu, R., 2015. Enhanced antimetastatic activity of etoposide using layered double hydroxide nano particles. J. Biomed. Nanotechnol. 11, 2158–2168.

Zou, K., Zhang, H., Duan, X., 2007. Studies on the formation of 5-aminosalicylate intercalated Zn–Al layered double hydroxides as a function of Zn/Al molar ratios and synthesis routes. Chem. Eng. Sci. 62, 2022–2031.

Abbreviations

5-FU 5-fluorouracil

AIDS acquired immune deficiency syndrome

ALCAP aluminium calcium phosphorous oxide

ASA acetyl salicylic acid

AUC area under curve

BCS Biopharmaceutics Classification System

BEZ 235-Dactolisib

CAM chloramphenicol

CFX cefuroxime

CFZ cefazolin

CHN carbon hydrogen nitrogen analysis

CIP ciprofloxacin

CP cisplatin

CPT captopril

DEX dextran

DIC diclofenac

DLS dynamic light scattering

ENP enalapril

FA folic acid

FBP flurbiprofen

FDA U.S. Food and Drug Administration

FITC fluorescein isothiocyanate

FTIR Fourier transform infrared spectroscopy

FUDR floxuridine

FV fluvastatin

Htt huntingtin gene

IBU ibuprofen

IFO ifosfamide

K dissolution rate constant

Ksp solubility product

LDH layered double hydroxide

LDL low-density lipoprotein

L-DOPA levodopa

LIS lisinopril

LMWH low molecular weight heparin

MDT mean dissolution time

miRNA micro ribonucleic acid

MRT mean residence time

MTX methotrexate

NP naproxen

NSAIDs non-steroidal anti-inflammatory drugs

ODNs oligodeoxynucleotides

OECD Organization for Economic Cooperation and Development

PAI poly amide-imide

PBS phosphate buffered saline

PER perindopril erbumine

PI3K phosphoinositide 3-kinase

PMP phenoxy methyl penicillin

PPT podophyllotoxin

SAED selected area (electron) diffraction

SEM scanning electron microscopy

shRNA short hairpin ribonucleic acid

siRNA small interfering ribonucleic acid

SSA specific surface area

SV simvastatin

TG-DTA thermogravimetry-differential thermal analysis

TMX tamoxifen

VP16 etoposide

XRD X-ray diffraction

ZCAP zinc calcium phosphorous oxide

A novel nanosized layered double hydroxide ceramic based extended release drug delivery system for cancer therapy

ORIGINALITY REPORT

6%
SIMILARITY INDEX

PRIMARY SOURCES

1	Suman Saha, Sayantan Ray, Rituparna Acharya, Tapan Kumar Chatterjee, Jui Chakraborty. "Magnesium, zinc and calcium aluminium layered double hydroxide-drug nanohybrids: A comprehensive study", Applied Clay Science, 2017 Crossref	563 words — 2%
2	Suman Saha, Sayantan Ray, Swapankumar Ghosh, Jui Chakraborty. "pH-dependent facile synthesis of CaAl-layered double hydroxides and its effect on the growth inhibition of cancer cells", Journal of the American Ceramic Society, 2018 Crossref	335 words — 1%
3	pubs.rsc.org Internet	91 words — < 1%
4	www.jaduniv.edu.in Internet	89 words — < 1%
5	Sk. Hasanur Rahaman, Arnab Bhattacharjee, Suman Saha, Monisha Chakraborty, Jui Chakraborty. "shRNA intercalation in CaAl-LDH nanoparticle synthesized at two different pH conditions and its comparative evaluation", Applied Clay Science, 2019 Crossref	68 words — < 1%